LIQUEFACTION AND INSTABILITY OF TAILINGS DEPOSITS DUE TO EARTHQUAKE FORCES

Hoda Ellaboudy Elsawaf

A Thesis

in

The Faculty

of

Engineering

Presented in Partial Fulfillment of the Requirements

for the degree of Master of Engineering at

Concordia University

Montreal, Quebec, Canada

August 1981

ABSTRACT

LIQUEFACTION AND INSTABILITY OF TAILINGS DEPOSITS DUE TO EARTHQUAKE FORCES

Hoda Ellaboudy Elsawaf

In the past decade there has been a dramatic increase in the size of tailings dams and mine waste deposits. Recent history indicates that the consequences of failure of a large mine waste deposit can be disastrous from the standpoint of both loss of life and environmental damage. Liquefaction and flow of tailings deposits due to earthquake forces is considered to be the main factor.

In many tailings deposits the profile consists of a layer of sand (D_{50} = 0.1 to 0.3 mm) overlying a continuous layer of saturated loose, very fine material (D_{50} = 0.01 to 0.03 mm), generally referred to as slimes.

This thesis presents a study of the response of the slime material to cyclic loading and its liquefaction characteristics. It was found that the material is inherently unstable and would liquefy under even small amplitude cyclic loading. The instability of the whole deposit during and after an earthquake is analyzed. It was shown that the most critical situation is when a bed of slime is deposited on a layer of coarser sandy material and that the most critical factor causing instability is the duration of earthquake. A solution for tailings deposits liquefaction and flow problems is introduced and verfied by experimental evidence.

ACKNOWLEDGEMENT

The author wishes to express her sincere appreciation to Dr. H.B. Poorooshasb, under whose supervision this work was carried out. His constructive guidance, cooperation and encouragement throughout all stages of this work were invaluable.

The author would like to thank Mr. Harold Leroux who offered valuable suggestions in designing the new parts for the triaxial apparatus.

Thanks are also due to Mr. Cydney Smith for his worthy help.

The author is grateful to the National Science and Engineering Council of Canada for the financial assistance.

The author's thanks also go to Miss Joan Armour for her judicious typing of the entire manuscript.

Last, but certainly not least, the author is grateful to her husband, Abdel Fattah, for his help, encouragement and understanding throughout the course of this work.

TABLE OF CONTENTS

LIST OF SYMBOLS

a_{max}	the maximum horizontal ground surface acceleration
A	the settling velocity of the sand grains
A'	the sample's corrected cross sectional area
B	the downstream slope angle
C	the settling velocity of the slime grains
e	the void ratio
E	Elasticity modulus
E_1, E_2	the active earth pressure
g	the gravity acceleration
G	shear modulus
h_o	the height of the sand layer
h_s	the height of the slime layer
H_c	the critical vertical height
k_o	the coefficient of earth pressure at rest
L	the distance of flow
n_d	the initial porosity of the slime layer
n_e	the final porosity of the slime layer
n_f	the final pososity of the sand layer
n_i	the initial porosity of the sand layer
n_s	the temporary porosity of the slime layer
N_o	the stability number
N_1	the corrected standard penetration resistance
p,p'	the total and effective mean normal stress
q	the shear stress
r	the stress ratio in the simple shear test

r_d	the depth reduction factor
r_o	the initial radius of the sample
R	the stress ratio in the triaxial test
u	the pore water pressure
t_o	the duration of the earthquake
u_x	the distance of flow after the earthquake ceases
$\bar{u}_x$	the distance of flow at the instant the earthquake ceases
$\dot{u}$	the pore water pressure generation rate
$\dot{u}_x$	the velocity of the flow
$\ddot{u}_x$	the acceleration of the flow
v_f	the volume of the tailings which flow
w	the weight of the tailings which flow
γ	the total unit weight of the soil
γ_o	the total unit weight of the sand layer
γ_{xy}	the engineering shear strain
$d\gamma^p, dv^p$	the plastic shear and volumetric strain increment component
$\delta v, \delta\epsilon$	the change in the volumetric and axial strain
θ	the slope inclination angle
ψ	the plastic potential function
ϕ	the angle of internal friction
ϵ_{ij}	the strain tensor
ϵ_{xy}	the shearing strain
$d\epsilon^p_{ij}$	the plastic strain increment vector
$d\epsilon_1, d\epsilon_3$	the major and minor principal strain increment
μ	Poisson ratio
σ, σ'	the total and effective normal stress
σ_{ij}	the stress tensor

σ'_{ij}	the effective stress tensor
σ_1, σ'_1	the total and effective major principal stress
σ_3, σ'_3	the total and effective minor principal stress
τ	the shear strength of soil
τ_{av}	the equivalent uniform cyclic shear stress induced by earthquake
$\Delta\tau$	the cyclic shear stress induced by the earthquake

LIST OF FIGURES

TO MY BELOVED MOTHER

CHAPTER 1

INTRODUCTION

In this chapter, the definition of liquefaction and the objectives of this thesis will be mentioned. The stress conditions in earthquake (equivalent loading), and the stress conditions in the triaxial cyclic loading test (compression-extension test) to simulate the earthquake stress conditions will be discussed. At the end of this chapter, a review of the previous studies in liquefaction, and the contents of this thesis will be presented.

1.1 Foreword

The principle of effective stress in soils may be stated by the relationship

$$\sigma'_{ij} = \sigma_{ij} - u\,\delta_{ij}$$

where σ'_{ij} is the so-called effective stress tensor, σ_{ij} is the applied stress tensor, and u is the pore water pressure. The symbol δ_{ij} represents the Kronecker delta tensor where $\delta_{ij} = 1\,(i=j)$, $\delta_{ij} = 0\,(i\neq j)$.

It has been demonstrated empirically that to a very close degree of approximation both strength and deformation of a soil sample are dependent on (but not necessarily a function of) the parameter σ'_{ij}, the effective stress.

Let the reference axis x_i be so chosen as to coincide with the principal directions of σ'_{ij} (coincidental with σ_{ij}) and let the major and minor principal stresses be $\sigma'_1 - \sigma'_3$. Denoting τ by the quantity $(\sigma'_1-\sigma'_3)/2 = (\sigma_1-\sigma_3)/2$ and by σ' the quantity $(\sigma'_1+\sigma'_3)/2$, then according to Coulomb's failure criterion:

$$\tau = \sigma' \sin \phi \qquad (1.1)$$

for a cohesionless soil. But

$$\sigma' = \frac{\sigma_1' + \sigma_3'}{2} = \frac{\sigma_1 + \sigma_3}{2} - u = \sigma - u$$

and hence

$$\tau = (\sigma - u) \sin \phi \qquad (1.2)$$

Cohesionless soils (sands, silts, sandy gravels, etc.) when sheared have a tendency to change their volumes due to particles overriding each other or due to collapse of locally unstable structure. In particular, loose samples of such soils have a great tendency to contract during a loading process because a loose structure is inherently unstable (even virgin dense samples are initially unstable). If a saturated loose sample of a cohesionless soil is tested under undrained conditions, i.e. no water is permitted to leave the sample, the tendency to contract would create positive pore water pressure in the sample and as loading proceeds progressively more pressure will be developed by the pore water. When the pore water pressure tends to levels comparable or equal to applied normal stress, σ, then according to equation (1.2)

$$\tau \to 0$$

as

$$(\sigma - u) \sin \phi \to 0 \qquad (1.3)$$

or as

$$u \to \sigma$$

This phenomenon which brings about an apparent lack of strength of the soil sample, is called "liquefaction". Note that liquefaction can also be brought about in a drained test by appropriately monitoring the applied stresses which are now equal to effective stresses (since the sample is tested drained).

Earthquake loading is essentially a cyclic loading of a soil element. If the sample is loose this loading process produces conditions similar to those indicated by equation (1.3). Evidence of such losses of strength are extensive, e.g. Niigata earthquake of 1964, Great Alaska earthquake of 1964. Both earthquakes produced extensive damage by causing foundation instability, large landslides, etc.

Tailing deposits are amongst the loosest deposits which can be encountered, hence they are very susceptible to liquefaction.

1.2 Objectives of This Research

The aim of this research is to study the effect of earthquakes on tailings deposits.

Specifically a soil element is subjected to a number of loading cycles under the so-called triaxial cyclic loading system, the pore water pressure and axial strains being measured continuously and then subjected to a direct loading process.

Stability at some simple deposits are subsequently investigated using the results obtained from these tests.

1.3 Stress Conditions in Earthquake; Equivalent Loadings

In the laboratory it is essential to load the sample in a manner which is equivalent to those encountered in the field. In the following, a method due to Seed and Idriss (1971), which was used in the present work, is described.

Fig. 1.1 shows an assumed idealized mode of loading during an earthquake. The sample is subjected to a sequence of stress reversals simulating the alternating forces applied by the earthquake.

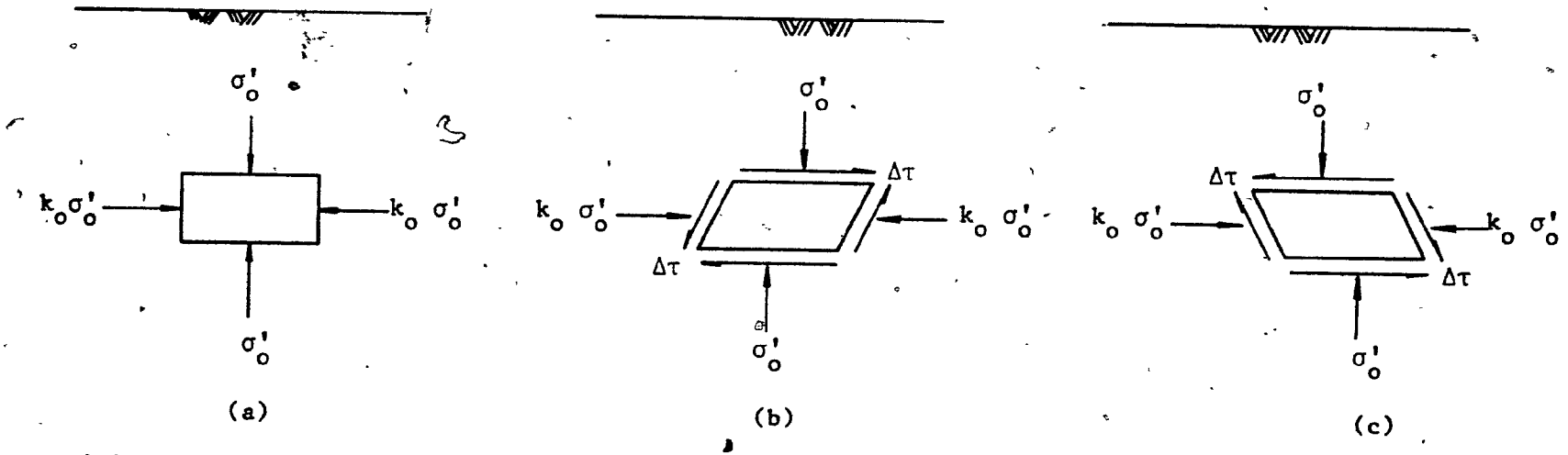

Initial Stresses Before Earthquake

Cyclic Load Sequence During Earthquake

Fig. 1.1 Idealized Stress Conditions for Element of Soil During an Earthquake

Before the earthquake the soil element is subjected to the principal stresses σ_o' and $k_o\ \sigma_o'$ where σ_o' is the effective overburden pressure, and k_o is the coefficient of earth pressure at rest (no lateral deformation).

During the earthquake the soil element is subjected to shearing stress, $\Delta\tau$ on the horizontal and vertical planes, which reverses directions many times during the earthquake period (Seed, 1979).

The amplitude of the exerted shear stress in the field varies randomly from one cycle to another (Fig. 1.2). A simple procedure by which a series of uniform cyclic stresses, assumed to be equivalent in their effect to the irregular stress sequence produced by an earthquake, would be determined was proposed by Seed and Idriss (1971). The method involves the computation of the equivalent uniform cyclic shear stress, τ_{av}, induced at any point in a soil deposit using the relationship:

$$\tau_{av} = 0.65 \cdot \gamma h \cdot \frac{a_{max}}{g} \cdot r_d \qquad (1.4)$$

in which a_{max} = maximum horizontal ground surface acceleration, γ = total unit weight, h = depth below ground surface, and r_d = depth reduction factor. The 0.65 factor assumes that the equivalent uniform shear stress, τ_{av}, is 65% of the absolute maximum shear stress. The depth reduction, r_d, recognizes that the soil is deformable and does not behave as a rigid body. The value of rd will decrease from 1.0 at the ground surface to much lower values at large depth as shown in Fig. 1.3.

The number of stress cycles over which the equivalent uniform shear stress is repeated may be evaluated either by using an appropriate weighting procedure or by adopting a representative number of cycles from studies of different magnitude earthquakes. Typical numbers of cycles first

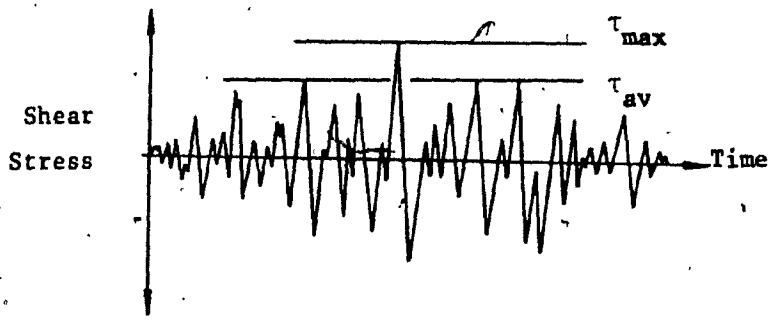

Fig. 1.2 Time History of Shear Stresses During Earthquake

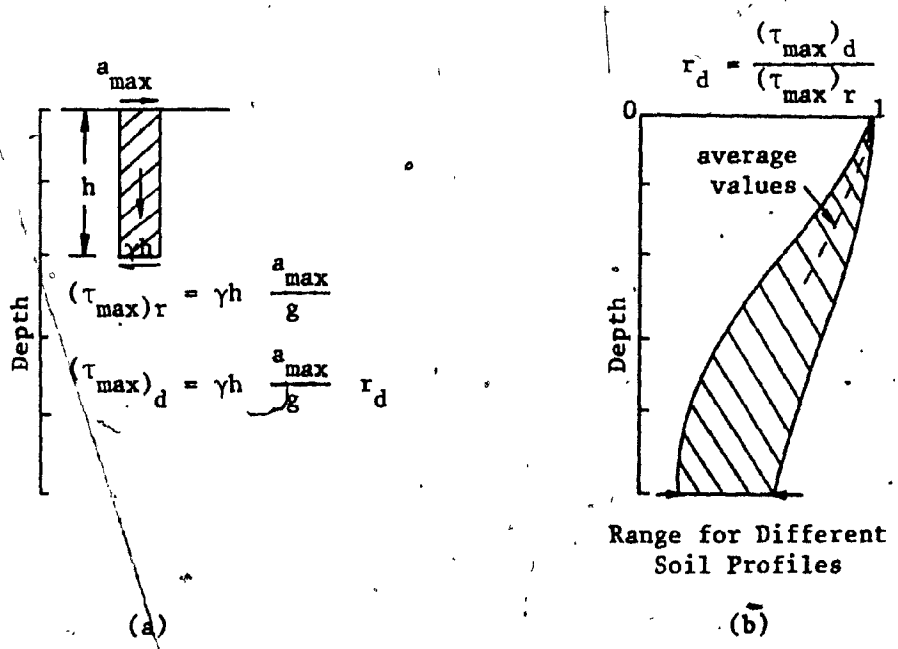

Fig. 1.3 Determination of Maximum Shear Stress

presented by Seed and Idriss (1971) have been updated by Lee and Chan (1972) and Seed et al (1975). In all cases, the number of cycles corresponding to an equivalent uniform shear stress (usually 0.65 τ_{max}) has been plotted as a function of the earthquake magnitude. Relationships developed by Seed et al (1975) are presented in Fig. 1.4.

Hence, the irregular shear stress cycles induced by the earthquake (Fig. 1.2) can be represented by equivalent number of uniform stress cycles (Fig. 1.5).

During the short period of earthquake shaking there would be no significant dissipation of the pore water pressures in the soil mass under study, so that its behaviour could be evaluated on the basis of undrained test conditions in the laboratory. Hence, earthquakes can be represented by undrained uniform cyclic loading conditions.

1.4 Stress Conditions in Cyclic Loading (Triaxial Cyclic Loading Test)

Cyclic loading triaxial tests have been used to simulate the cyclic loading condition induced by the earthquake.

Fig. 1.6 (Col. 1) shows three stress conditions at different stages of a cyclic loading test. In condition a, the sample is subjected to an all-around pressure. The Mohr diagram for this stress condition is a point (Col. 2) and the stress on plane xx is equal to σ_3. In condition b the vertical stress is increased by an amount $\Delta\sigma/2$ and the horizontal stress is decreased by an equal amount, the resulting Mohr diagram is shown in Col. 2. It is seen that the normal stress on plane xx is still equal to σ_3 but a shear stress equal to $\Delta\sigma/2$ has also been induced. Finally in condition c, the vertical stress is reduced by $\Delta\sigma/2$ but the horizontal stress is increased by this amount. Again, the resulting stress condition produces

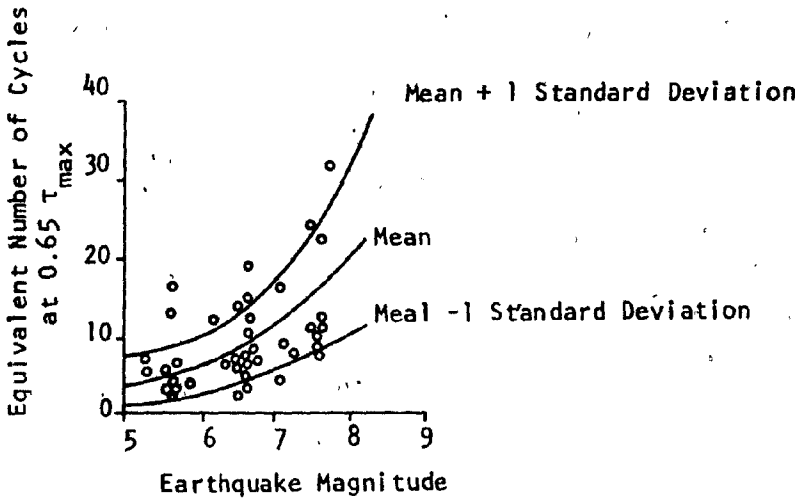

Fig. 1.4 Equivalent Numbers of Uniform Stress Cycles

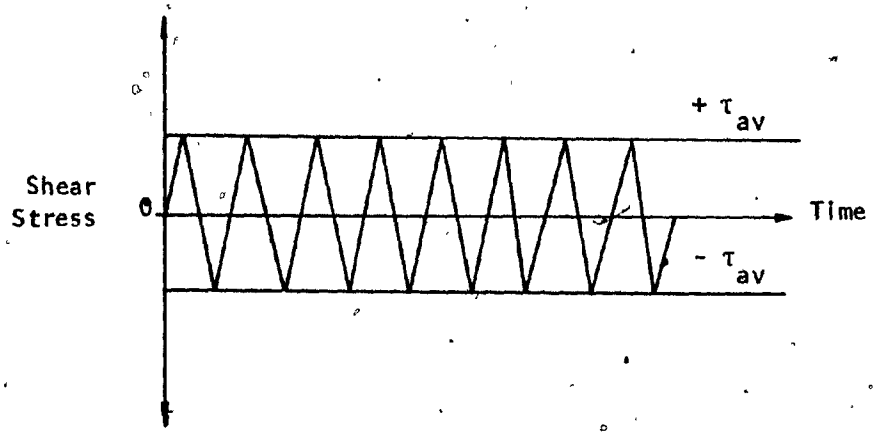

Fig. 1.5 Equivalent Uniform Stress Cycles

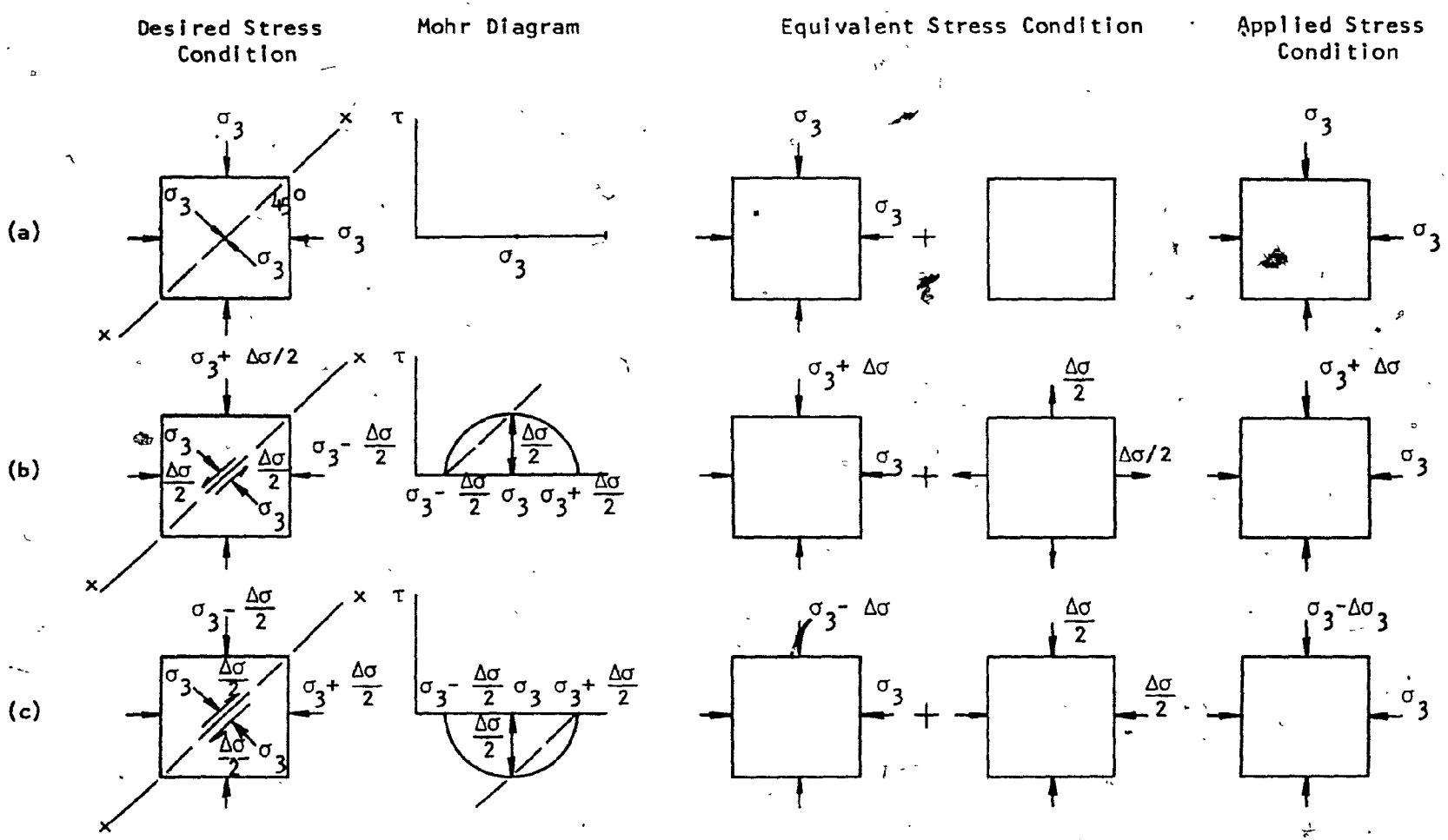

Fig. 1.6 Stress Conditions for Triaxial Test on Saturated Soil Under Simulated Earthquake Loading Conditions

a stress equal to σ_3 on plane xx but a shear stress of $\Delta\sigma/2$ acting in the opposite direction to that for condition b.

Thus, by bringing the sample to equilibrium under a confining stress condition and then cycling the vertical and horizontal stresses between conditions b and c in Fig. 1.6, the stress conditions on plane xx will be the same as those on a horizontal plane during an earthquake (Fig. 1.1). The effects of the intermediate stress are neglected as is customary in triaxial testing.

The cyclic stress changes required to induce the desired stress conditions required that at all stages of loading the mean of the major and minor principal stresses should be maintained constant. This condition might be termed "constant mean principal stress" and, if the effects of the intermediate principal stress are neglected, maintenance of this condition would provide the desired stress condition.

The application of simultaneous cyclic changes in both the vertical and horizontal stresses acting on a test specimen to maintain a constant mean principal stress condition is a difficult test procedure. However, in working with saturated soils this difficulty can readily be overcome. For example, the desired stress condition shown by conditions b (Fig. 1.6, Col. 1) can be induced on a test specimen by the simultaneous application of the two stress conditions shown in Col. 3, direct addition of the two stress conditions in Col. 3 produces the same stress as those indicated in Col. 1. Thus, the desired stress condition can be induced by increasing the axial stress on the specimen by an amount $\Delta\sigma$, keeping the lateral stress constant, and simultaneously reducing the all-around confining pressure on the specimen by an amount $\Delta\sigma/2$. However, the effects of the reduction in all-around confining pressure are well known. It would simply reduce the pore-water

pressure in the saturated sample by $\Delta\sigma/2$ without causing any change in effective stresses in the sample. Because the deformation of the sample is caused only by changes in effective stress, the deformations of the specimen would be the same whether the change in confining pressure were made or not. In fact, if the reduction in confining pressure were omitted from the test procedure, the effective stresses and the strains in the sample would be just the same as if it were included, but the pore water pressures would be too high by $\Delta\sigma/2$. Thus, the effects of the desired stress condition b in Col. 1 can be determined by applying the stress conditions shown in Col. 4 and simply correcting the measured pore water pressures as explained above. Strains and effective stresses would require no correction at all.

Similarly, the desired stress condition shown by condition c (Fig. 1.6, Col. 1) can be induced by the application of the two conditions shown in Col. 3, that is by reducing the vertical stess by $\Delta\sigma$ and applying an increase in all-around pressure equal to $\Delta\sigma/2$. The effects of the desired stress condition therefore can be determined by applying only the reduction in vertical stress and correcting the pore-water pressures by increasing them by $\Delta\sigma/2$. It is, of course, necessary that the cyclic stress $\Delta\sigma$ should not exceed the initial confining pressure σ_3, as the vertical stress σ_1 must remain compressive at all times.

Thus, it follows that the effects of the desired cyclic stress conditions, corresponding to those in Fig. 1.1, can be determined by subjecting a test specimen of saturated soil to cyclic changes in deviator stress $\pm\Delta\sigma$ and maintaining the lateral pressure σ_3 constant, provided $\Delta\sigma$ is less than σ_3 and appropriate corrections are made to the measured pore water pressure (Seed and Lee , 1966).

This test procedure has been used for the following studies.

1.5 Review of Previous Liquefaction Studies

1.5.1 The "Critical Void Ratio" concept

Probably the first attempt to determine conditions under which liquefaction might occur was the "critical void ratio" approach suggested by A. Casagrand, 1936. It was noted that during shearing dense sands tend to expand whereas loose sand tends to decrease in volume, thus, for any sand there will be some initial void ratio, termed the critical void ratio, for which no volume change during drained shear, and correspondingly, no pore water pressure changes during undrained shear, will occur. It was reasoned, therefore, that sand deposits having a void ratio above the critical value and therefore tending to contract during shear, would under undrained conditions, develop a positive pore water pressure that would possibly be large enough to produce liquefaction. Conversely, deposits having an initial void ratio below the critical value would tend to dilate during shear, produce a decrease in pore-water pressure and a corresponding increase in effective stress under undrained conditions, so that high strength and stability would be developed.

It was subsequently noted that the critical void ratio is not a constant value for a given sand but that it depends on the confining pressure to which the sand is subjected (Casagrand, 1938) because dilation tendencies are smaller at high confining pressures, the critical void ratio decreases as the confining pressure increases. Thus, it has been concluded that a saturated sand at any given density is potentially less stable under a high confining pressure (producing compression characteristics) than under a low confining pressure (producing dilatant characteristics).

This approach can provide a valuable guide to the behaviour of saturated sands subjected to the kind of loading for which the critical void ratio is established. However, as Casagrand (1936) noted in presenting the concept of a critical void ratio, volume changes under cyclic loading conditions are quite different from those occurring under one-direction static loading conditions, and it could hardly be expected that the critical void ratio concepts would be applicable to earthquakes or vibratory loading conditions.

1.5.2 The shaking table method

The inadequacy of the critical void ratio concept for the vibratory loading problems has led to attempts to establish the conditions producing liquefaction in terms of the acceleration at which liquefaction can be observed to develop (Prakash and Mathur, 1965). Usually this is done by placing saturated sand in a box on a shaking table and recording the table accelerations at which liquefaction occurs. However, such results are inevitably influenced by the duration and frequency of the table motions to which the sand is subjected and possibly also by the geometry and deformation characteristics of the container in which the saturated sand is placed. Thus, it is difficult to extrapolate the results to field conditions.

1.5.3 The standard penetration resistance method

After Alaska and Niigata earthquakes of 1964, more comprehensive collections of site conditions at various locations where some evidence of liquefaction or no liquefaction was known to have taken place was presented by Seed and Peacock 1971, and used as a basis to determine the relationship

between field values of cyclic stress ratio, τ_{av}/σ'_o (in which τ_{av} = the average horizontal shear stress induced by an earthquake, and σ'_o = the initial effective overburden pressure on the soil layer involved, stress ratio has been determined by the relationshp $\tau_{av}/\sigma'_o = 0.65\ a_{max}/g \cdot \gamma h/\sigma'_o \cdot r_d$ as mentioned before), and the relative density of the sand, as determined from the Standard Penetration Resistance. The most recent form of this data collection is shown in Fig. 1.7 (Seed, Mori and Chan). Values of stress ratio known to be associated with some evidence of liquefaction or no liquefaction in field are plotted as a function of the corrected average penetration resistance N_1 of the sand deposit involved. Thus for any given site and a given value of maximum ground surface acceleration, the possibility of liquefaction can readily be obtained with the aid of the chart (Fig. 1.7) by determining values of N_1 for the sand layer involved, reading off a lower bound value of τ_{av}/σ'_o for sites where some evidence of liquefaction is known to have occurred, and comparing this value with that induced by the design earthquake for the site under investigation.

Limitations of this procedure include the following 1) empirical charts of this type do not take into account all the significant factors affecting liquefaction such as duration of shaking, magnitude of earthquake, etc. 2) the standard penetration resistance of a soil is not always determined with reliability in the field and its value may vary significantly depending on the boring and sampling conditions used for its determination.

It appeared necessary to investigate the behaviour of soils under controlled conditions of stress or strain and under cyclic loading conditions, so laboratory tests based on simulations of the earthquake stress condition (Fig. 1.1) have been the principal means of studying liquefaction.

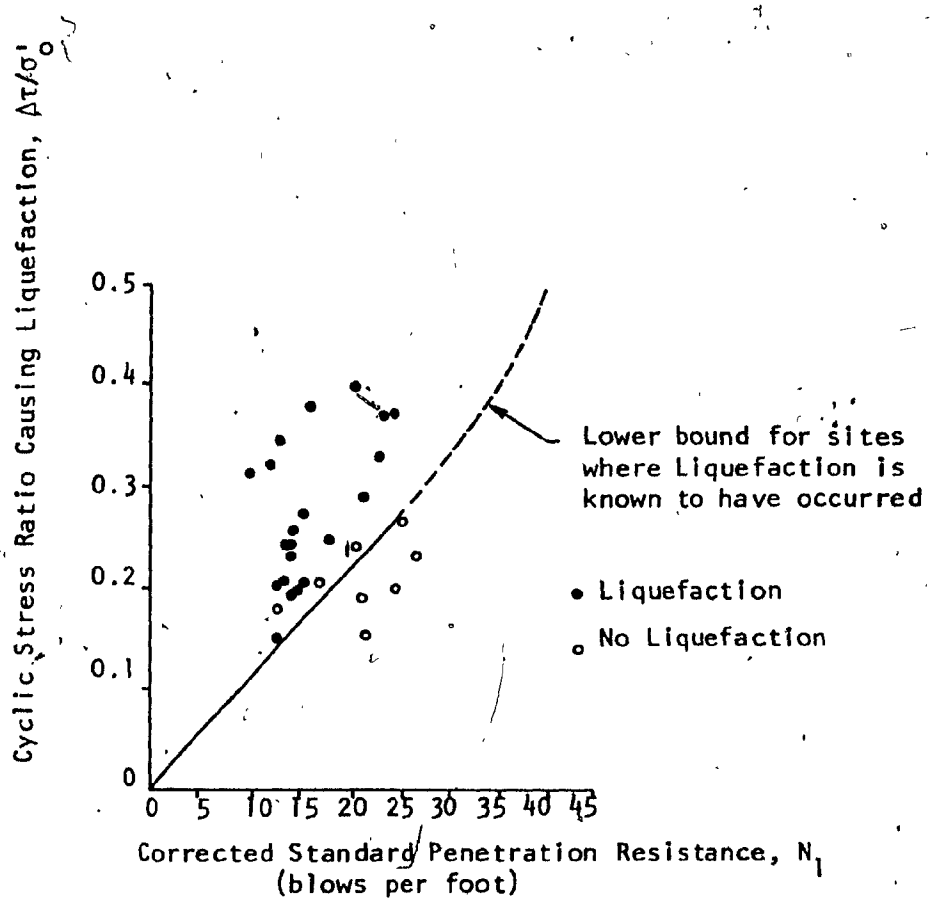

Fig. 1.7 Correlation Between Stress Ratio Causing Liquefaction in the Field and Penetration Resistance of Sand

1.5.4 The cyclic triaxial test

The cyclic triaxial test has been widely used (Seed and Lee 1966, Lee and Seed 1967, Finn, Pickering and Bransby 1971) to study the various factors controlling the liquefaction characteristics of sand. Samples of saturated sand are initially consolidated under all-around confining pressure and then subjected to uniform cyclic deviator stress with a frequency of 2 cycles per second (stress-controlled pulsating load test) under undrained conditions (Fig. 1.8a). Stress conditions on a plane at 45° through the sample approximate those on the horizontal planes in the field.

In such tests, the pore water pressure at the end of each stress cycle increases progressively with increasing number of cycles. The rate of pore water pressure development accelerates as liquefaction is approached (the pore water pressure equal to the confining pressure), at which point strain amplitude rapidly increases as shown in Fig. 1.9 (See and Lee, 1966).

The study of the factors affecting liquefaction concluded that the higher the cyclic stress or strain to which the sand is subjected, the smaller is the number of stress cycles required to induce liquefaction. The lower the confining pressure acting on a sand, the lower the cyclic stresses, strains, or the number of cycles required to induce liquefaction. The looser the sand the lower the cyclic stresses, strains or the number of cycles required to induce liquefaction. The cyclic stresses required to induce liquefaction or failure of initially unstressed elements of saturated sand are considerably smaller than those required to induce failure under static loading conditions (Lee and Seed, 1967).

In the triaxial test it is only possible to produce the desired stress changes by consolidating the sample initially under all-around confining stress corresponding to $k_o = 1$. If any other initial stress condition is used, there is no plane in the sample which receives the desired

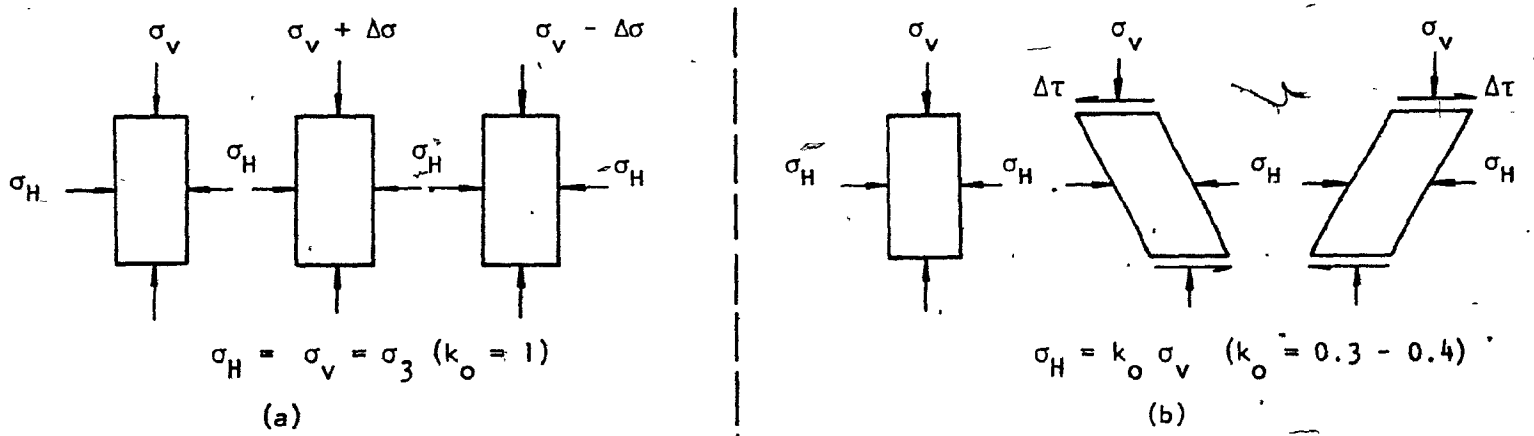

Fig. 1.8 State of Stress for Samples Under:
(a) Triaxial Test Conditions
(b) Simple Shear Test Conditions

Initial Void Ratio = 0.87

Initial Confining Pressure = 2.0 kg/sq cm

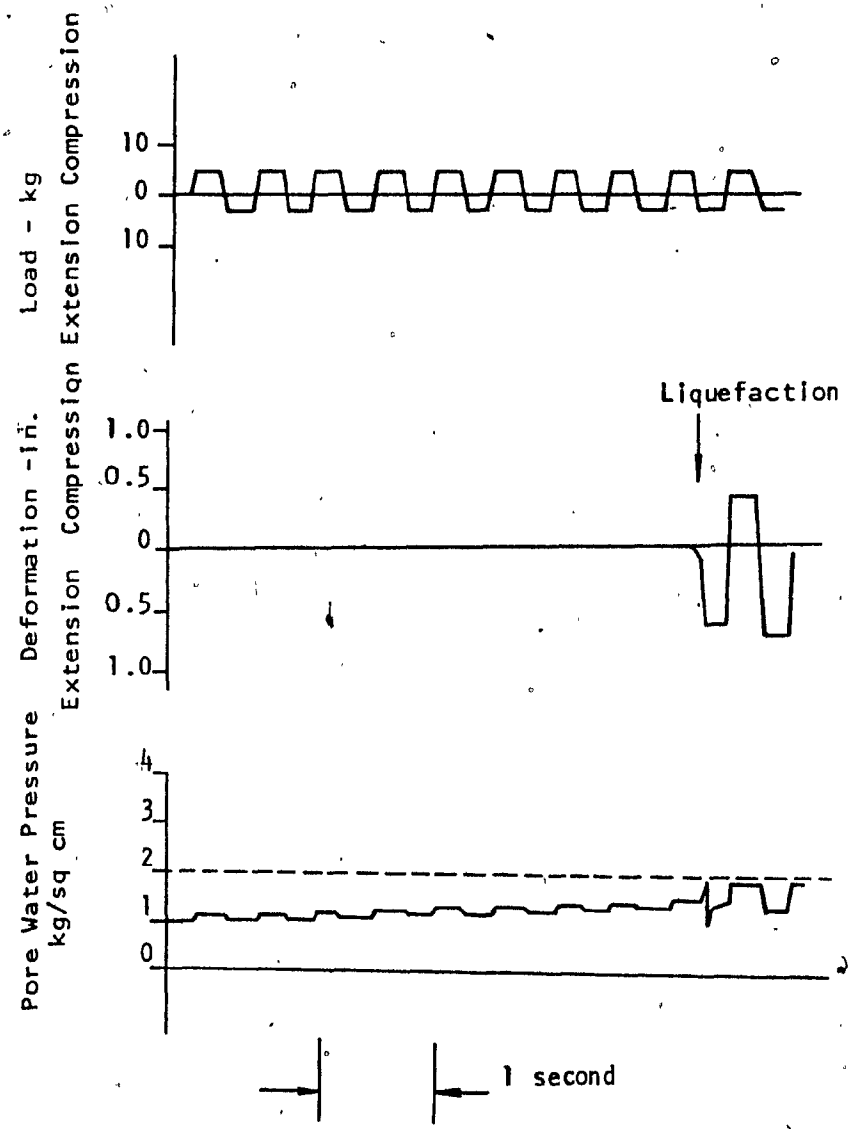

Fig. 1.9 Record of Typical Pulsating Load Test on Loose Sand

symmetrical changes in shear stress, corresponding to those on the horizontal plane in the field. The use of $k_o = 1$ condition in the test procedure (rather than the actual field condition of about 0.4) together with a failure criterion expressed in terms of the rate $\Delta\sigma/2\sigma_3$ will cause the stresses inducing failures or liquefaction in triaxial tests to be higher than those inducing failure in the field.

1.5.5 Cyclic simple shear test

To overcome the theoretical limitations of the cyclic triaxial test (Peacock and Seed, 1968) the cyclic simple shear apparatus was developed by Peacock and Seed (1968) and Finn et al (1971) to more closely simulate field conditions. In this test, rectangular samples of saturated sand are consolidated by a vertical stress σ_v under k_o conditions (zero lateral deformation), and a cyclic horizontal shear stress, $\Delta\tau$ applied with frequency of 2 cycles per second, with drainage prevented and with zero lateral deformation conditions maintained (Fig. 1.8b). In this type of test the build up of pore water pressure is similar in form to that in the cyclic triaxial test except that cyclic fluctuations in pore water pressure are relatively small.

In the simple shear test, there are difficulties encountered in ensuring a uniform shear stress across the width of the sample and along the vertical faces of the test specimen, which leads to non-uniformities in stress and strain conditions near the edge, and at the top and base of the sample. There are difficulties too in preparing test specimens in a uniform condition representative of field conditions because of the difficulties in enclosing test specimens to maintain constant volume or uniform strain, or both (Seed and Peacock 1971). These difficulties have

made the use of cyclic triaxial tests more widely used to simulate the cyclic stress condition in the field during the earthquake.

1.5.6 New method of comparison of triaxial and simple shear data

A comparison was made between the cyclic shear stress ratio $\Delta\sigma/2\sigma_3'$ causing liquefaction after certain number of cycles in the triaxial test, and the cyclic shear stress ratio $\Delta\tau/\sigma_v'$ in the simple shear test causing liquefaction after the same number of cycles in the case where the effective confining pressure σ_3' in the triaxial is equal to the effective vertical pressure σ_v' in the simple shear. The triaxial tests give higher results as shown in Fig. 1.10a. However, a new method of comparison has been developed by Finn et al 1971, taking the difference in the initial confining stress system for each test into account. In this method the mean normal effective stress is considered rather than the actual normal effective stress acting on the sample. The mean normal effective stress in the triaxial test is equal to $(\sigma_3'+\sigma_3')/2=\sigma_3'$. In the simple shear test it is equal to $1/2\ (\sigma_v' + k_o\ \sigma_v')$. Hence, the cyclic shear stress ratio is equal to $R=\Delta\sigma/2\sigma_3'$ in the triaxial and equal to $r=2\Delta\tau/(\sigma_v'+k_o\sigma_v')$ in the simple shear. Comparing these ratios at $\sigma_3' = \sigma_v'$ at the same number of cycles causing liquefaction, the two tests give identical results as shown in Fig. 1.10b.

1.6 Contents of the Thesis

In Chapter 1 the liquefaction phenomenon is defined. The objectives of this thesis are reviewed. The stress conditions in earthquake, and in triaxial cyclic loading tests are discussed. A review of the previous studies in liquefaction is presented.

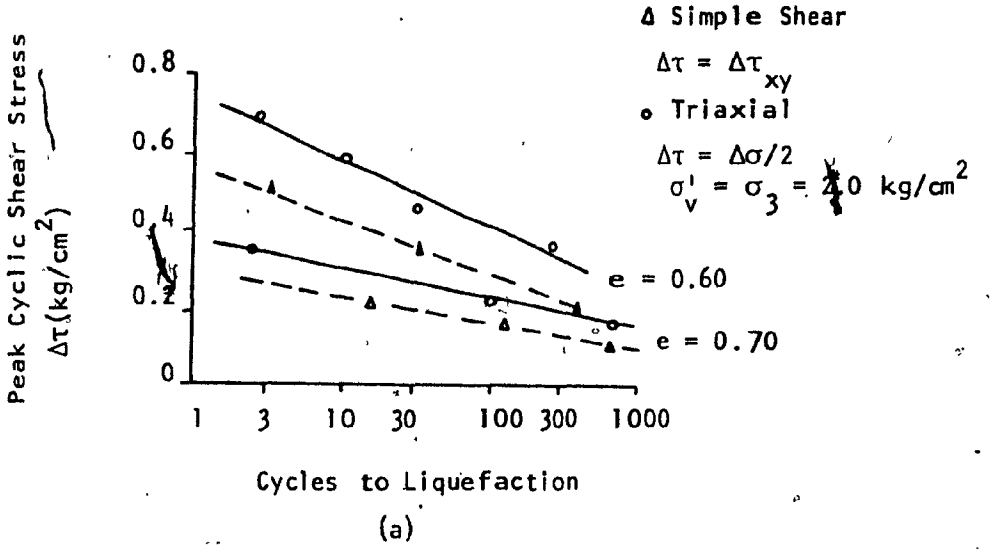

(a)

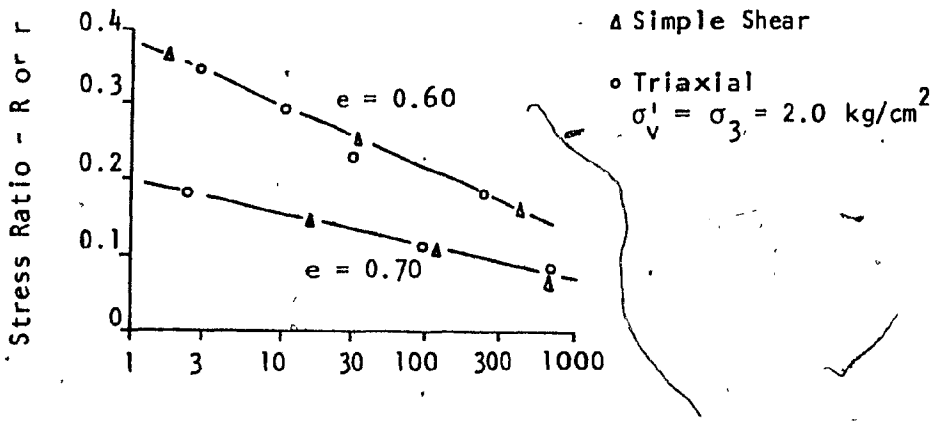

(b)

Fig. 1.10 Comparison of Liquefaction Resistance of Ottawa Sand In Simple Shear and Triaxial Tests

The testing program of the triaxial cyclic loading tests (compression-extension tests) to study the liquefaction characteristics of the tailings deposits is described in Chapter 2.

In Chapter 3, the instability of the tailings deposits during and after earthquake is analyzed. A quantitative analysis of settling and liquefaction for different tailing deposits profiles is discussed. Finally, a solution for liquefaction and flow problems of tailings desposits due to earthquake is introduced and verified by experimental evidence.

The research results are concluded in Chapter 4.

CHAPTER 2

LIQUEFACTION OF TAILINGS DEPOSITS DUE TO EARTHQUAKE FORCES

In this chapter the series of triaxial cyclic loading tests (compression-extension tests) performed to study the liquefaction characteristics of the tailings deposits soil will be reviewed. The testing material, test apparatus, including the new parts designed especially for these special tests, and the sample preparation, will be described. The behaviour of the testing material, the slimes, under cyclic stress application, and under static loading following liquefaction, will be discussed together with the factors influencing liquefaction. A comparison will be made between the static loading following liquefaction and the conventional static loading, and between the cyclic stresses causing liquefaction or failure, and the static loading causing failure. At the end of this chapter, the results of the tests will be analyzed.

2.1 Test Material

The soil used in this work is a silty soil called slime, and forms the underlying material of the tailing deposits. It is a fine material (D_{50} = 0.01 to 0.03 mm) of liquid limit ≃ 36%, plastic limit ≃ 33%, and plasticity index = 3%. According to the Unified Soil Classification System, the plasticity chart, it can be classified as MI. These are inorganic silts and very fine sands with intermediate plasticity or compressibility and of fair to poor drainage characteristics. The slime is cohesionless material with cohesion intercept, c = 0.

2.2 Test Apparatus

Cyclic loading tests (compression-extension tests) were performed on the slime using strain controlled triaxial apparatus with a very slow strain rate of .0008 inch/min. The slow strain rate was chosen because the slime is sufficiently impervious that pore pressure equalization in the sample occurs after lengthy stress application. Hence, the use of a slow loading rate permits the pore water pressure to develop and equalize in the sample and avoids developing gradient or unequal pore pressures in it.

Two new parts were designed for the tests in this work to allow for the application of compression and extension deviator stresses on the sample in the same test (the cyclic loading condition). The new parts are a special ram, as shown in Fig. 2.1, and a special top cap, as shown in Fig. 2.2.

The ram consists of a cylinderical stainless steel rod and a stainless steel ball of 1.104 inch diameter brazed to the rod's upper end. The rod is of .495 inch diameter and 5.733 inches high. It is connected at its lower end to a cylindrical pin of 0.1 inch diameter, and 0.759 inches long, by a set screw at the bottom of the ram. The ball is supported by upper and lower 2 inch square aluminum machined out blocks of .488 inches high. The two blocks are kept apart at constant distance by four spacers of 1.124 inches high and 0.367 inch diameter, fixed to the blocks. There is a bolt of 3/4 inch diameter at the top of the ram, which connects it to the proving ring before the test, by placing the bolt in a threaded hole at the bottom of the proving ring. The hole is the same size as the bolt, and is fastened by a nut. The ball ensures that, during the test, the ram applies axial load acting at the center line of the sample, so preventing eccentricity. There are two marks on the ram: a vertical and a horizontal one. The horizontal mark is at a distance of 1.141 inches from the ram

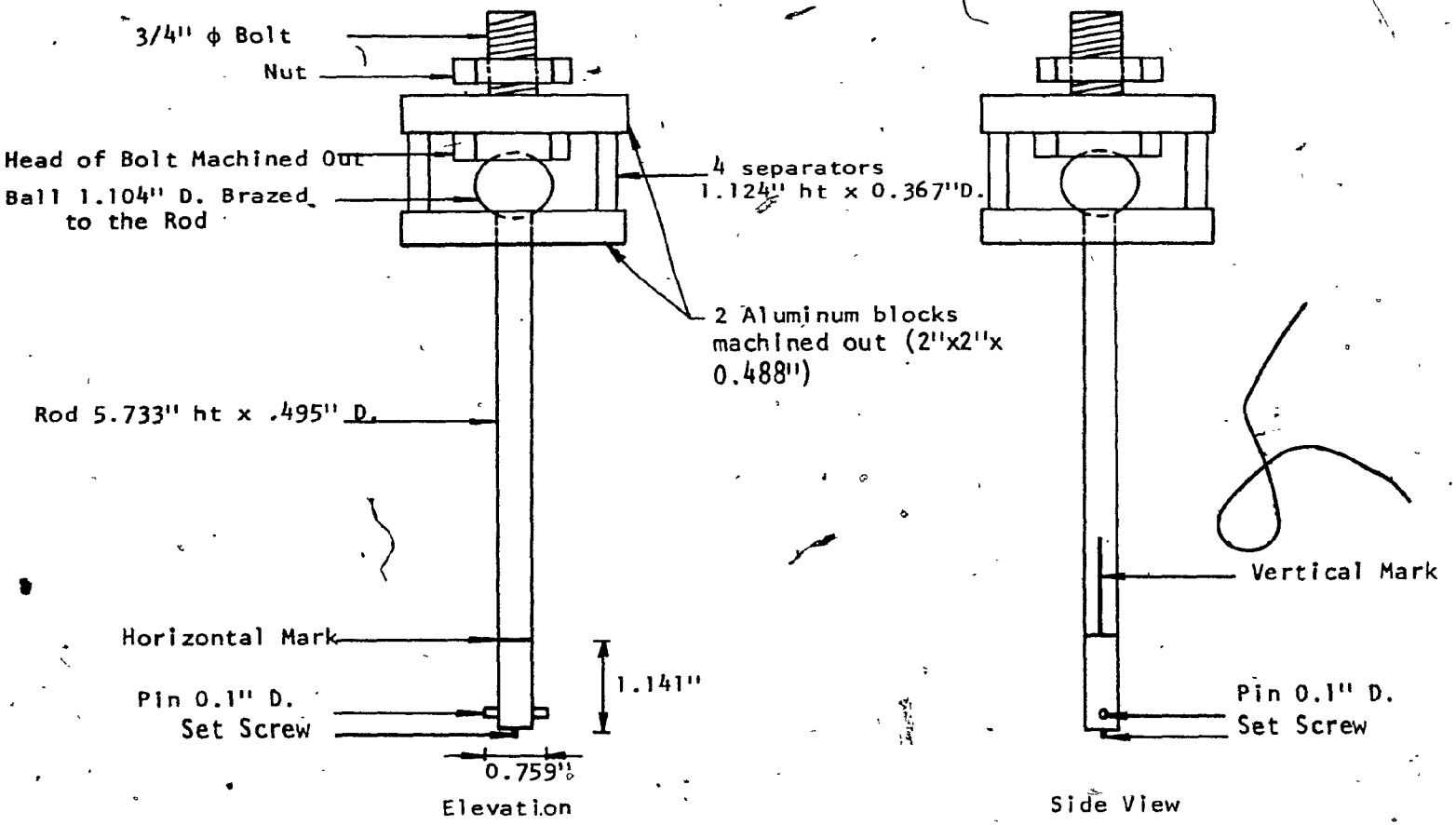

Fig. 2.1 The New Ram for the Triaxial Cyclic Loading Tests

bottom which is the distance the ram should be inserted into the top cap to touch the sample. The vertical mark determines the position of the pin inside the top cap.

The second part is a special top cap, as shown in Fig. 2.2. The cap is of two parts, connected together: the lower cylindrical plexiglass part is 1.962 inches in diameter and 1.5 inches in height, and the higher cylindrical brass part is 1.118 inches in diameter, and 0.801 inches in height, 0.433 inches of that height being inside the lower plexiglass part. There is a hole in the upper part, along its depth, of the same size and shape as the ram and the pin. Along this hole the ram can move only vertically, upwards or downwards. Under this hole in the lower part of the cap, there is a cylindrical hole 0.19 inches high and 0.759 inches in diameter, along which the ram can move vertically, upwards and downwards with a play of 0.09 inch depth. It can also rotate 90^{o} in one direction and 270^{o} in the other direction due to a vertical stopper at the perimeter of the hole.

Before testing, the ram is inserted into the top cap until just before the horizontal mark is at the surface of the cap, to ensure that the ram does not hit the sample. The cell is fixed to the base by the nuts and so takes its position in the triaxial machine. The ram is connected to the proving ring by the upper bolt and the nut. Then the confining pressure is applied to consolidate the sample. During consolidation the top cap moves downward along the ram as the sample settles, due to the decrease in its volume. The maximum allowable settlement for the sample to settle while the ram is still inside the top cap is 1.141 inch (the top cap hole depth), which is always more than the consolidation settlement. Thus the ram will not leave the top cap during consolidation.

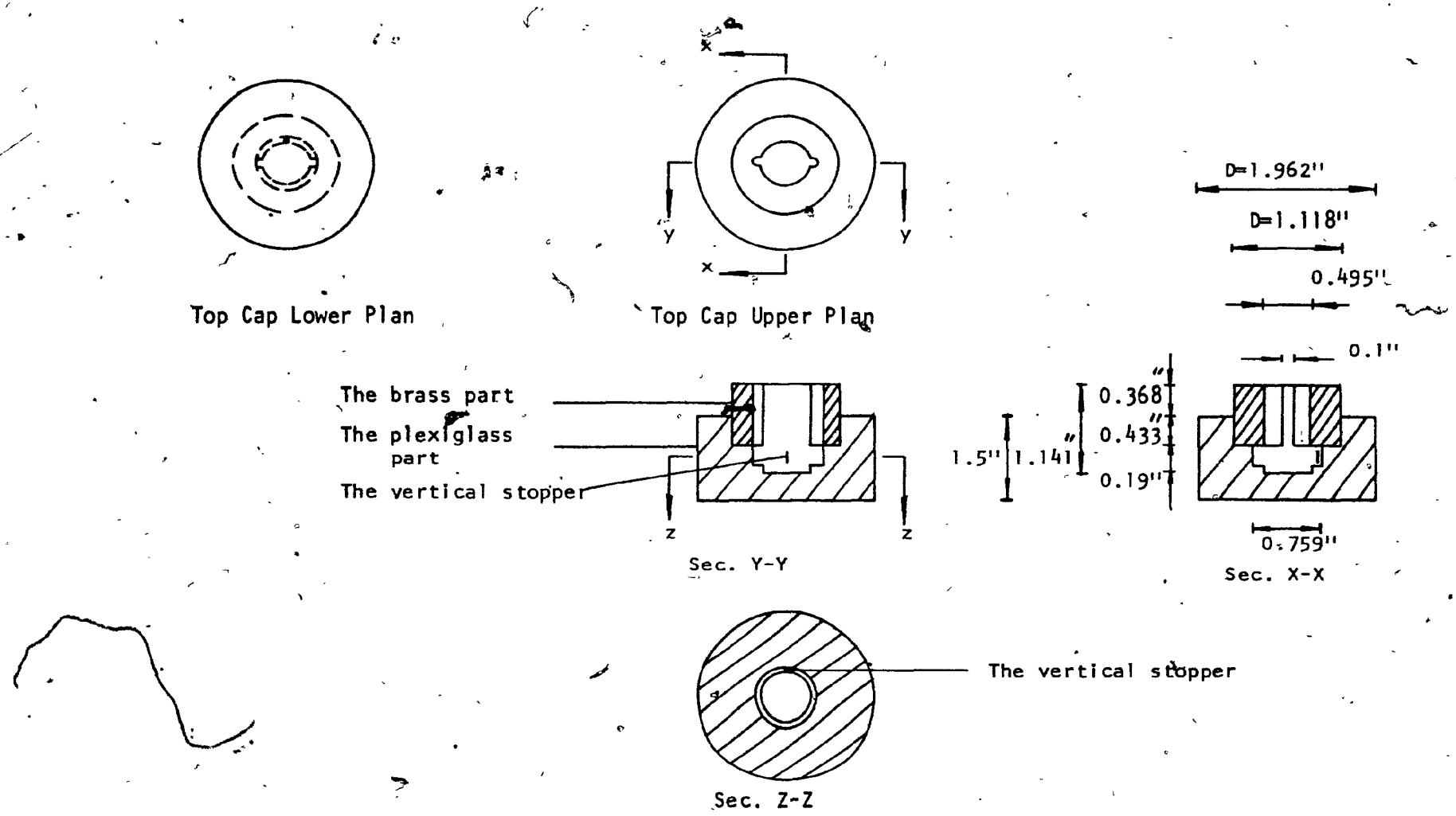

Fig. 2.2 The New Top Cap for the Triaxial Cyclic Loading Tests

After consolidation and before applying the cyclic loading, the triaxial cell is moved upward to insert the ram into the top cap again, until its lower part touches the sample (the horizontal mark is at the surface of the top cap) and the ram is rotated about 45^{o} - 90^{o} just before the ram's pin hits the vertical stopper, that is, the vertical mark on the ram is about 45^{o} - 90^{o} from the top cap hole as shown in Fig. 2.3. After this, the ram is locked into the top cap and will not leave the top cap and the sample during the extension cycle of the test. The test can now be started.

The ram travels a distance of 0.09 inches, which is equal to the play inside the top cap without applying any load on the sample (the deviator stress dial gauge reads zero). Hence there is no deformation in the sample at the end of each half cycle when the deviator stress changes from compression to extension, and from extension to compression, as shown in Fig. 2.4a. In view of this, the play is reduced from the displacement recorded on the displacement dial gauge and the corrected stress displacements are obtained as shown in Fig. 2.4b.

2.3 Sample Preparation

Samples of 2 inch diameter and 4 inch height were prepared for the tests. The material was mixed well to homogenize it before sampling. Every sample in the membrane inside the forming mould was consolidated by the external axial load for about two hours. A hanger weighing 4.27 lb. was put on the top cap on the sample for about one hour, then five pounds load was added to the hanger for another hour. During the external consolidation the sample was connected to the burrette to drain the water. At the end of two hours a negative pressure was applied on the sample by

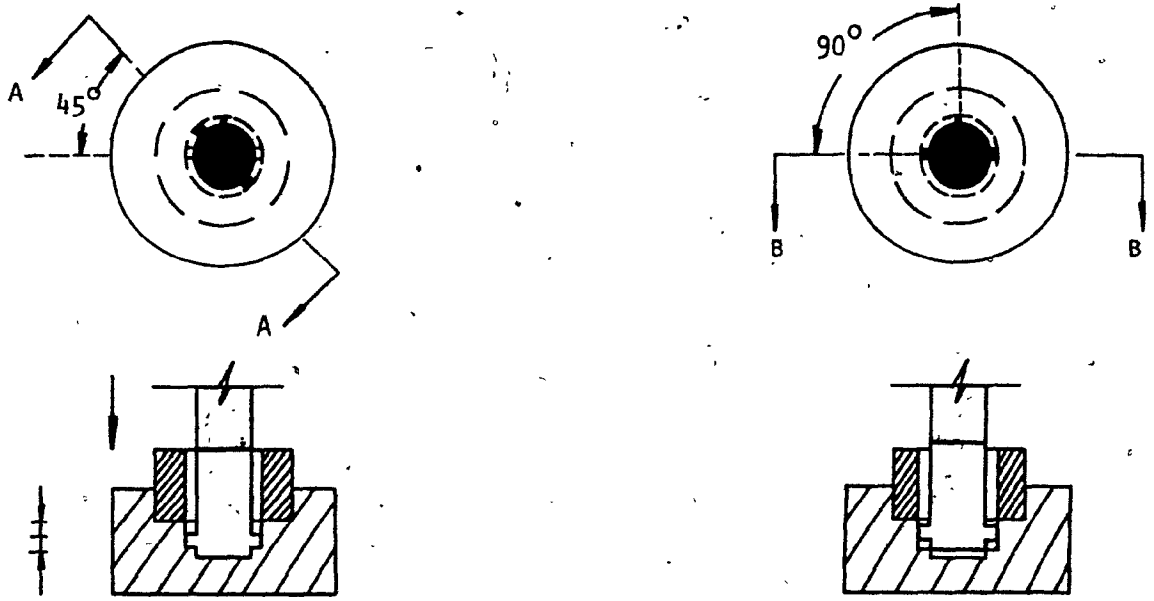

Fig. 2.3 The Ram Inside the Top Cap

A: During Testing:
(a) Compression
(b) Extension

B: Before Testing (During Consolidation)

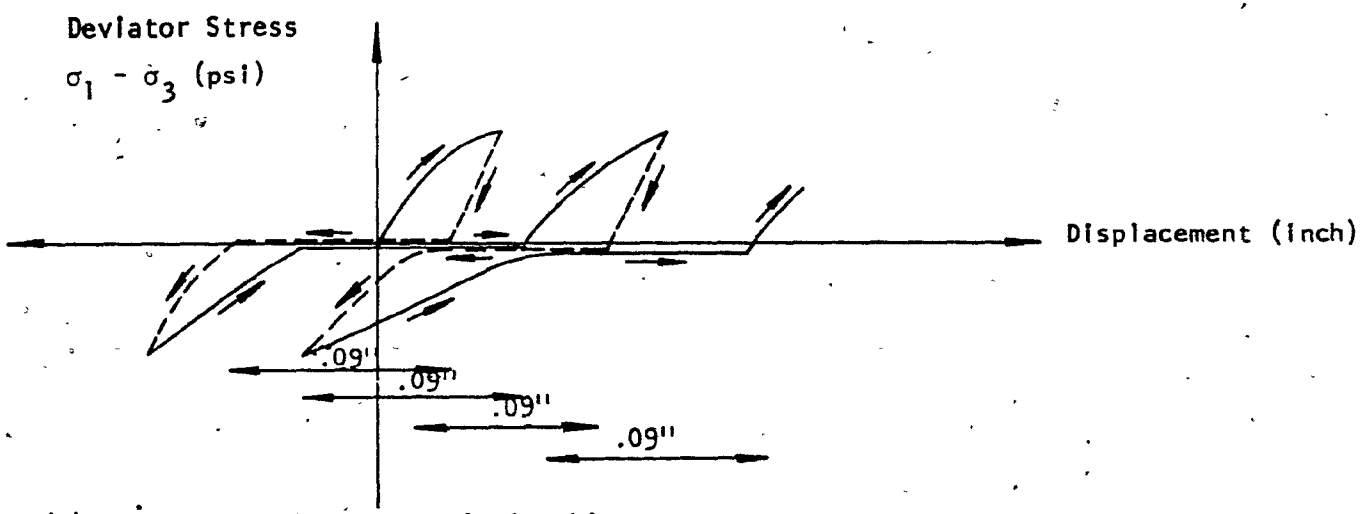

(a) Stress-Displacement Relationship

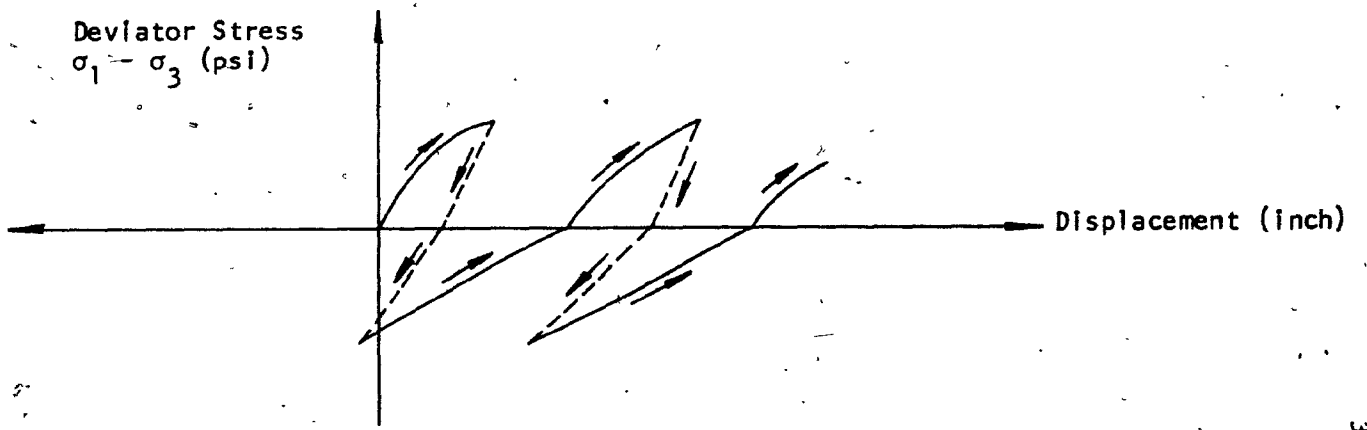

(b) Corrected Stress-Displacement Relationship

Fig. 2.4 Stress-Displacement Relationship During Cyclic Loading

lowering the burrette about 20 inches below the level of the sample middle height. The external consolidation and the negative pressure were applied to obtain firm samples, since the material in its initial condition is very soft. After so, the forming mould is taken out and the dimensions of the sample height and diameter are measured.

Then, the sample was consolidated under an all-round confining pressure of 5 lb per sq.in. for about 20 hours, which is approximatley equal to the confining pressure on the slime element in the field condition. The change in the volume of the sample during consolidation was measured and subtracted from the initial volume.

2.4 Description of Tests

Cyclic deviator stress of $\pm \Delta\sigma, \pm (\sigma_1 - \sigma_3)$, of constant amplitude was applied on the saturated sample. The cyclic stress did not exceed the confining pressure, σ_3 = 5 psi, so that the vertical stress, σ_1 was compressive at all times for all tests. The vertical displacement was measured by a dial gauge attached to the cell. The deviator stress load was measured by a dial gauge connected to the proving ring. The dial gauges were set to zero before testing. The pore water pressure during the undrained tests was measured by a Null Indicator and a manometer. The axial strain was calculated as the vertical displacement, divided by the sample height after consolidation. The deviator stress was calculated as the load read by the proving ring dial gauge, divided by the sample cross section area during the test: $A' = \pi r_o^2 \left[1 - \frac{1}{2} (\delta v - \delta\epsilon_1)\right]^2$, where r_o is the initial radius of the sample = 1 inch, δv = the change in the volumetric strain which is equal to zero for undrained tests, and $\delta\epsilon_1$ = the change in axial strain.

2.5 Behaviour of Slime Under Cyclic Stress Application

One sample was consolidated under 5 lb per sq in confining pressure. The water content after consolidation was about 58%. A cyclic deviator stress of ± 1.2 lb per sq in was applied by the strain controlled triaxial machine at a constant strain rate of 0.0008 inch/min, as shown in Fig. 2.5a. The resulting changes in axial strain, measured and corrected pore water pressure were measured and are shown in Fig. 2.5b,c,d.

It is noted that the sample showed gradually increasing deformation while pore water pressure built up gradually during the cycles. During the ninth cycle, the pore water pressure increased to a value equal to the applied confining pressure and the sample developed a larger strain than during the previous cycles. In fact, the soil had liquefied. The effective confining pressure was reduced to zero, as shown in the plot of effective stresses on the 45^{o} plane (effective stress path Fig. 2.5e) during the test.

2.6 Behaviour of Slime Under Quasi-Static Loading Following Liquefaction

The effect of cessation of cyclic loading and the application of a static load to a liquefied sample of slime is studied here. This simulates the case of applying a static shear stress on the liquefied slime layer after the earthquake ground motions cease. The shear stress can be caused, for example, by the own weight of the inclined slime layer.

The effect of quasi-static loading on a liquefied sample of slime is shown in Fig. 2.6(a,b,c,d). The sample was first caused to liquefy by the cyclic loading pattern shown in Fig. 2.5, and when the liquefaction started the cyclic loading was stopped. The pore water

Cyclic Stress = ± 1.2 lb per sq. in.

Confining Pressure, σ_3 = 5 lb per sq. in.

Water Content ≈ 58%

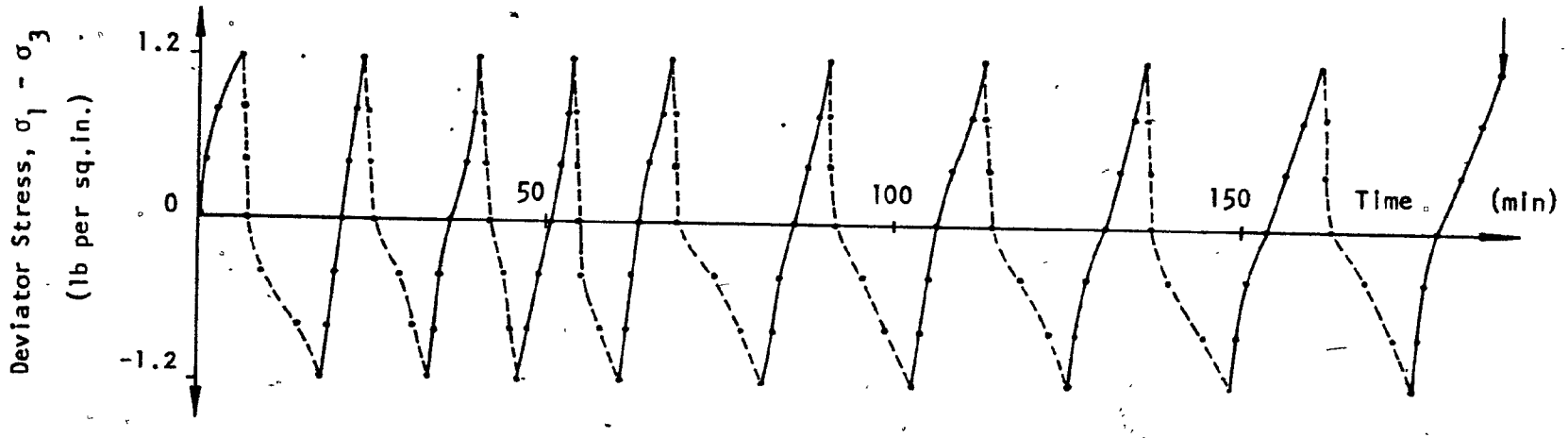

Fig. 2.5a Cyclic Loading Test

Deviator Stress vs. Time

Cyclic Stress = ± 1.2 lb per sq. in.

Confining Pressure, σ_3 = 5 lb per sq. in.

Water Content ≈ 58%

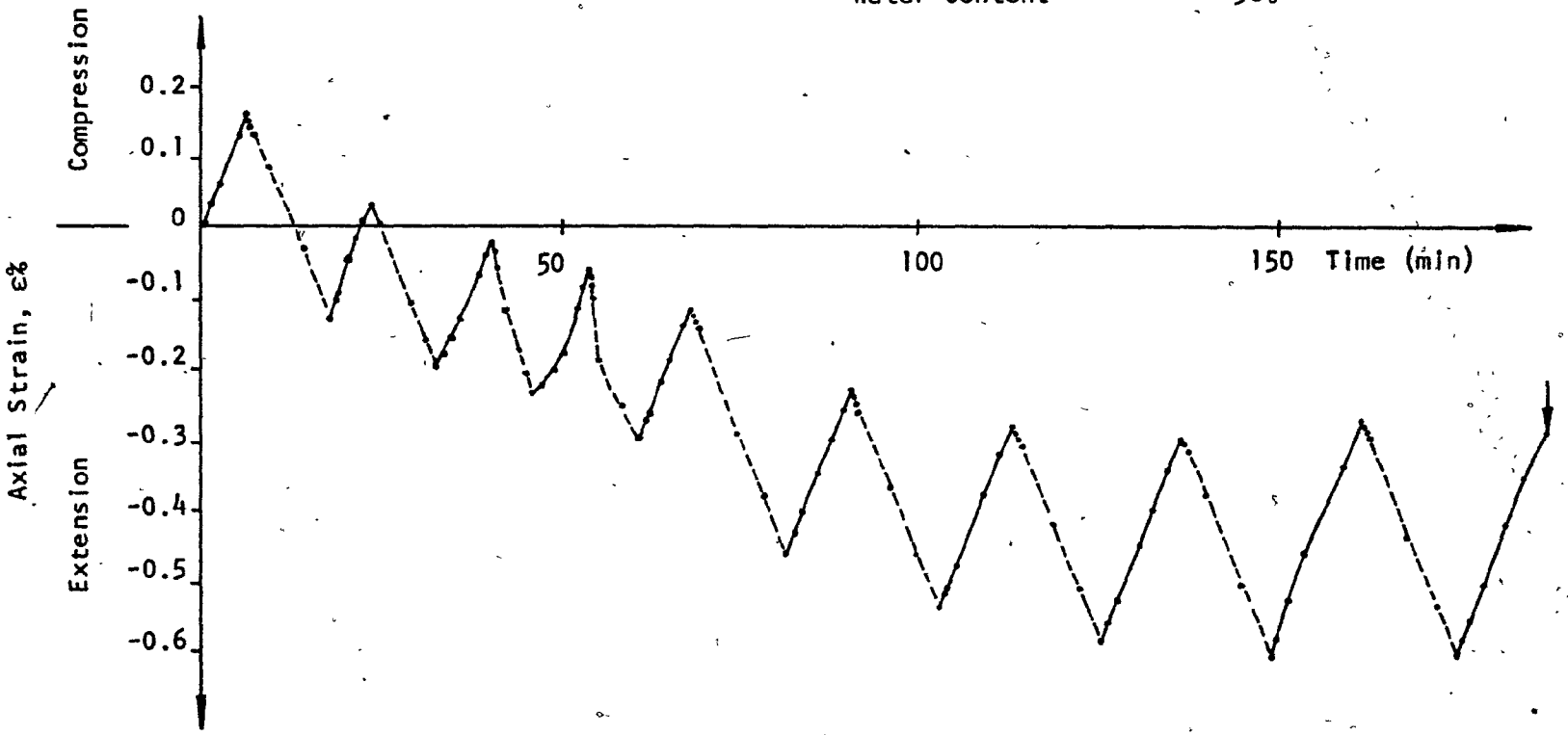

Fig. 2.5b Cyclic Loading Test

Axial Strain vs. Time

Cyclic Stress = ± 1.2 lb per sq. in.

Confining Pressure, σ_3 = 5 lb per sq. in.

Water Content ≈ 58%

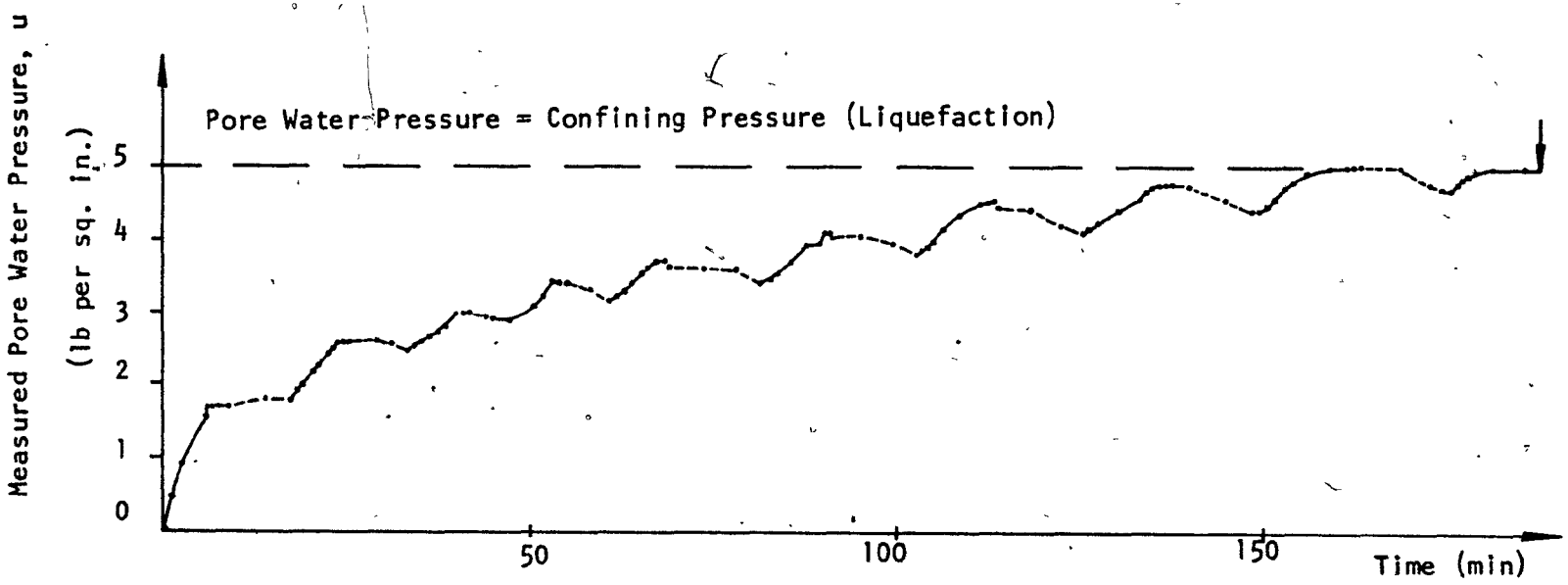

Fig. 2.5c Cyclic Loading Test

Measured Pore Water Pressure vs. Time

Cyclic Stress = ± 1.2 lb per sq.in.

Confining Pressure, σ_3 = 5 lb per sq.in.

Water Content ≃ 58%

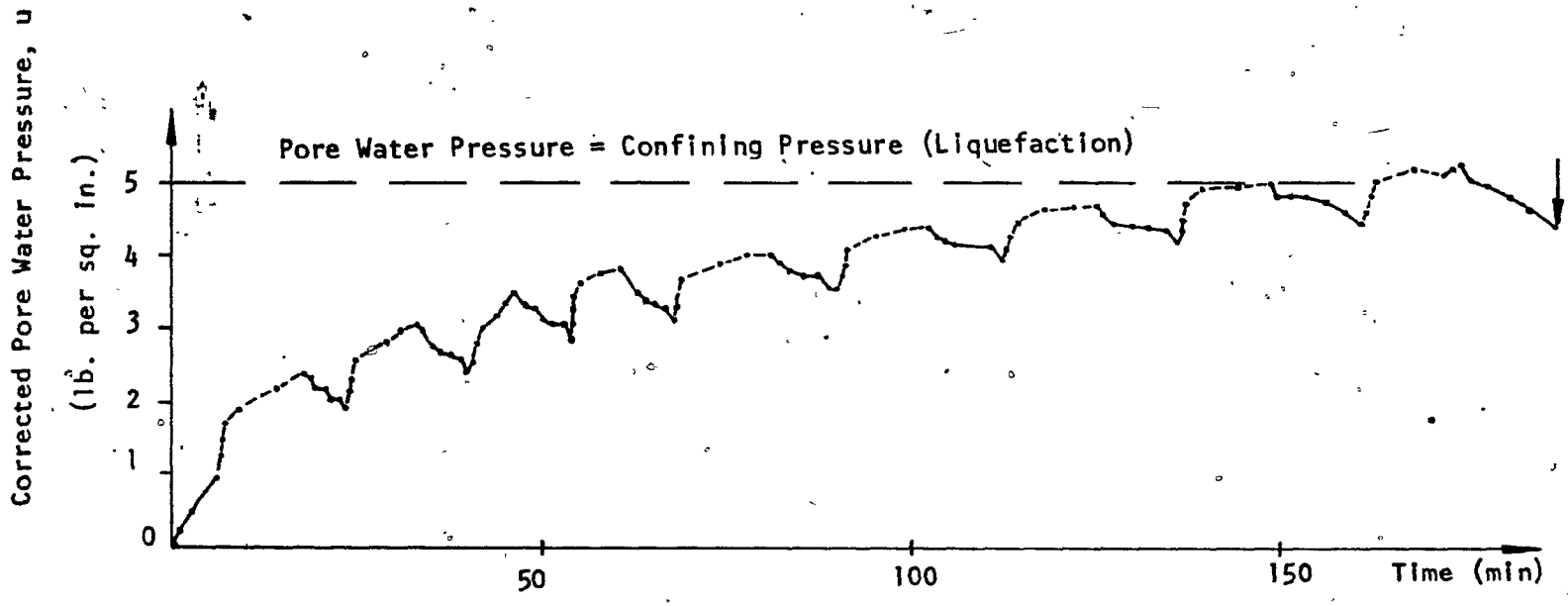

Fig. 2.5d Cyclic Loading Test

Corrected Pore Water Pressure vs. Time

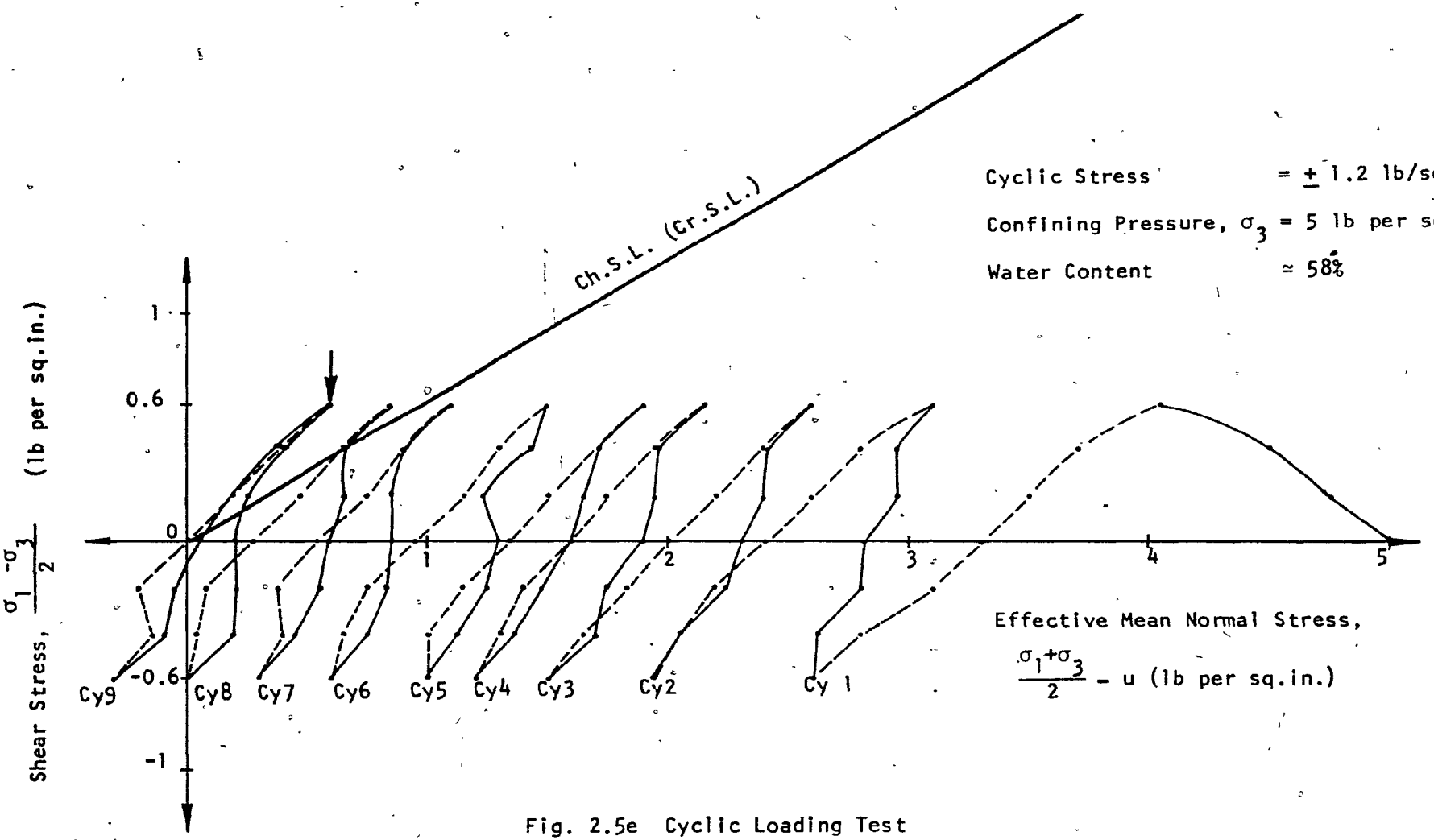

Fig. 2.5e Cyclic Loading Test

Effective Stress Path (Shear Stress vs Mean Normal Stress)

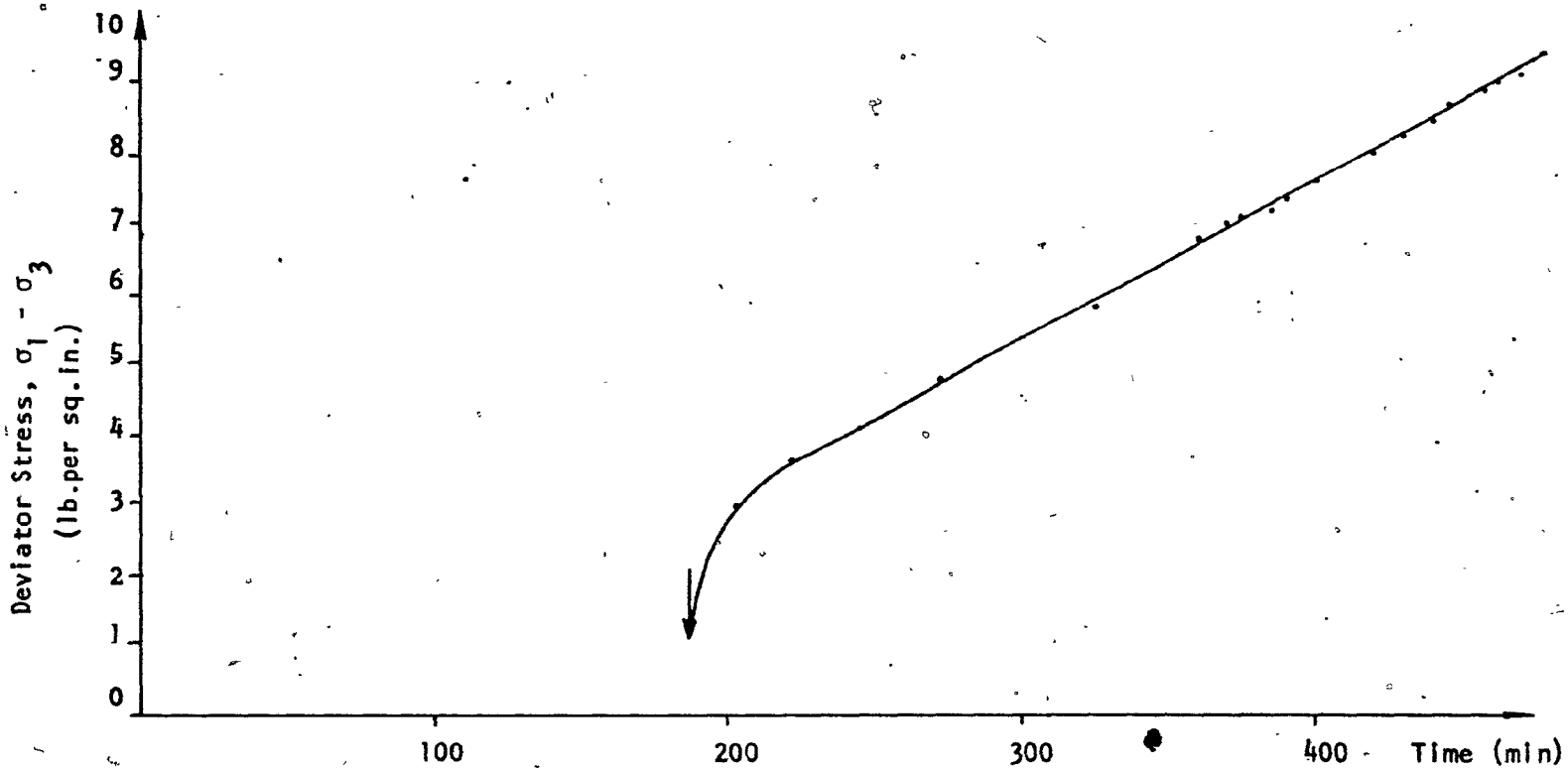

Fig. 2.6a Static Loading Following Liquefaction

Deviator Stress vs Time

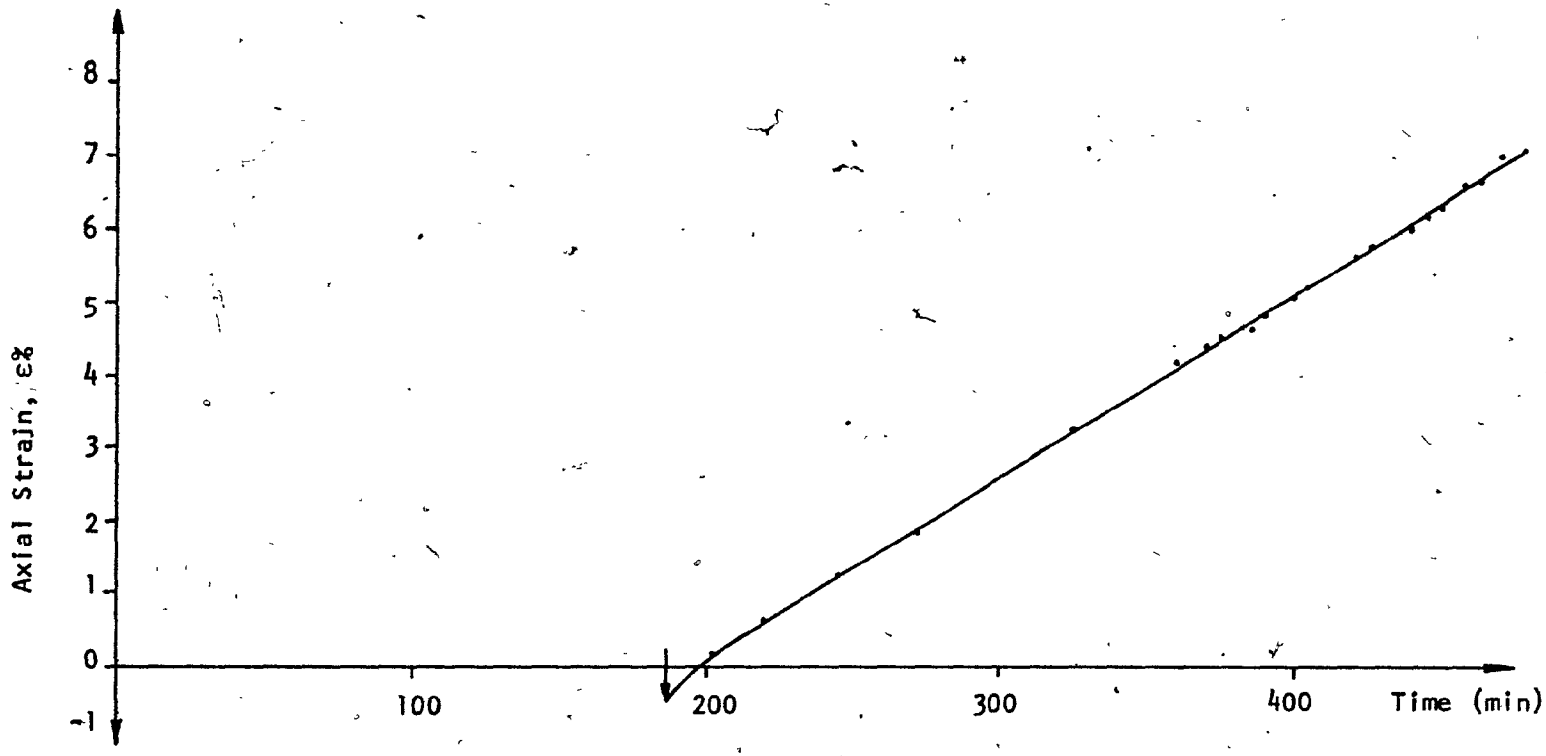

Fig. 2.6b Static Loading Following Liquefaction

Axial Strain vs Time

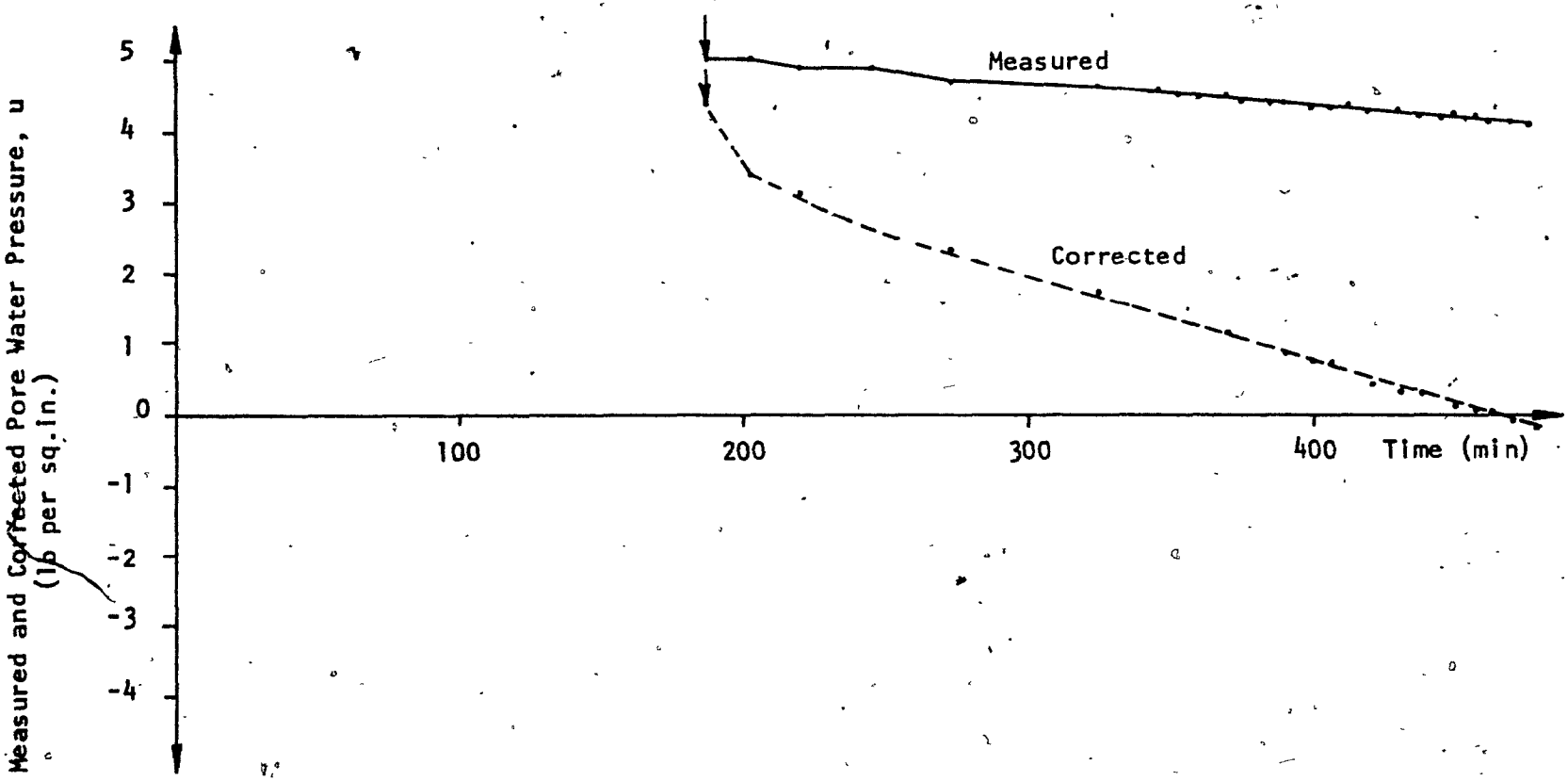

Fig. 2.6c Static Loading Following Liquefaction

Measured & Corrected Pore Water Pressure vs Time

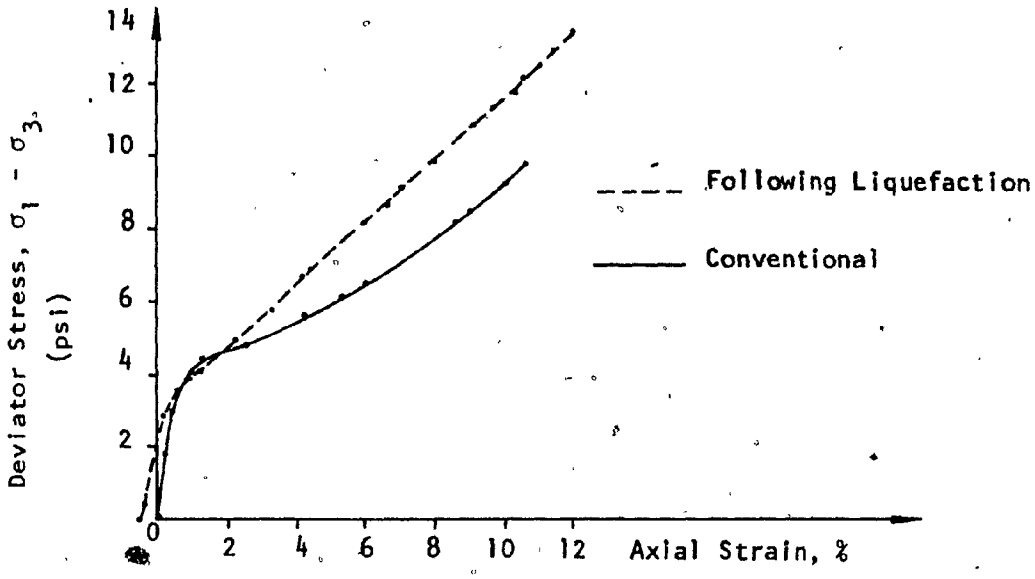

(a) Stress-Strain Relationships

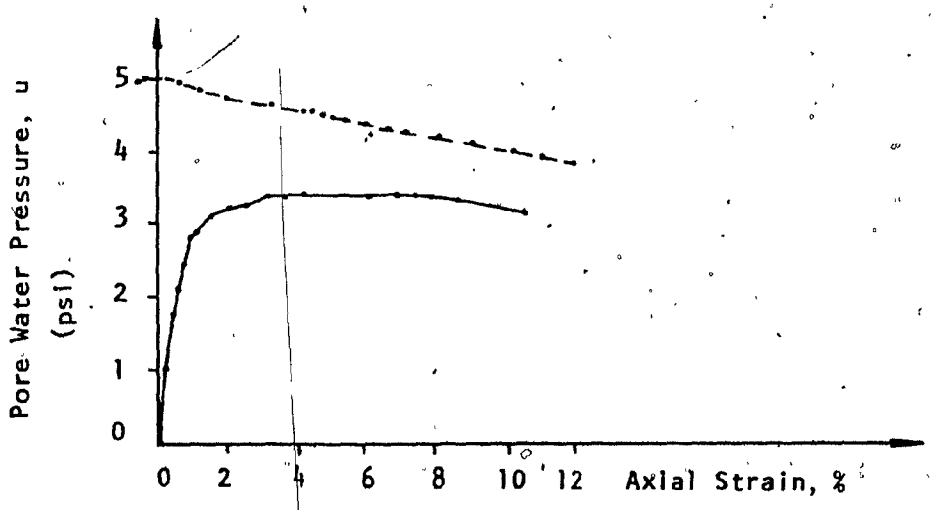

(b) Pore Water Pressure - Strain Relationships

Fig. 2.7 Comparison Between Static Loading Following Liquefaction and Conventional Static Loading

pressure in the sample was equal to the applied confining pressure. At this stage the sample was subjected to static loading applied at the same constant rate of strain, .0008 in/min. The pore water pressure started to decrease as shown in Fig. 2.6c, and the sample dilated, which caused an increase in the effective stress, as shown in Fig. 2.6d. The sample did not fail under the static loading following liquefaction even until it was deformed by a value of 13% of its original height, when the test was stopped. The angle of internal friction of the sample was 52.5°, calculated as $\sin^{-1} \frac{\sigma_1-\sigma_3}{2} / (\frac{\sigma_1+\sigma_3}{2} - u)$. This means that the soil possesses a high shear strength.

2.7 Comparison Between the Static Loading Following Liquefaction and the Conventional Static Loading

A sample with water content after consolidation similar to that of the previous test sample (Fig. 2.6), was consolidated under 5 psi confining pressure. The sample was subjected to monotonic static loading under the undrained condition at a strain rate of .0008 in/min.

The stress-strain, pore water pressure-strain relationship and the stress path for both tests are shown in Fig. 2.7 (a,b,c).

It is noted that the liquefied sample under static loading has a higher shear strength than the one subjected to conventional static loading not following cyclic loading. The angle of internal fraction ϕ, for the first sample is 59.2°, at 10.5% axial strain, and it is equal to 46.5° at the same axial strain for the second test.

This result is contrary to the result observed by Castro and Christian (1976). Castro and Christian stated that the static undrained shear strength of the sample subjected to static loading following cyclic loading is equal or very close to the static undrained shear strength for

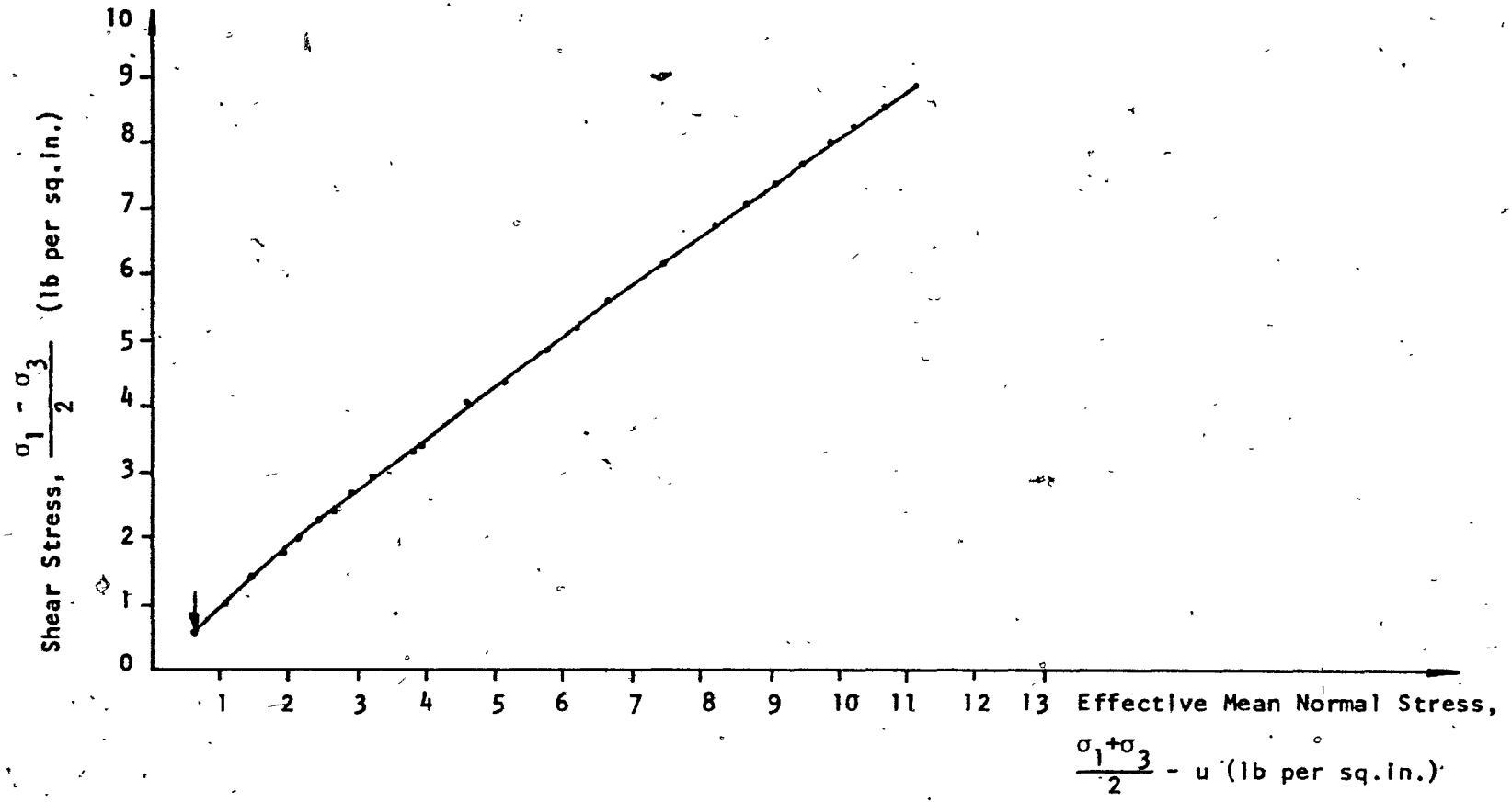

Fig. 2.6d Static Loading Following Liquefaction

Effective Stress Path (Shear Stress vs Mean Normal Stress)

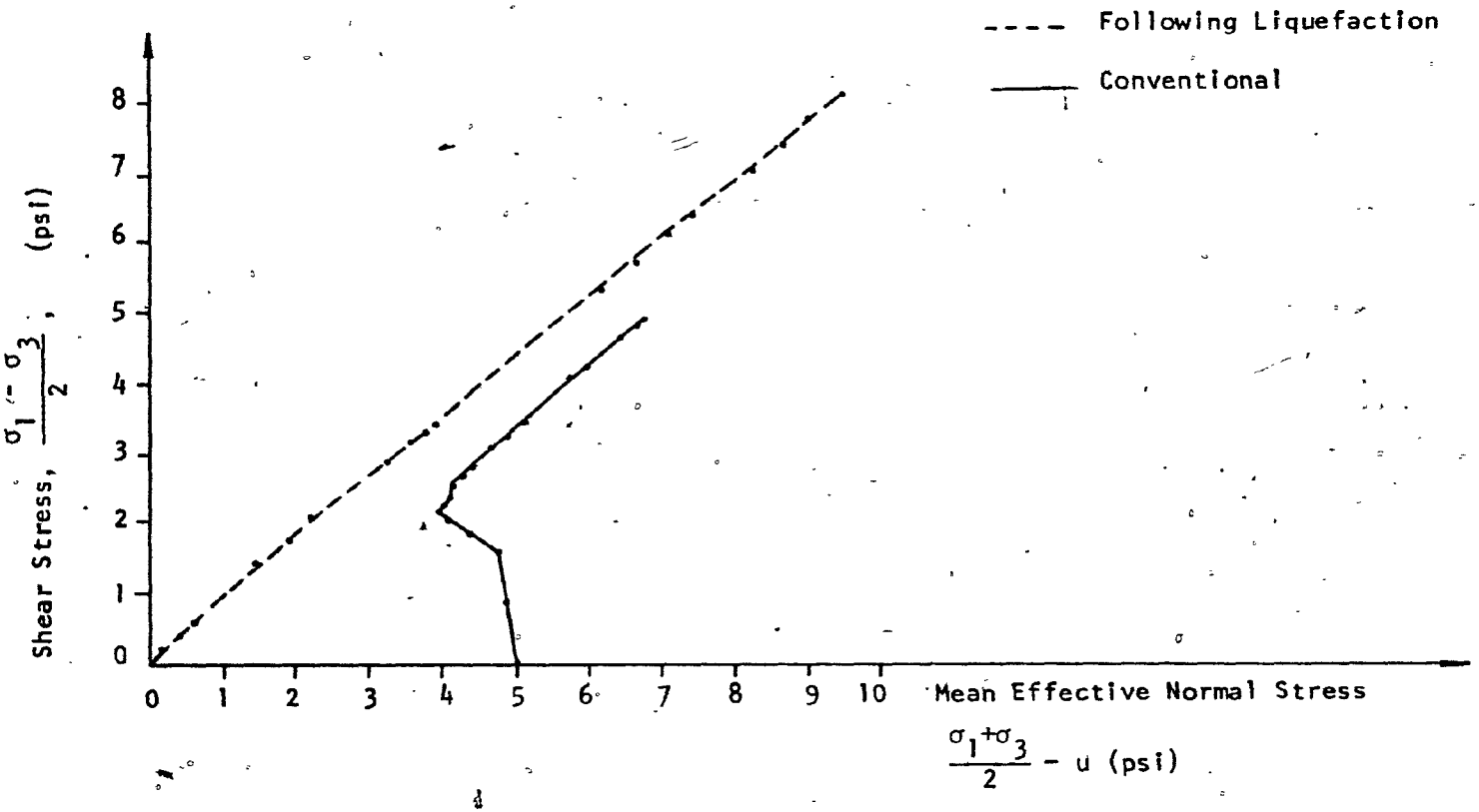

(c) Effective Stress Path

Fig. 2.7 Comparison Between Static Loading Following Liquefaction and Conventional Static Loading

samples that fail without initial cyclic loading. It appears that in the test carried out in the course of this investigation the cyclic loading has rearranged the particles in such a manner as to produce a higher shear strength. This may be due to the fact that the conventional undrained test described previously was only strained to an axial strain of 10.5%. Above this level of straining the results were felt not to be accurate enough in view of the inhomogenuity induced in the sample.

2.8 Influence of Water Content on Liquefaction

A major factor in developing liquefaction in a saturated soil is its water content. To study the effect of this factor, a sample was prepared the same way as mentioned before, and consolidated in the moulding form for 3 hours. The sample was initially consolidated under a confining pressure, σ_3, of 5 lb per sq in. The water content after consolidation was 41%, which is less than that of the first sample, Fig. 2.5, by 17%. The sample was subjected to cyclic stress application of the same magnitude as in the first test, $\pm$ 1.2 lb per sq in as shown in Fig. 2.8a. The resulting axial strain and measured and corrected pore water pressure were measured, as shown in Fig. 2.8b, c, d. The effective stress path is shown in Fig. 2.8e.

It was noted that the pore water pressure increases gradually but at a lower rate than in the first test, with high water content. So, the effective stress decreased gradually during the cycles, as shown in Fig. 2.8e. The sample gradually lost its shear strength, and hence its resistance to deformation, so that the axial strain increased cycle by cycle as shown in Fig. 2.8b. The pore water pressure did not increase to the value of the

Cyclic Stress = ± 1.2 lb per sq.in.

Confining Pressure, σ_3 = 5 lb per sq. in.

Water Content ≈ 41%

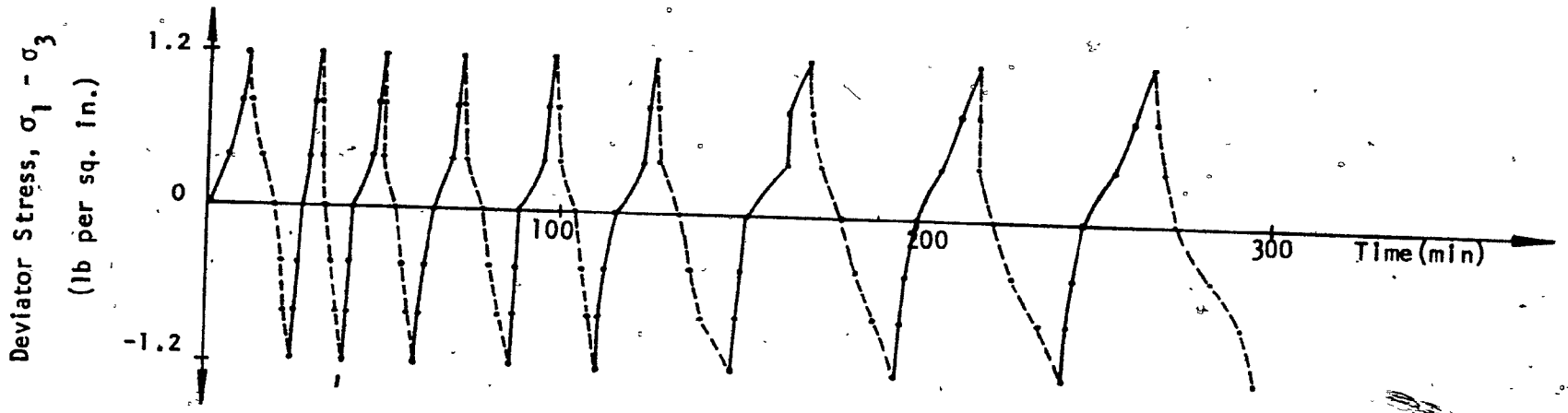

Fig. 2.8a Cyclic Loading Test
Deviator Stress vs Time

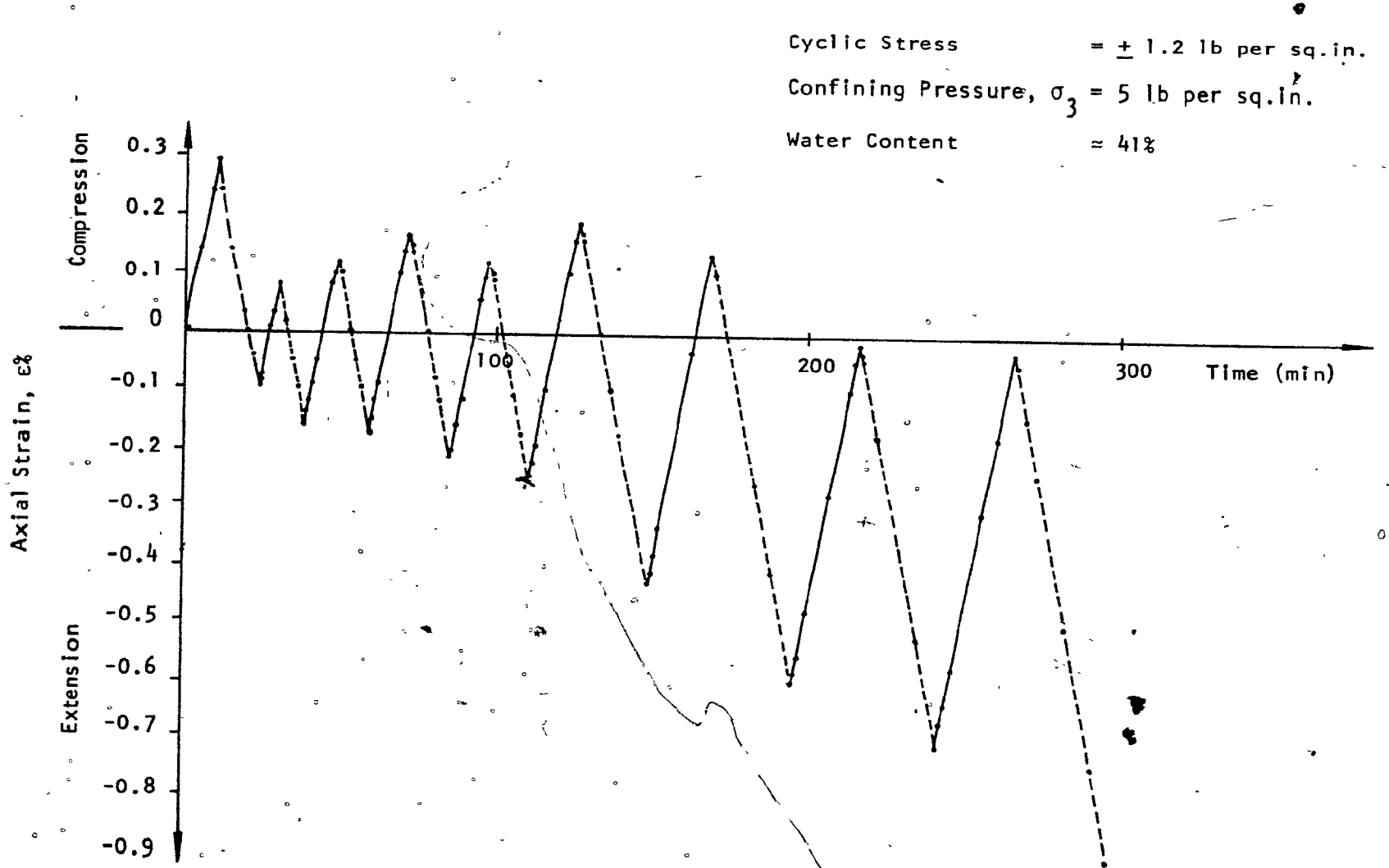

Fig. 2.8b Cyclic Loading Test
Axial Strain vs Time

Cyclic Stress = ± 1.2 lb per sq.in.

Confining Pressure, σ_3 = 5 lb per sq.in.

Water Content ≃ 41%

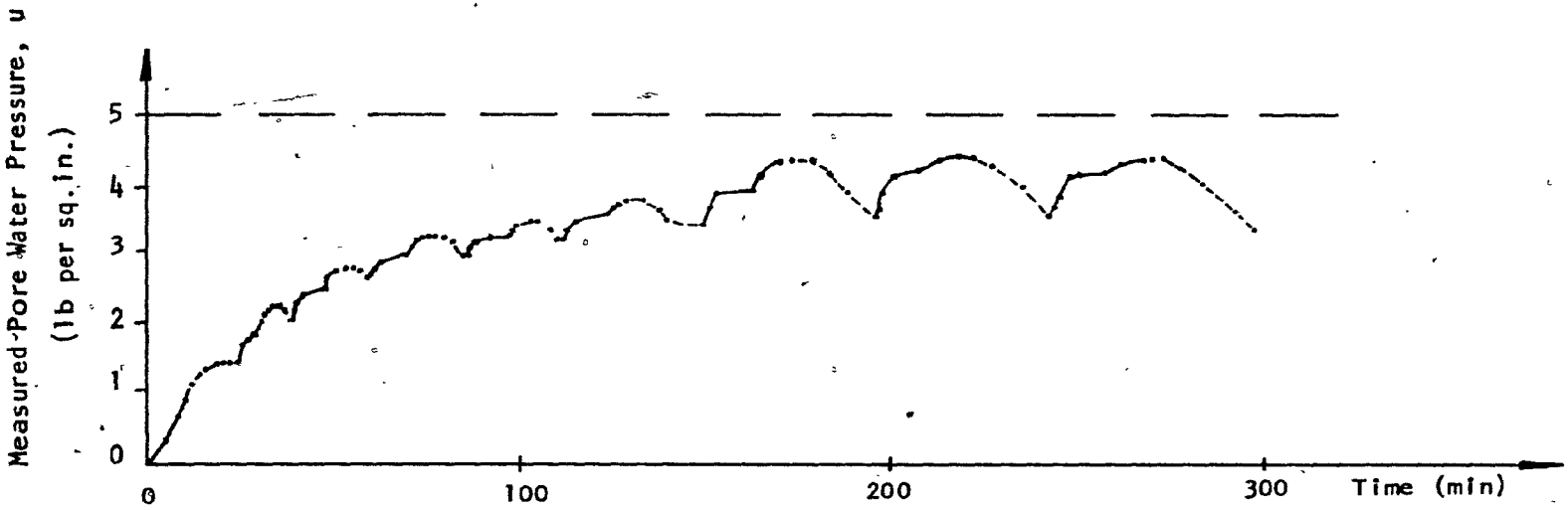

Fig. 2.8c Cyclic Loading Test
Measured Pore Water Pressure vs Time

Cyclic Stress = ± 1.2 lb per sq.in.

Confining Pressure, σ_3 = 5 lb per sq.in.

Water Content = 41%

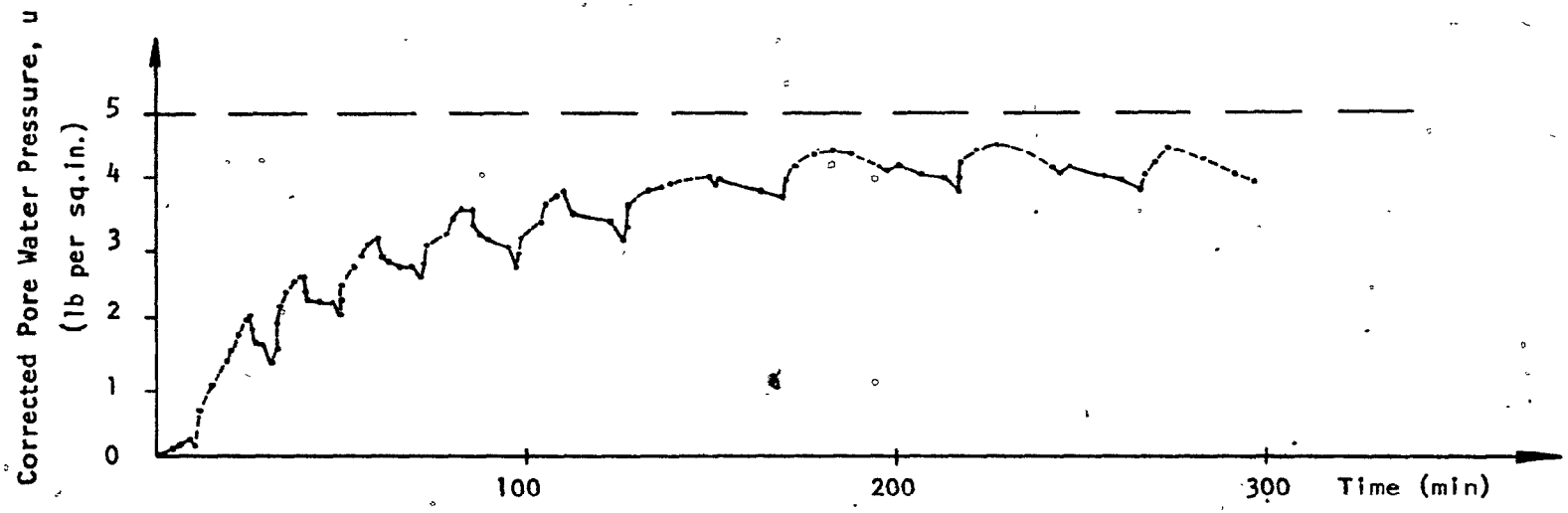

Fig. 2.8d Cyclic Loading Test

Corrected Pore Water Pressure vs Time

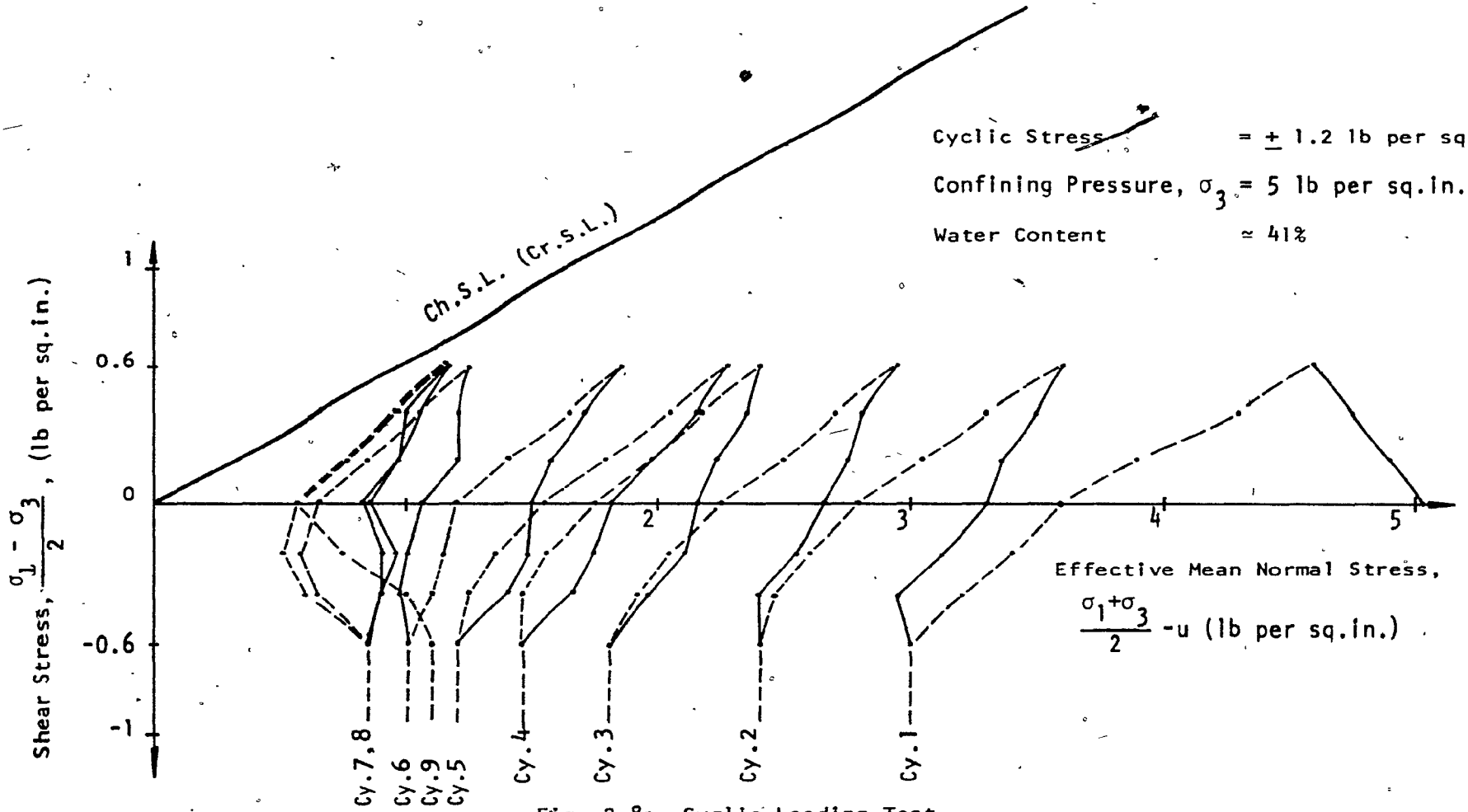

Fig. 2.8e Cyclic Loading Test

Effective Stress Path (Shear Stress vs Mean Normal Stress)

confining pressure at the ninth cycle as in the first test. Thus, the case of zero effective stress had not been reached, and the sample had not liquefied.

It can be concluded from this test that the lower the water content of the sample the greater the number of cycles required to cause liquefaction. This result confirms the previous finding that the slime of low water content may not be liquefied during an earthquake of a certain intensity and duration but the soil of high water content may be liquefied easily under the same conditions.

2.9 Influence of Cyclic Stress Level on Liquefaction

Another factor which influences the development of liquefaction in saturated slime is the cyclic stress level to which the slime is subjected. To study this factor's effect, a sample was prepared the same way as mentioned before and was found to have the same water content after consolidation as in the first test, Fig. 2.5. The sample was consolidated under the same confining pressure of 5 lb per sq in, and the water content after consolidation was 60.5%, which differs only 2.5% from the water content of the first sample. Cyclic stress of $\pm$ 4 lb per sq in was applied to the sample, as shown in Fig. 2.9a. The resulting axial strain, and measured and corrected pore water pressure, were as shown in Fig. 2.9b,c, d. The effective stress path is shown in Fig. 2.9e.

It was noted that the pore water increases only during the first loading cycle. It started decreasing during the second loading cycle and continued decreasing during the third one. This means that because of the high cyclic stress application on the sample, the pore water pressure started to dissipate and the sample started to dilate during the application of

Cyclic Stress = ± 4 lb per sq.in.

Confining Pressure, σ_3 = 5 lb per sq.in.

Water Content ≈ 60.5%

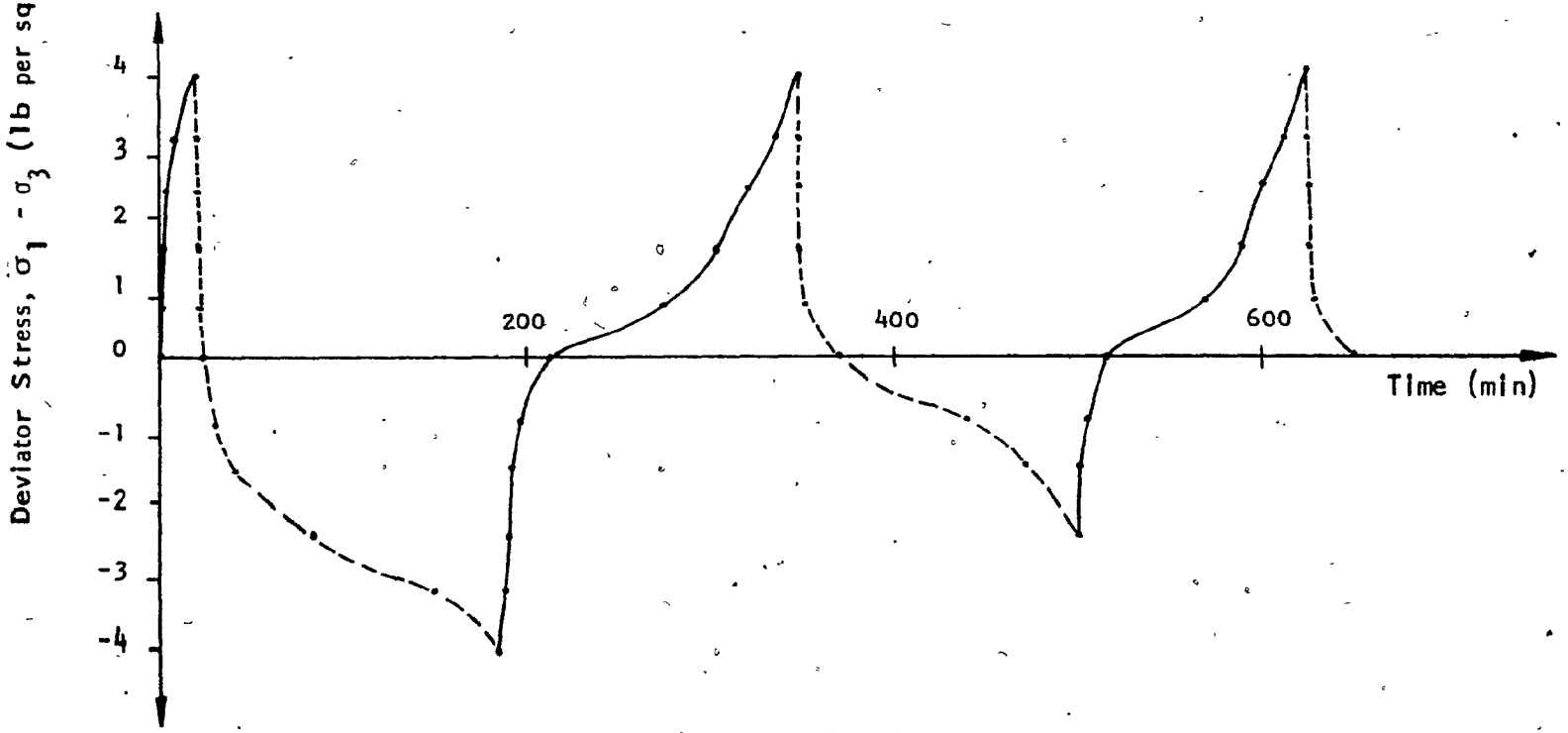

Fig. 2.9a Cyclic Loading Test

Deviator Stress vs Time

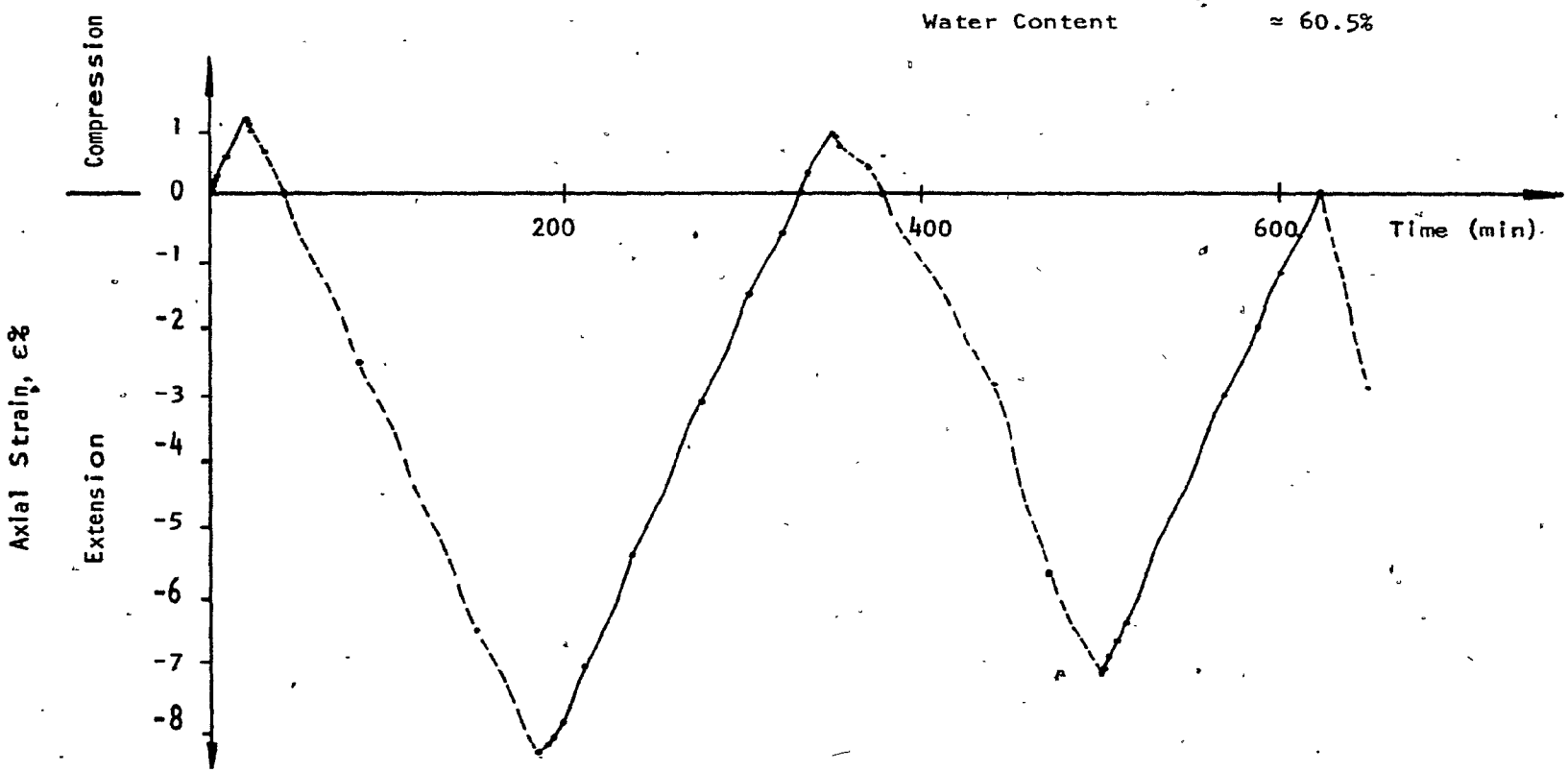

Fig. 2.9b Cyclic Loading Test
Axial Strain vs Time

Cyclic Stress = ± 4 lb per sq.in.

Confining Pressure, σ_3 = 5 lb per sq.in.

Water Content ≈ 60.5%

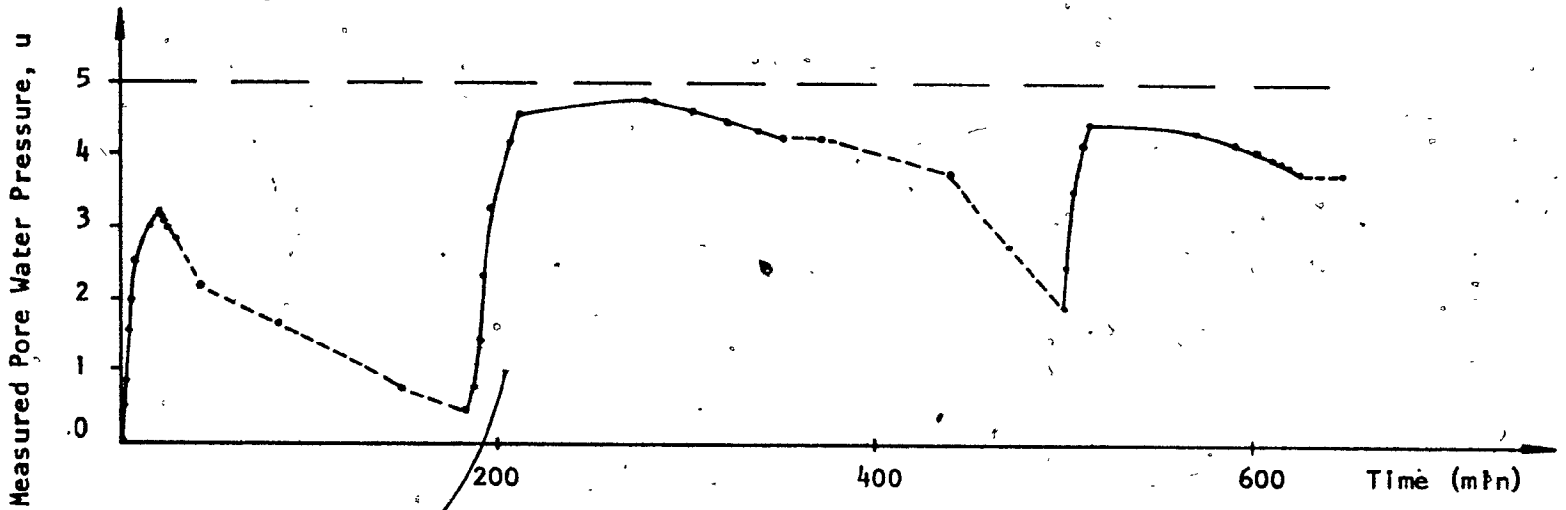

Fig. 2.9c Cyclic Loading Test
Measured Pore Water Pressure vs Time

Cyclic Stress = ± 4 lb per sq.in.

Confining Pressure, σ_3 = 5 lb per sq.in.

Water Content = 60.5%

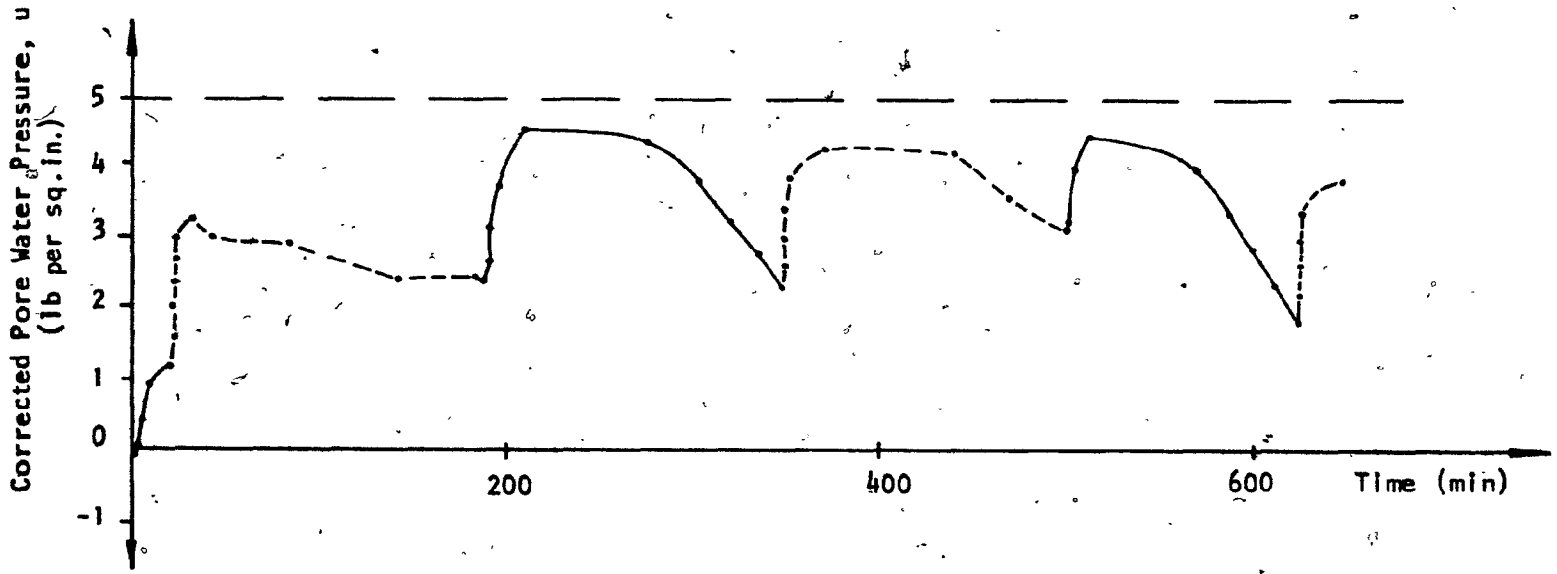

Fig. 2.9d Cyclic Loading Test
Corrected Pore Water Pressure vs Time

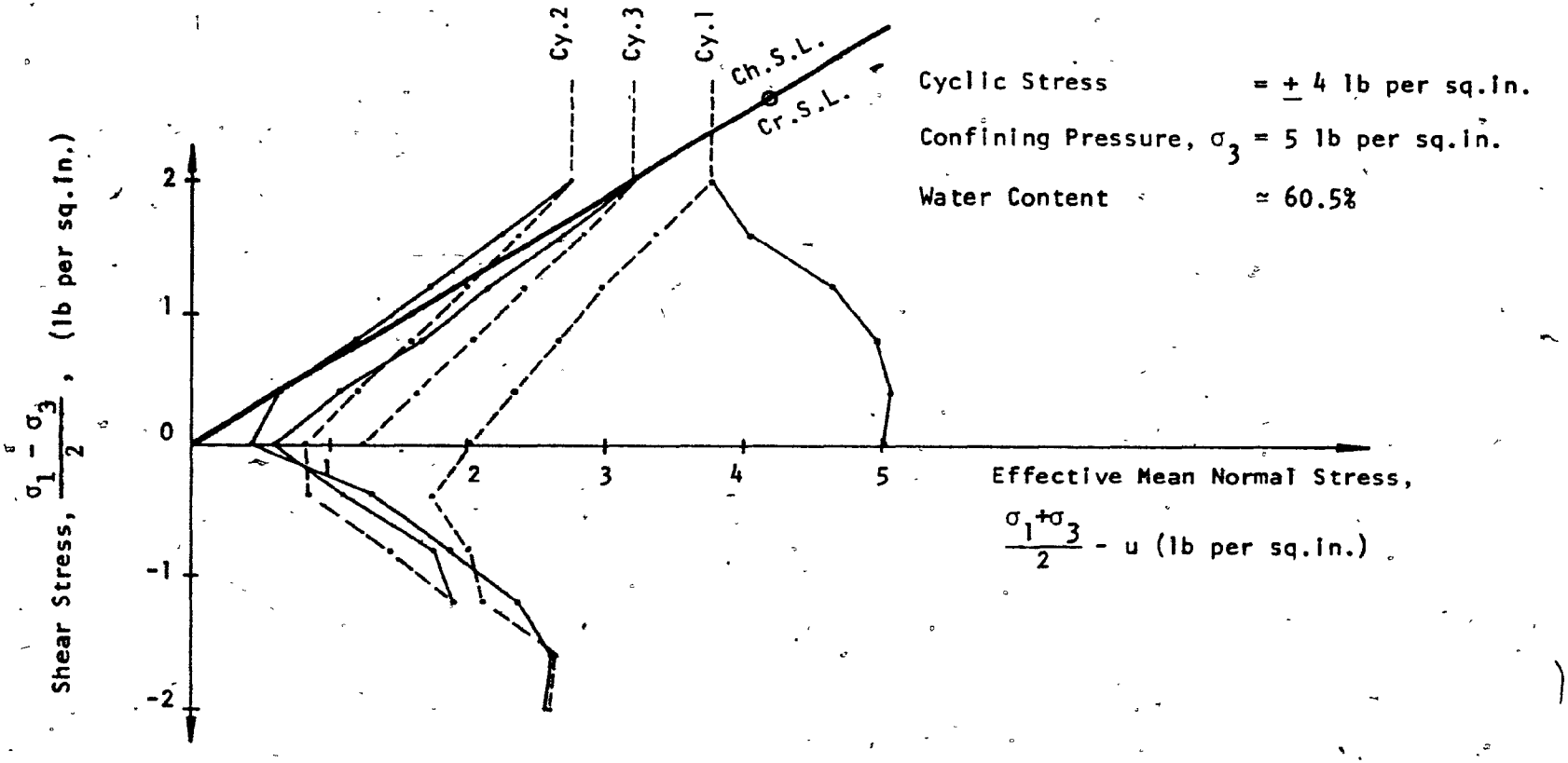

Fig. 2.9e Cyclic Loading Test

Effective Stress Path (Shear Stress vs Mean Normal Stress)

the cyclic loading before the pore water pressure reached the value of the confining pressure (zero effective stress). Thus, the sample lost only part of its shear strength during the first cycle, but started regaining that loss during the second cycle. In other words, the dissipation of the pore water pressure during cyclic loading means that it will not increase again and hence the sample will not be liquefied.

This test implies that a sample of certain water content under certain confining pressure is more likely to become liquefied under low cyclic stress as in test Fig. 2.5, than a sample of the same water content and under the same confining pressure, subjected to high cyclic stress.

2.10 Influence of Water Content and Cyclic Stress Level Combined on Liquefaction

To study the effect of water content and cyclic stress combined on liquefaction, a test was performed on a sample of water content of 49% after consolidation, under 5 lb per sq in confining pressure. The sample was subjected to cyclic stress of $\pm$ 2.4 lb per sq in, as shown in Fig. 2.10a. The water content of the sample is less than that of the first sample, Fig. 2.5, by 9% and the cylic stress is higher by $\pm$ 1.2 lb per sq in. The resulting strain, pore water pressure, and the effective stress path are shown in Fig. 2.10b,c,d,e.

During this test, the pore water pressure increased during the first, second and third loading cycles, but it started to dissipate during the fourth and the fifth cycles. The pore water pressure did not increase to the value of the confining pressure, so the sample had not liquefied. The sample lost shear strength during the first, second, and third cycles because of the increase in the pore water pressure and the resulting decrease in the effective stress during these cycles, as shown in Fig. 2.10e. But

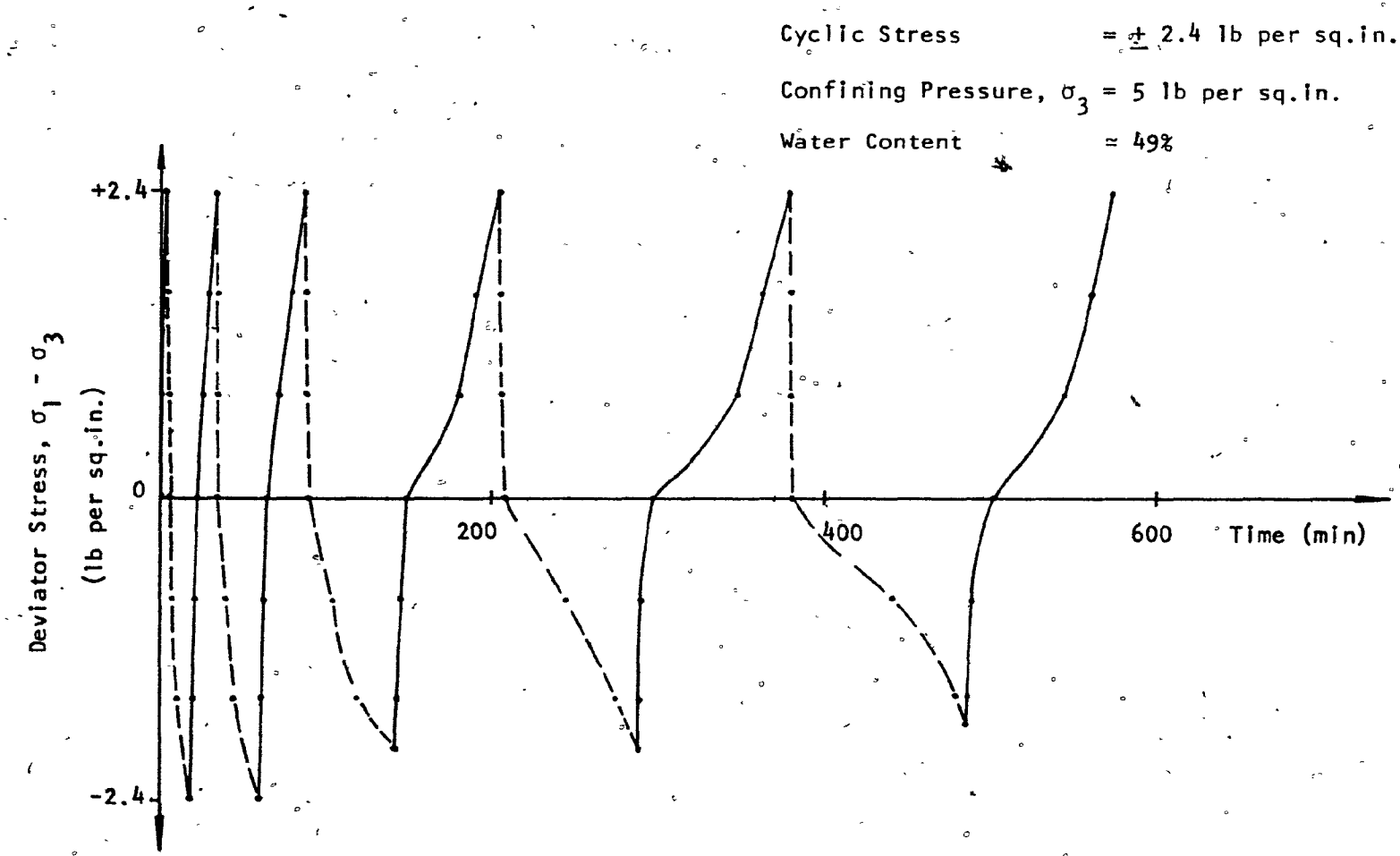

Fig. 2.10a Cyclic Loading Test
Deviator Stress vs Time

Cyclic Stress = ± 2.4 lb per sq.in.

Confining Pressure, σ_3 = 5 lb per sq.in.

Water Content ≈ 49%

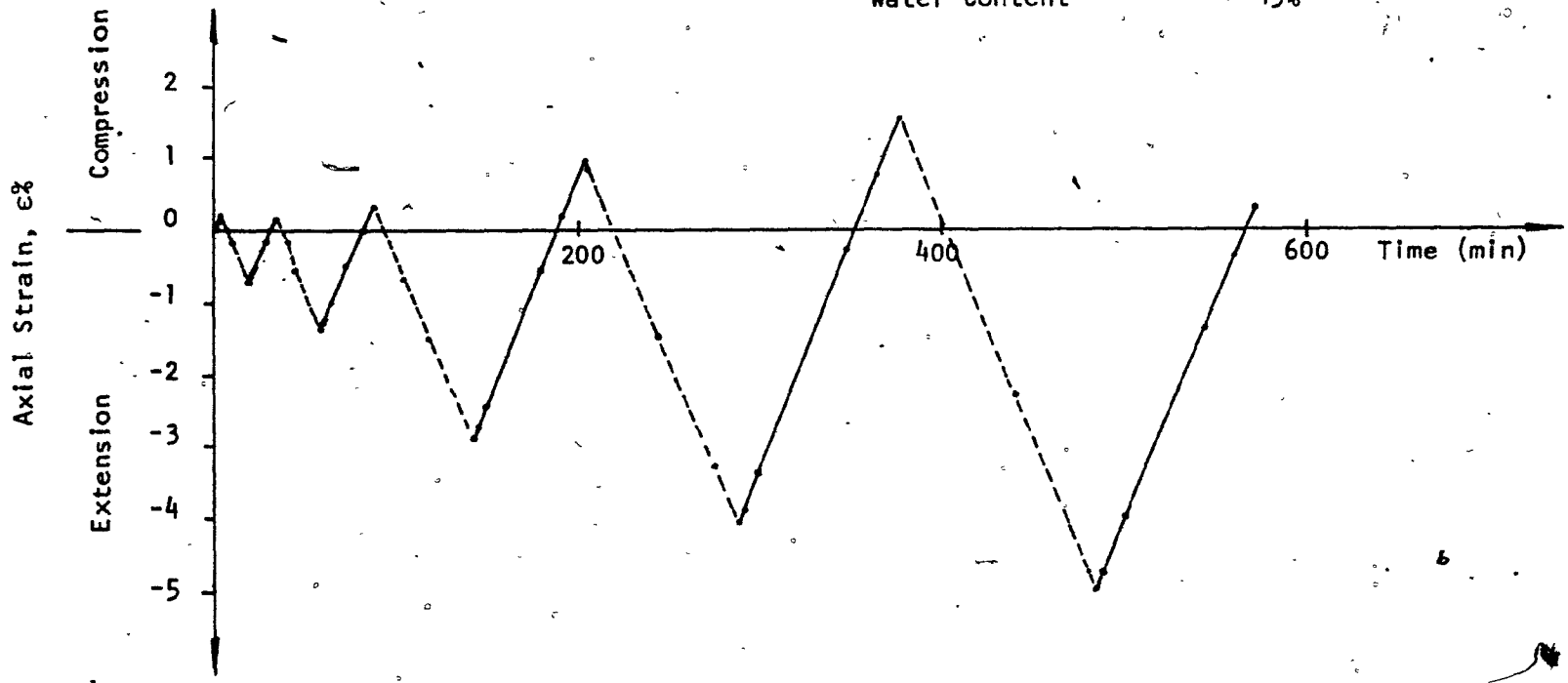

Fig. 2.10b Cyclic Loading Test
Axial Strain vs. Time

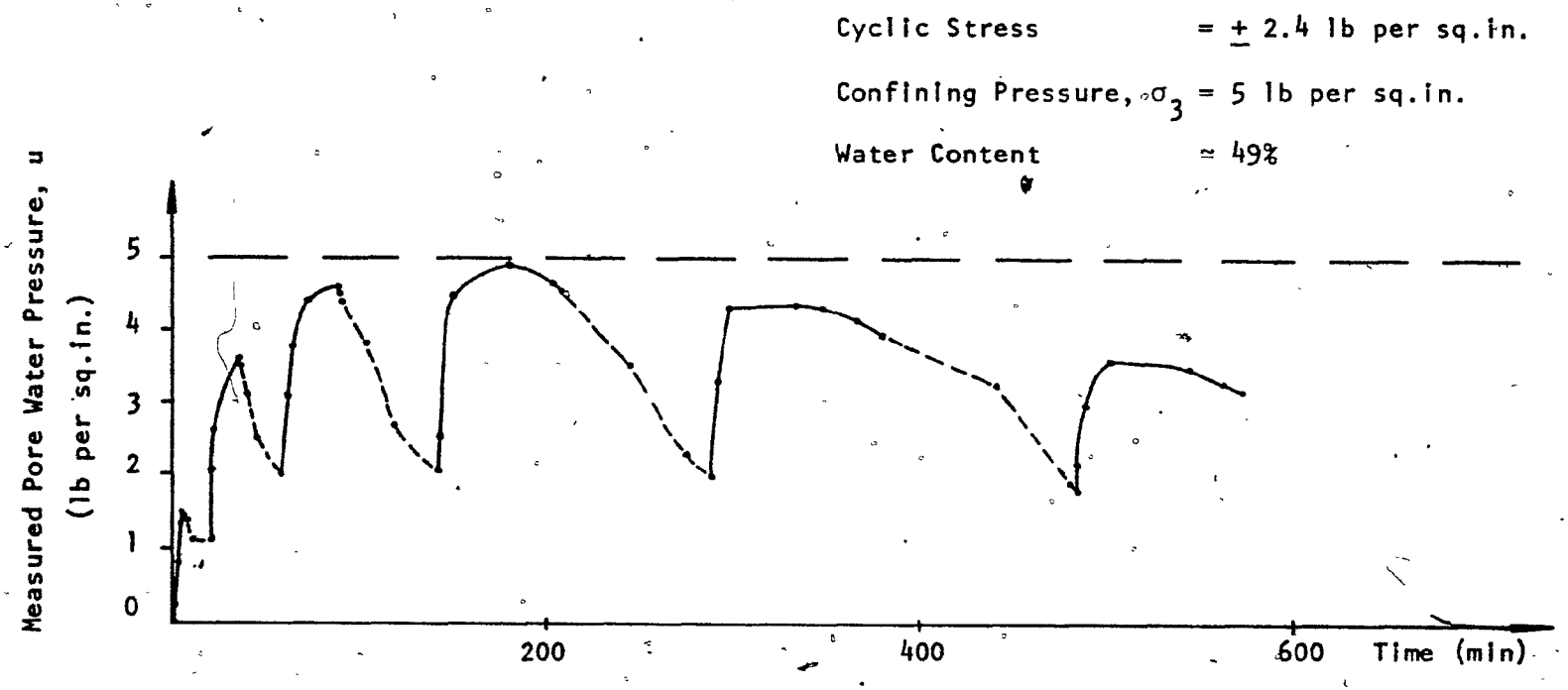

Fig. 2.10c Cyclic Loading Test
Measured Pore Water Pressure vs Time

Cyclic Stress = ± 2.4 lb per sq.in.

Confining Pressure, σ_3 = 5 lb per sq.in.

Water Content ≈ 49%

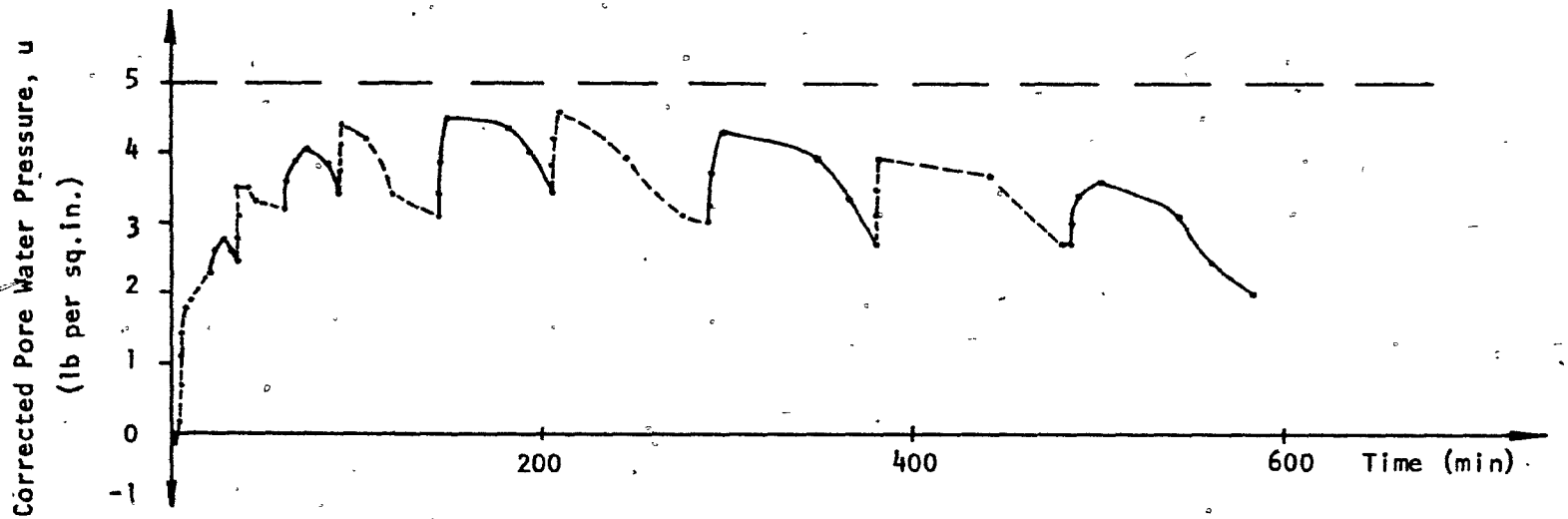

Fig. 2.10d Cyclic Loading Test
Corrected Pore Water Pressure vs Time

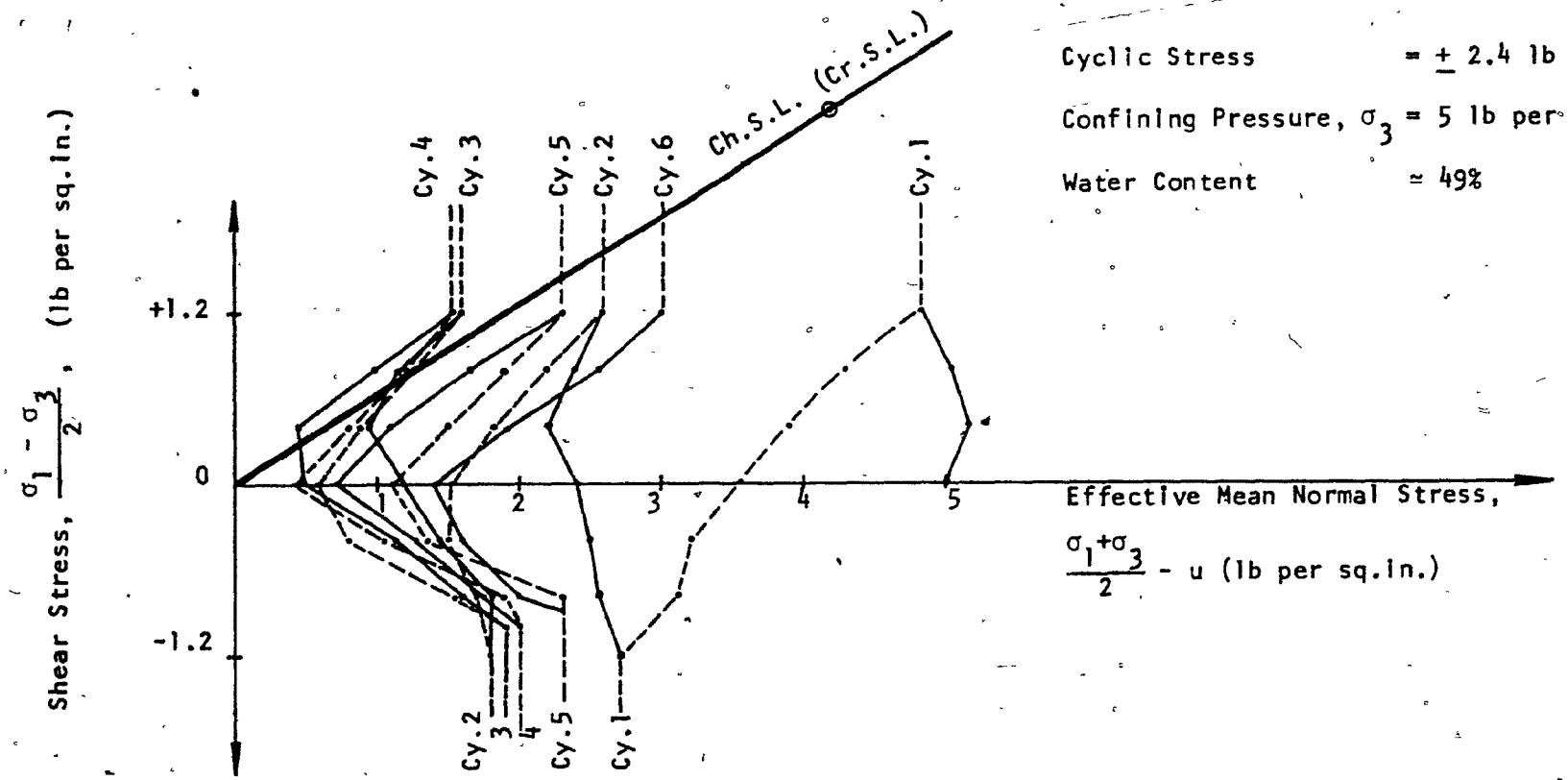

Fig. 2.10e Cyclic Loading Test

Effective Stress Path (Shear Stress vs Normal Stress)

the sample regained shear strength during the fourth cycle because of the decrease in the pore water pressure and the resulting increase in the effective stress.

It is therefore concluded that the slime of high water content (58%) under low cyclic shear stress (± 0.6 lb per sq in) (Fig. 2.5) is more likely to become liquefied than that of lower water content (49%) under higher cyclic shear stress (± 1.2 lb per sq in) (Fig. 2.10).

The results of the tests showing the effects of the water content of the sample and the level of the cyclic stress it is subjected to are shown in Fig. 2.11.

2.11 Stress-Strain Relationships During Cyclic Loading

A typical stress-strain relationship during cyclic loading is shown in Fig. 2.12a, for example for a sample of 49% water content under cyclic stress of ± 2.4 lb per sq in. It is observed that the strain increases cycle by cycle due to the loss of the shear strength of the sample and hence the loss of its resistance to deformation during cyclic loading application, as shown in Fig. 2.12b.

2.12 Comparison Between Cyclic Stresses Causing Liquefaction and Static Loading Causing Failure

It is noted that the cyclic deviator stresses required to induce liquefaction or failure are, in general, substantially lower than stresses required to cause failure under static loading conditions.

Fig. 2.13 presents a comparison of strengths for samples having an initial water content after consoidation ≈ 58%, and tested at the same confining pressures 5 psi, and at the same strain rate, .0008 in/min, as

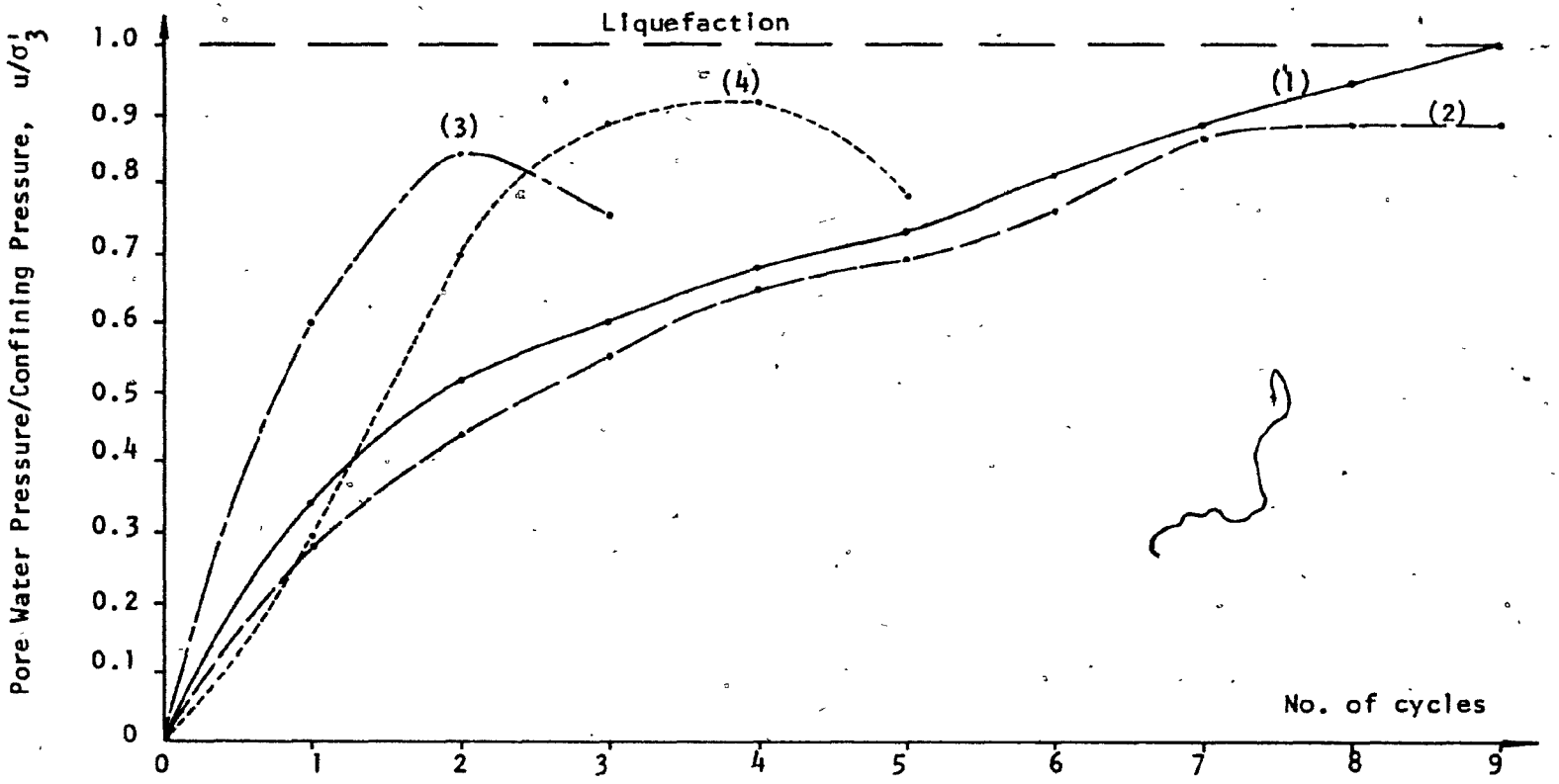

Fig. 2.11 Test Results

Test (1) w_c = 58%, cyclic stress = $\pm$ 1.2 psi ; Test (2) w_c = 41%, cyclic stress = $\pm$ 1.2 psi

Test (3) w_c = 60.5%, cyclic stress = $\pm$ 4 psi ; Test (4) w_c = 49%, cyclic stress = $\pm$ 2.4 psi

Cyclic Stress = ± 2.4 lb per sq.in.

Confining Pressure, σ_3 = 5 lb per sq.in.

Water Content ≃ 49%

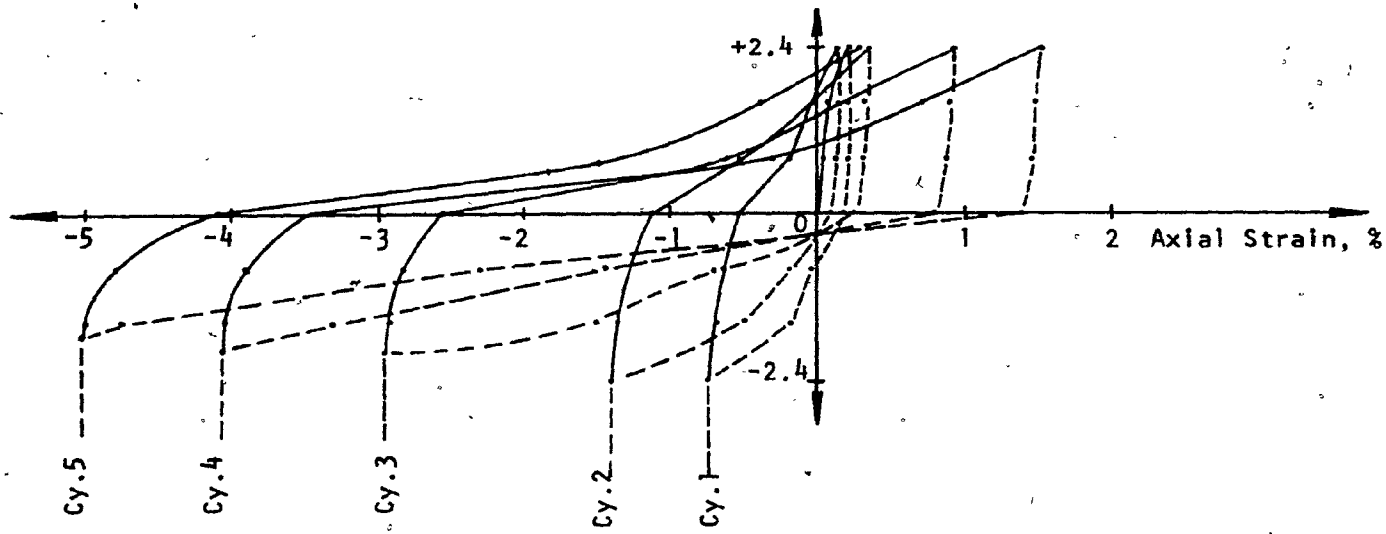

Fig. 2.12a Cyclic Loading Test
Stress-Strain Relationship

Cyclic Stress = ± 2.4 lb per sq.in.

Confining Pressure, σ_3 = 5 lb per sq.in.

Water Content = 49%

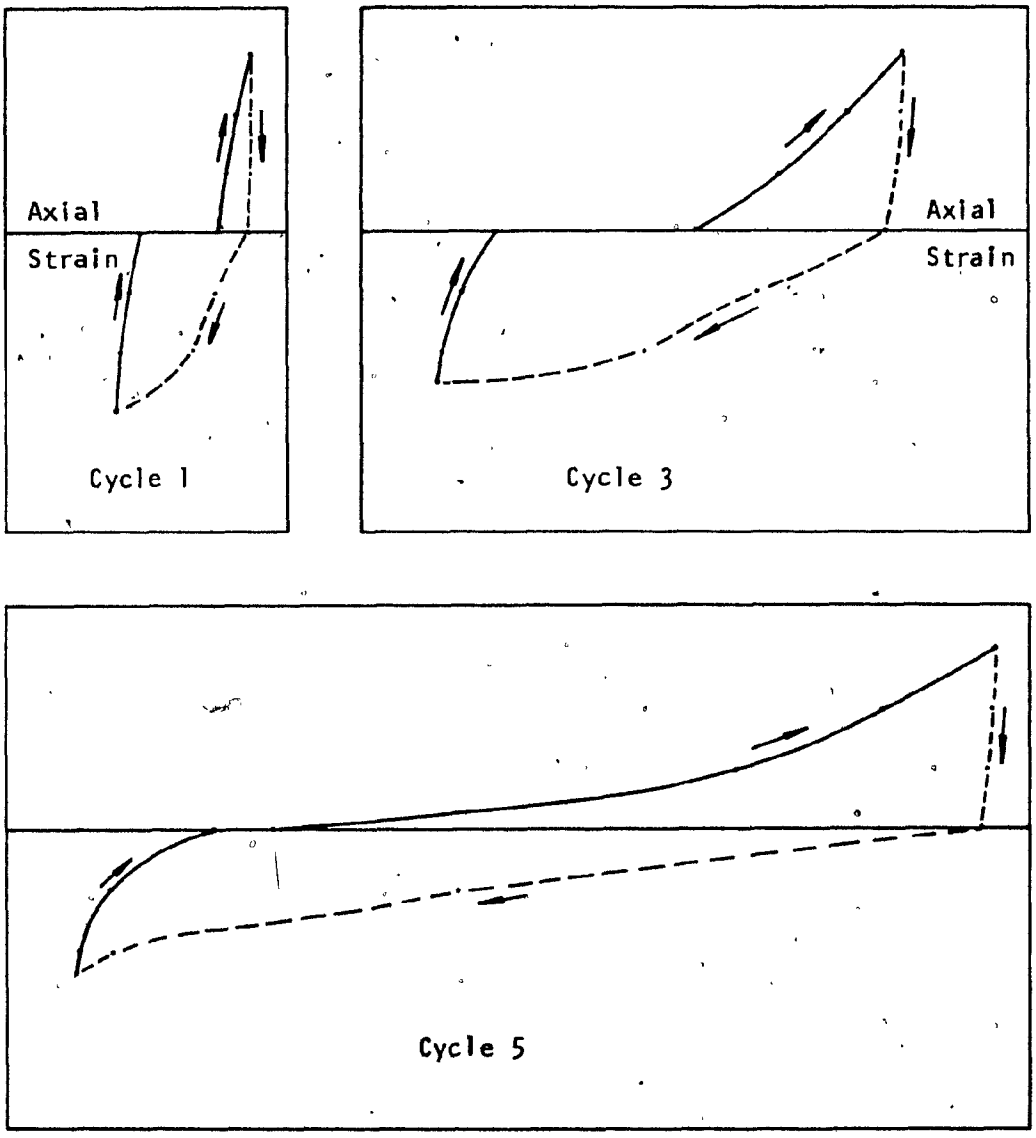

Fig. 2.12b Cyclic Loading Test
Stress-Strain Relationship

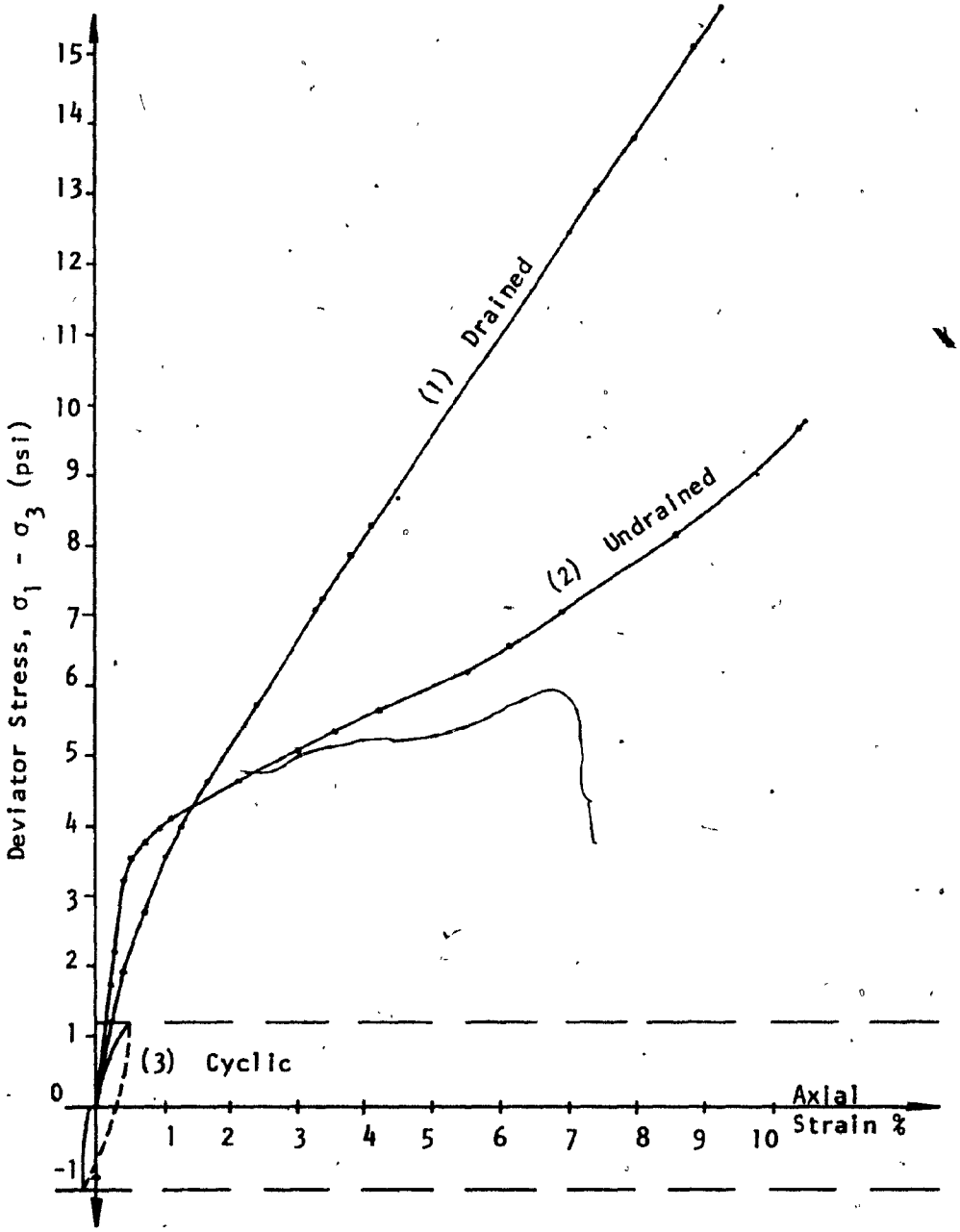

Fig. 2.13 Comparison of Cyclic Stresses Causing Liquefaction (3) and Static Loading Causing Failure (1), (2)

follows: (1) Deviator stress required to cause failure in static drained test (2) deviator stress required to cause failure in static undrained test (3) cyclic deviator stress required to cause liquefaction after nine loading cycles.

2.13 Analysis of Test Results

2.13.1 Triaxial conventional tests

In part one of this section, the results of the tests carried out are analyzed in the light of a concpet proposed by Luong (1981). In part two, the rationale for Luong's concept is examined using certain energy concepts first proposed by Poorooshasb and Roscoe (1961), and in the light of plasticity formulations for the cohesionless media proposed by Poorooshasb, Holubec and Sherbourne (1966). In fact, it is shown that the projection of the "Characteristic State Line" on the $\tau - \sigma$ plane coincide with the projection of the "Critical State Line" on the same plane.

The "Characteristic State" Concept

Test results agree with the concept of "The Characteristic State" for cohesionless soils, introduced by Luong (1981) for sands. "The Characteristic State" is defined in drained conventional triaxial tests by a deviator stress level q/p $(= \frac{(\sigma_1-\sigma_3)/2}{(\sigma_1+\sigma_3)/2})$ corresponding to a zero plastic (irreversible) volumetric strain rate (constant volume), or in undrained conventional triaxial tests by an effective deviator stress level q/p' $(= \frac{(\sigma_1-\sigma_3)/2}{[(\sigma_1+\sigma_3)/2]-u})$ corresponding to a zero pore water pressure generation rate (constant pore water pressure).

Figure 2.14 illustrates stress-axial strain and volumetric strain-axial strain curves for two slime samples which were tested under 5 and 20 psi

effective confining pressures, as obtained in the conventional compression drained tests with σ_1 increasing. The curves are similar and each shows an initial volume decrease (sample contractancy) followed by constant volume or volume increase (sample dilatancy).

Fig. 2.15 illustrates stress-axial strain and pore water pressure-axial strain curves for two other samples tested under 5, and 20 psi effective confining pressure, as obtained in the conventional compression undrained tests. A pore water pressure increase characterizes the first stage of both tests. As the deviator stress increases the pore pressure generation rate, $\dot{u}$ decreases, passing through zero to become negative: that is, the pore pressure was constant then started to decrease. This pore water pressure generation behaviour parallels phases of contractancy and dilatancy in a drained test.

The stress level corresponding to either the zero volume change rate, $\dot{\varepsilon}_v^p = 0$, (constant volume) in a drained test or the zero pore water pressure generation rate, $\dot{u} = 0$ (constant pore pressure) in an undrained test defines the "Characteristic State Line, Ch.S.L." which is practically the same for the two sets of tests under 5 and 20 psi, confining pressures as shown in Fig. 2.16a,b.

The Characteristic State Line defines the region of contractancy behaviour of the slime ($\dot{\varepsilon}_v^p > 0$, $\dot{u} > 0$), beyond which the soil dilates ($\dot{\varepsilon}_v^p < 0$, $\dot{u} < 0$) and experiences large irreversible deformations. Continuous dilatancy may lead to failure.

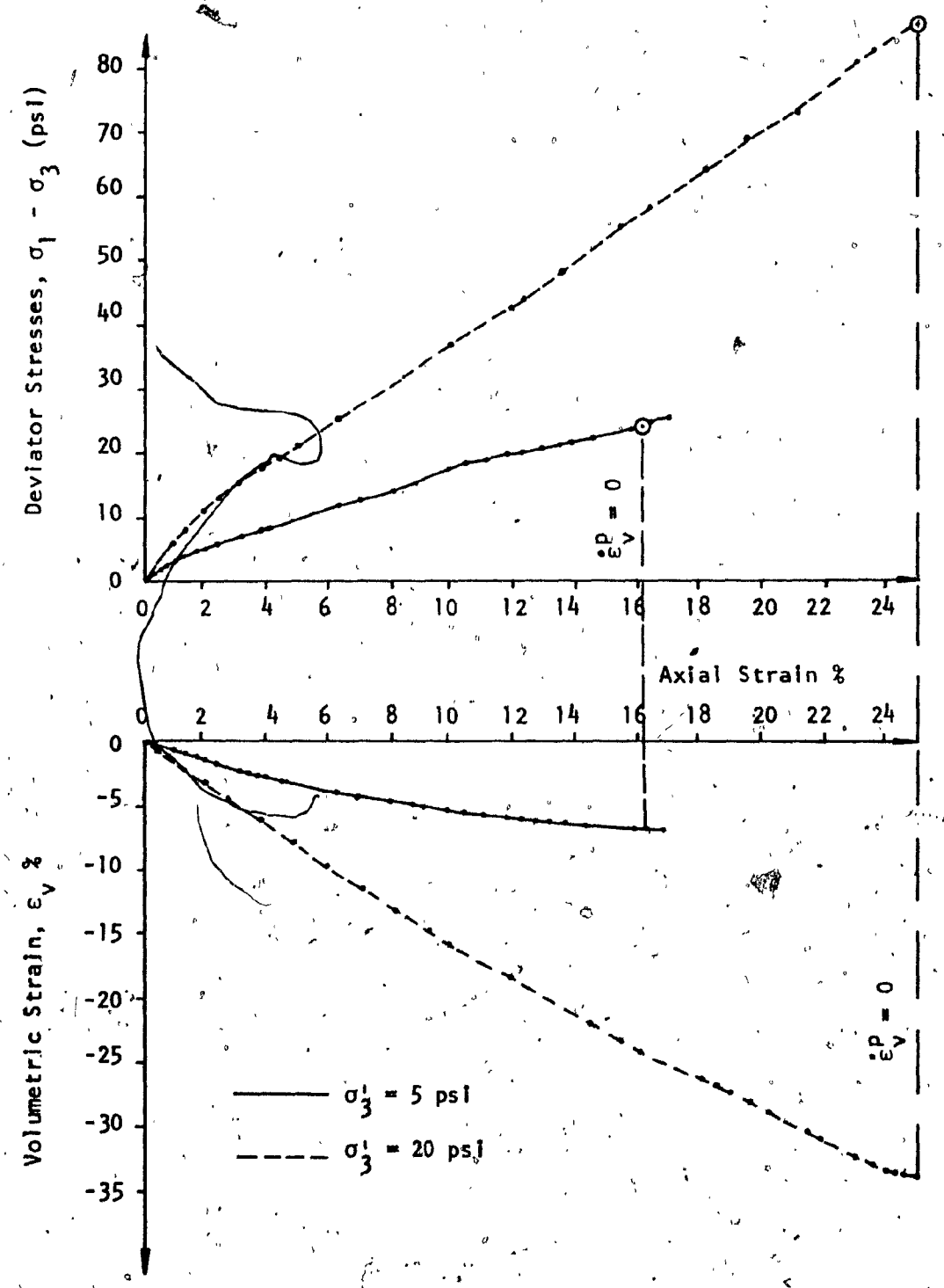

Fig. 2.14 Characteristic State for Drained Tests

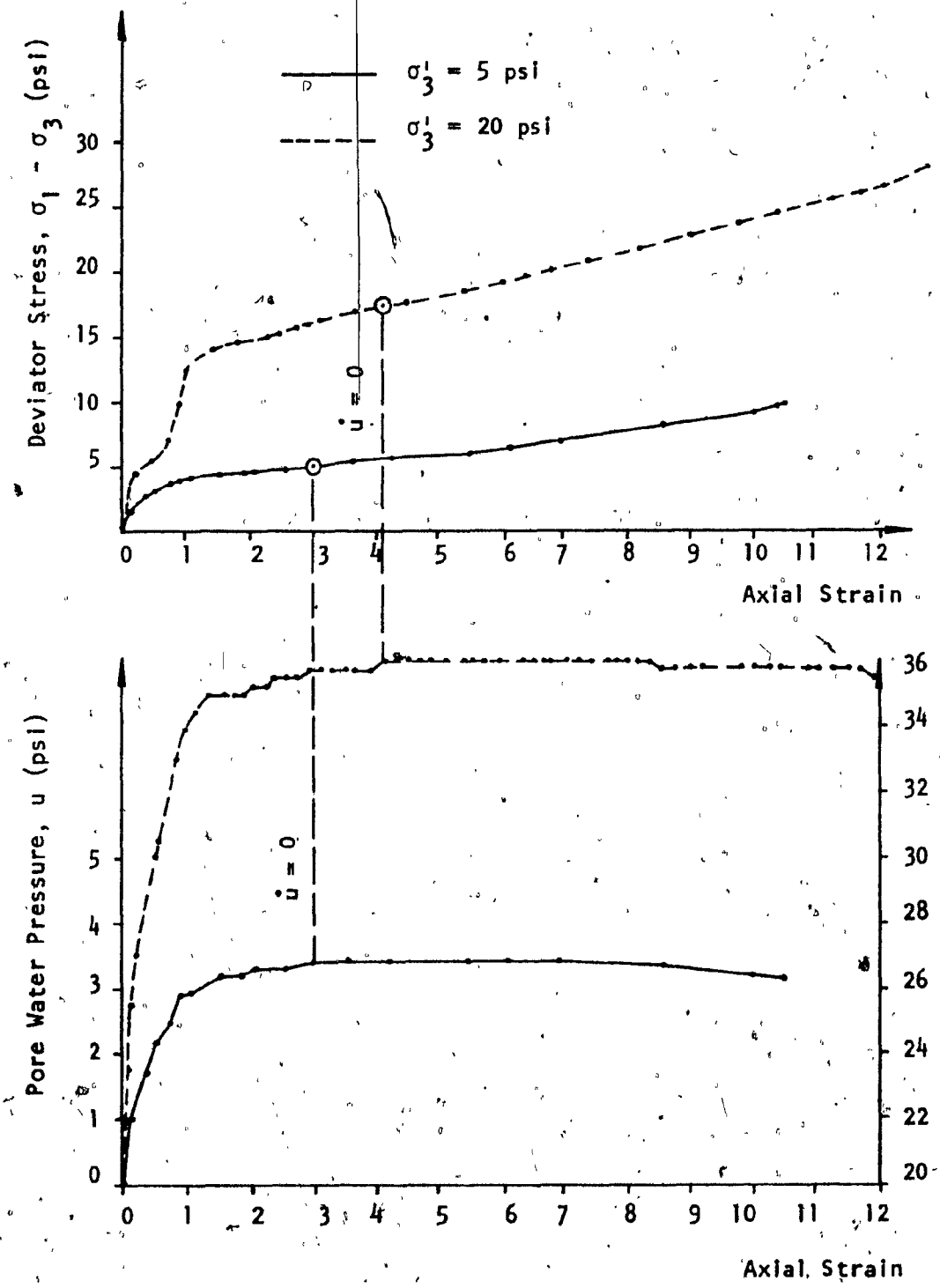

Fig. 2.15 Characteristic State for Undrained Tests

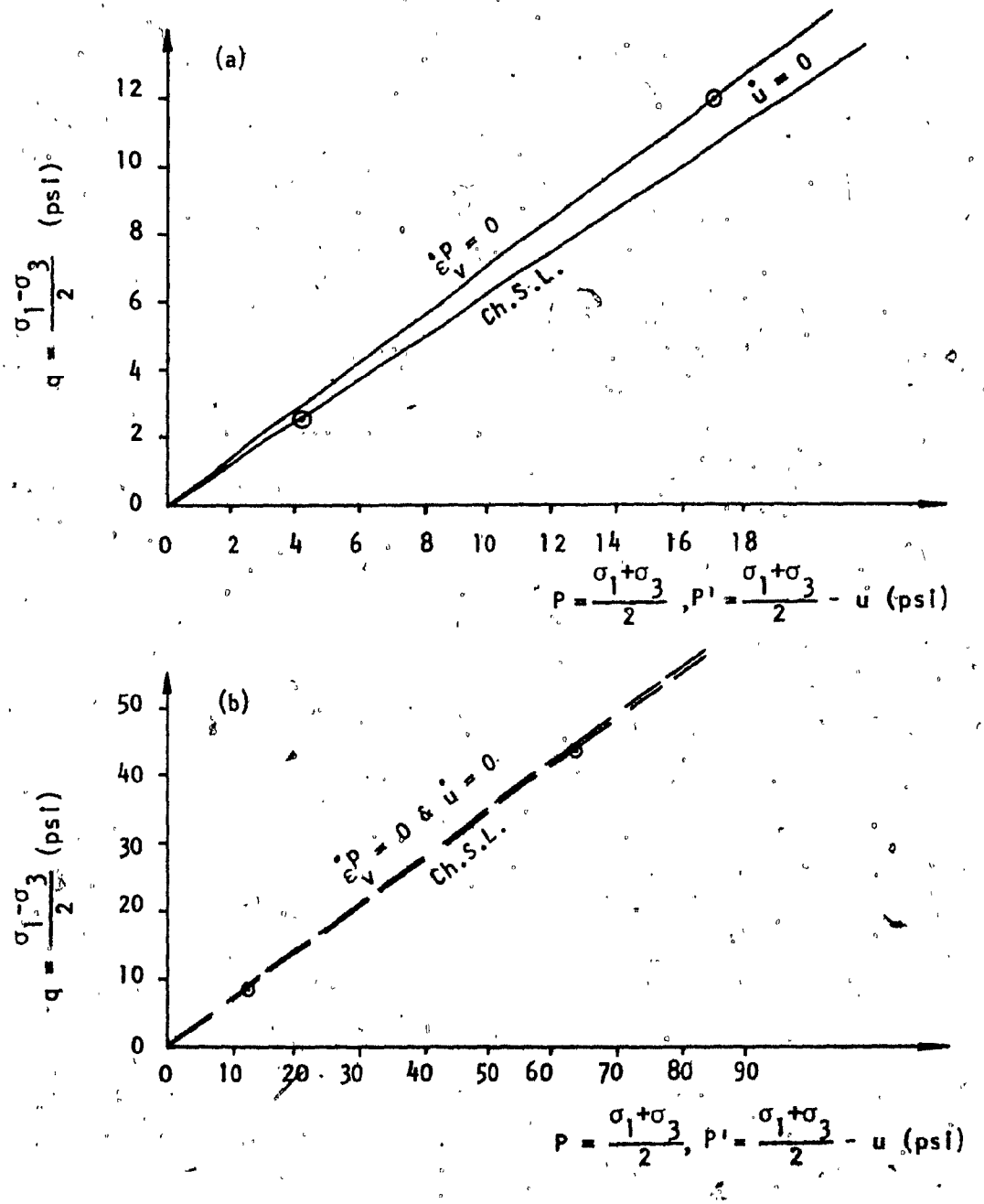

Fig. 2.16 The "Characteristic State Line" Ch.S.L. for (a) Tests of $\sigma_3' = 5$ psi; (b) Tests of $\sigma_3' = 20$ psi

The "Critical Void Ratio" Concept

Poorooshasb and Roscoe (1961) suggested energy correction for the observed shear strength in triaxial drained tests equal to $P \frac{\delta v/\delta \epsilon_1}{1 - \frac{1}{3}(\delta v/\delta \epsilon_1)}$, where $P = \frac{1}{3}(\sigma_1 + 2\sigma_3)$, δv is the change in the volumetric strain, $\delta \epsilon_1$ is the change in the axial strain. Hence,

$q_{corrected} = q_{observed}$ - energy correction where q = deviator stress, $\sigma_1 - \sigma_3$.

$$q = S\,P - P \frac{\delta v/\delta \epsilon_1}{1 - \frac{1}{3}(\delta v/\delta \epsilon_1)}$$

where S is a constant

$$\frac{q}{P} = S - \frac{\delta v/\delta \epsilon_1}{1 - \frac{1}{3}(\delta v/\delta \epsilon_1)} = S - \frac{\delta v}{d\epsilon_1 - \frac{1}{3} dv}$$

$$\frac{q}{P} + \frac{\delta v}{\delta \epsilon_1 - \frac{1}{3} \delta v} = S$$

if $\delta v = 0$ $\quad \frac{q}{P} = S$ (on the C.V.R.L.)

if $\delta v > 0$ $\quad \frac{q}{P} < S$ (below the C.V.R.L.)

if $\delta v < 0$ $\quad \frac{q}{P} > S$ (above the C.V.R.L.)

The "Critical Void Ratio" line (C.V.R.L.) is defined as the line in the stress plane ($\tau - \sigma$ plane) which passes through origin and the stress state at which the corrected deviator is equal to the observed deviator stress, that is, the energy correction equal to zero. In other words, the change in the volumetric strain δv is equal to zero. Hence, the soil volume is constant, as shown in Fig. 2.17. The soil contracts and its volume decreases in the drained conditions ($\delta v > 0$) or the pore pressure increases in the undrained conditions if the deviator stress is

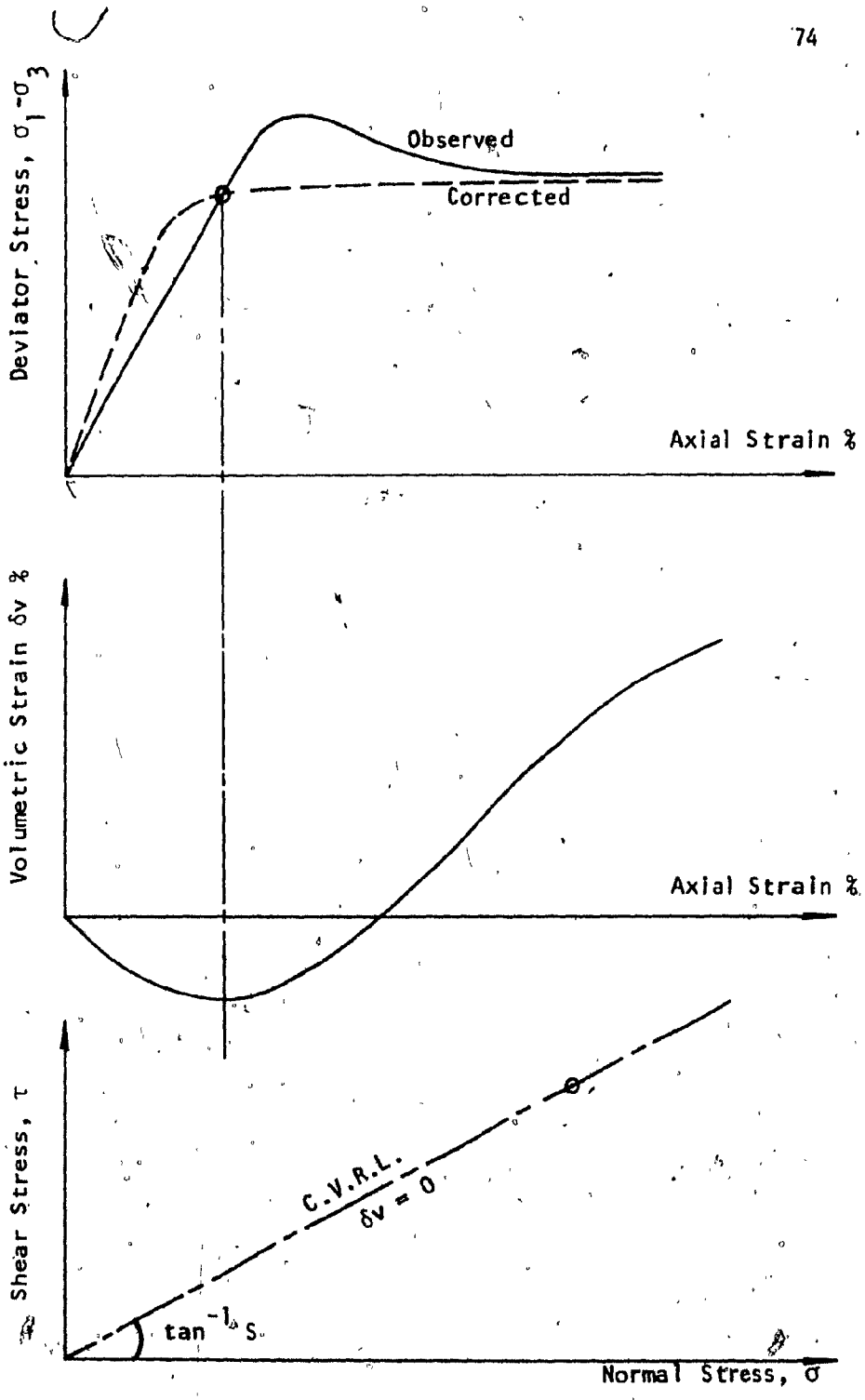

Fig. 2.17 The "Critical Void Ratio Line" (C.V.R.L.) After Poorooshasb and Roscoe (1961)

lower than the "Critical Void Ratio Line" ($q/p < S$). If the deviator stress is higher than the "Critical Void Ratio Line" ($q/p > S$), the soil dilates and its volume increases in the drained condition ($\delta v < 0$), or the pore pressure decreases in the undrained condition.

Test results agree with the "Critical Void Ratio" concept, hence the "Critical Void Ratio Line" is the same as the "Characteristic State" line suggested by Luong (1981).

The "Critical State" Concept

Before defining the "Critical State" concept two concepts should be defined. They are the plastic strain increment vector and the plastic potential function.

The plastic strain increment vector $d\varepsilon_{ij}^p$ is the incremental change in the strain associated with the incremental change in the stress. It is the resultant of two components, the plastic shear strain increment component $d\gamma^p = (d\varepsilon_1 - d\varepsilon_3)/2$, and the plastic volumetric strain increment component $d_v^p = (d\varepsilon_1 + d\varepsilon_3)/2$ for triaxial tests where $\sigma_2 = \sigma_3$, $(\varepsilon_2 = \varepsilon_3)$. Poorooshasb, Holubec, and Sherbourne (1966) showed that for cohesionless soils, the gradient of the plastic strain increment vector $d_v^p/d\gamma^p$ is independent of the gradient of the stress increment vector dq/dp, being a function only of the state of the element. In other words, for a point in the stress plane $\tau - \sigma$, i.e. $(q = (\sigma_1 - \sigma_3)/2 - p = (\sigma_1 + \sigma_3)/2)$ plane, the plastic strain increment vectors have gradients which are the same for all the loading stress paths passing through that point. The plastic strain increment vector $d_v^p/d\gamma^p$ depends only on the stress state (q,p) and the void ratio of the soil at that point e, i.e. $d_v^p/d\gamma^p = f(q,p,e)$, Poorooshasb, Holubec and Sherbourne (1966).

The plastic potential ψ is a function of the stress state and the void ratio of the soil element. These authors showed that it is rational to express the function ψ in the form:

$$\psi = P\,\psi'(\eta, e),$$

where $\eta = q/p\ (= \tau/\sigma)$.

The gradient of the plastic potential function ψ determines the inclination of the plastic strain increment vector associated with an incremental change of stress.

The "Critical State Line" (Cr.S.L.) is defined by the line passing through origin and the points of the zero plastic strain increment vector gradient, $d_v^P/d\gamma^P = 0$ (vertical plastic strain increment vectors in the stress plane, as shown in Fig. 2.18). The vertical plastic strain increment vector means that the volumetric strain increment component is equal to zero and the plastic strain increment is equal to the shear strain increment component only, $(d_v^P/d\gamma^P = 0)$. In other words, at these points there is no change in the volume (constant volume) in drained tests or there is no change in the pore water pressure in undrained tests. If the deviator stress applied on the soil is lower than the "Critical State Line" Cr.S.L., the soil will contract. That is, it decreases in volume in drained condition, $(d_v^P/d\gamma^P > 0)$ or the pore pressure increases in undrained conditions. If the deviator stress is higher than the "Critical State Line", Cr.S.L., the soil will dilate: it increases in volume in drained condition $(d_v^P/d^P < 0)$, or the pore water pressure decreases in undrained conditions.

The "Critical State Line" for two conventional drained tests under confining pressure of 5 psi and 20 psi is shown in Fig. 2.19. The results of these tests agreed with the concept. Hence, it is noted that the volume of the sample for both tests was decreasing until the deviator stress reached the "Critical State Line", when the volume started to be constant.

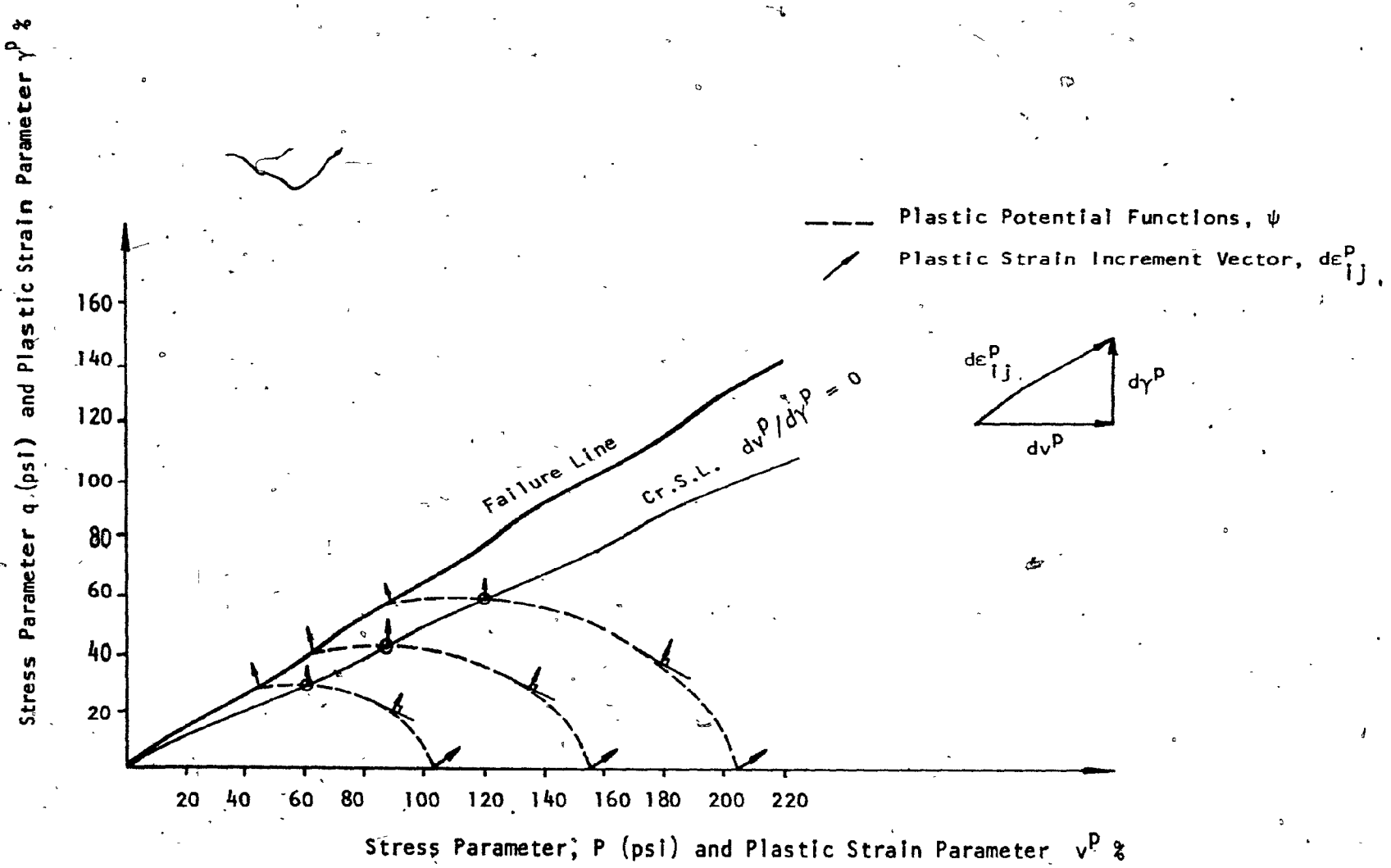

Fig. 2.18 The "Critical State Line" Cr.S.L.

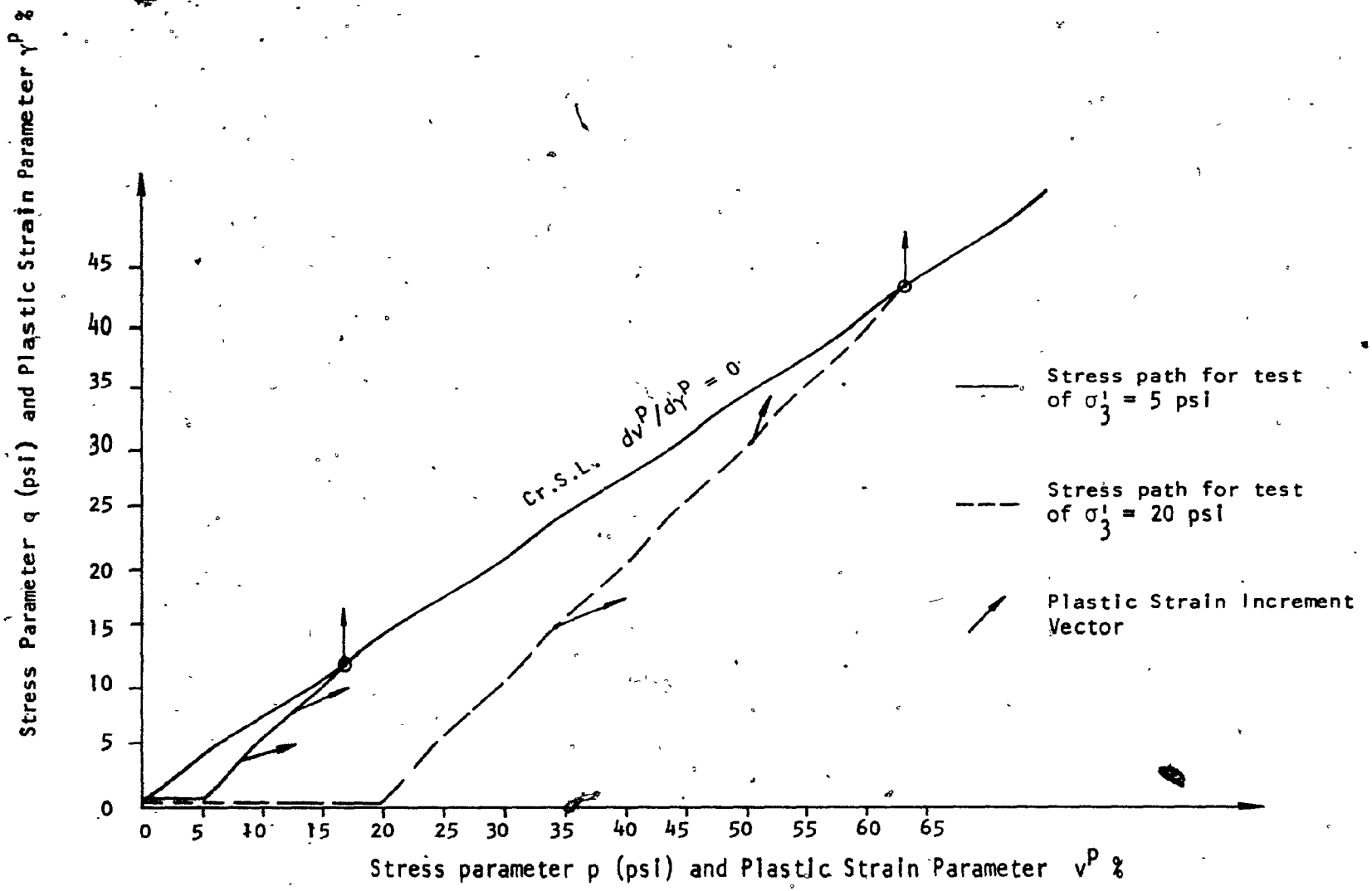

Fig. 2.19 The "Critical State Line" Cr.S.L. For Drained Tests

2.13.2 Triaxial undrained cyclic loading tests

It was seen that liquefaction of saturated slime was observed under an undrained alternating loading on both sides of zero deviator stress (compression–extension tests). Each load cycle reduces the mean effective stress as a result of increases in pore water pressure. This process continues as long as the mean deviator stress is lower than the Characteristic State Line, Ch.S.L. (Critical State Line, Cr.S.L.), as shown in Fig. 2.5e, Fig. 2.8e. After several alternating load cycles, the mean effective stress reduces to zero with a deviator stress on an unloaded path. Liquefaction is occurring when the effective stress is zero.

The contractancy behaviour (or increase in the pore water pressure) of the slime was obtained each time the mean deviator stress level is lower than the Characteristic State Line, Ch.S.L. (Critical State Line, Cr.S.L.), as shown in Fig. 2.9e, where the pore water pressure increases only in the first loading cycle, and in Fig. 2.10e, where the pore pressure increases only in the first and second loading cycles.

The dilatancy behaviour (or decrease in the pore water pressure) of the slime during cyclic loading was evident only when the mean deviator stress level becomes higher than the Characteristic State Line, Ch.S.L. (Critical State Line, Cr.S.L.), as shown in Fig. 2.9e, where the pore pressure started to decrease in the second loading cycle, and in Fig. 2.10e when the pore pressure started to decrease in the third and fourth loading cycle.

These concepts explain the reason why the slime under high value of cyclic stress was not likely to liquefy, because the mean deviator stress levels were higher than the Characteristic State Line. Hence, the pore water pressure dissipated during the cyclic loading and the zero effective mean stress condition was not reached, as shown in the tests in Fig. 9, 10.

CHAPTER 3

INSTABILITY OF TAILINGS DEPOSITS DUE TO EARTHQUAKE FORCES

In this chapter, the instability of tailings deposits during and after the earthquake will be studied. The results will be compared with a simplified procedure for predicting the distance of flow introduced by Lucia, Duncan and Seed (1980), although the two solutions are not exactly the same. Quantitative analysis of settling and liquefaction for different tailings deposits profiles will be discussed, determining the condition of the liquefaction process to be completed, and the estimated time of liquefaction. At the end of this chapter, a simple solution for liquefaction, and flow problems of tailings deposits due to earthquakes, will be introduced and verified by experimental evidence.

3.1 Behaviour of Tailings Deposits Soils at Liquefaction:

Tailings are frequently angular, bulky grained sand and silt (slimes) particles. It has been known that slimes particles (Chapter 2 of this thesis) and sand (Seed and Lee, 1966) are susceptible to rapid and large reduction in strength, due to very minor disturbances if they are deposited in a loose condition and they are saturated.

Tailings are commonly deposited using hydraulic methods, where the particles separate by size due to gravity in a peripheral discharge system or by cycloning (Dobry and Alvarez 1967). As they settle in the water in which they were transported, tailings often accumulate in loose deposits. In most tailings deposits, all voids between the particles are filled with water.

Rapid loading of this type of soil structure, either by seismic (like earthquakes) or by static means, results in a rapid build up in pore pressures. The induced shear stresses are resisted at the points of contact between soil particles because the water in the voids has no shear strength. The soil particles move under the shear stresses and tend to densify, which results in compression in the pore fluid. This transference of compressive stress to the pore water results in reduced compressive forces at interparticle contacts, and a consequent weakening of the soil structure. After a small amount of strain, particle to particle contact may be lost, and complete breakdown of the structure may occur. This "liquefaction" phenomenon results in nearly completed loss of strength

The breakdown in structure and the loss of particle to particle contact results in the earthquake induced shear stresses being transferred to the water in the soil, which has no shear strength. The soil mass is then driven by forces for which it does not have sufficient resistance, resulting in the onset of the "flow" of the mass. This flow of the liquefied tailings has resulted in many deaths, moreover severe environmental polution might occur, the degree of which depends on the nature of the tailings and their proximity to rivers and streams. In recent years, for example, Chilean tailings dams failed due to 1965 earthquake, and Mochikoshi tailings dam due to 1978 earthquake may be sited. During flow, at any given time, there is always some particle to particle contact, and this results in some small shear resistance for the flowing soil mass. This shear strength is termed the residual strength, and the magnitude of the residual strength is a function of the soil type and its initial density.

The flowing soil mass will come to rest when the shearing resistance in the soil due to its residual strength is higher than, or equal to, the shear stress.

3.2 Simplified Procedure for Predicting the Distance of Flow (for a definite slope, after the earthquake ceases) By Lucia, Duncan and Seed (1980)

A study of some case histories indicated a consistent pattern of behaviour of the liquefied tailings deposits during and after earthquakes. Liquefied soils have a low shear strength which enables them to come to rest on small slopes. All of the liquefied saturated tailings materials continued to flow until they reached an inclination of 1^{o} to 4^{o}.

The authors assumed that the flowing soil mass will come to rest when the shearing resistance in the soil, due to its residual strength, is equal to the shear stress induced by the low slope angle. Hence, at the moment the flow stopped, the shear strength of the liquefied mass required to give a safety factor of 1.0 was calculated. (This assumption neglects inertia forces, considering that they are negligible at low velocities, just before the flow stops).

The authors considered the most critical mode of failure is as shown in Fig. 3.1. They found that considering the shear along the base, and active pressure at the back of the liquefied wedge, required greater shear strength than the most critical circular or noncircular slip surfaces. This mechanism was therefore used by them to develop dimensionless stability charts. For this condition, the equation of stability can be written for a factor of safety of unity as follows:

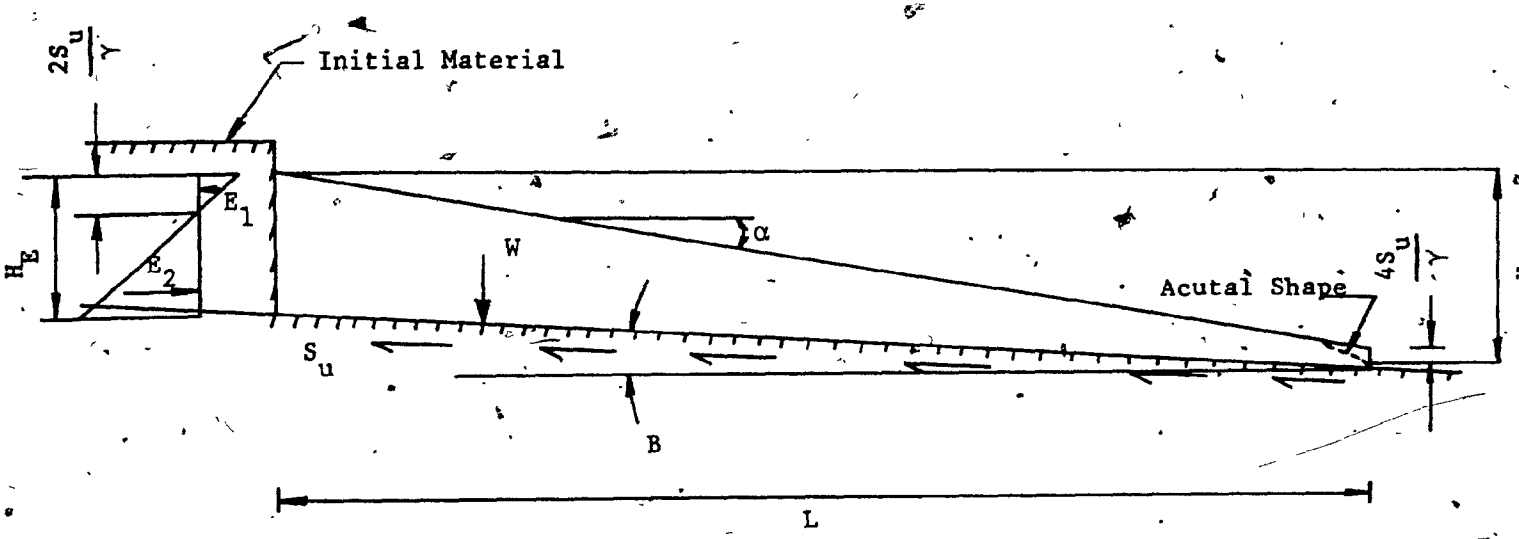

Fig. 3.1 Idealized Cross Section

$$F.S. = \frac{\text{Shear Strength (Residual Strength, } S_u)}{\text{Shear stress}} = 1.0$$

Shear stress - shear strength = 0

According to Fig. 3.1:

$$w \sin B + E_2 \cos B - \frac{S_u \cdot L}{\cos B} - E_1 \cos B = 0 \qquad (3.1)$$

Equation (3.1), in a dimensionless form is as follows:

$$\frac{w \sin B}{\gamma H_T^2} + \frac{E_2 \cos B}{\gamma H_T^2} - \frac{S_u \cdot L}{\gamma H_T^2 \cdot \cos B} - \frac{E_1 \cos B}{\gamma H_T^2} = 0 \qquad (3.2)$$

Equation (3.2) can be solved in terms of the dimensionless parameter, N_o where

$$N_o = \frac{\gamma H_T}{S_u} \qquad (3.3)$$

where γ is the total unit weight of the tailings

H_T as shown in Fig. 3.1

S_u the residual shear strength of the tailings after liquefaction and during the flow. S_u can be determined by using values for similar materials.

B the downstream slope angle.

N_o varies with α and B. The authors established charts to directly determine the stability number, N_o for given values of α and B. The distance, L, through which liquefied tailings may flow before coming to rest, can be estimated based on these charts as follows:

1. Determine the value of N_o for a number of assumed values of α from the charts. For each of these values, calculate H_T where

$$H_T = \frac{N_o S_u}{\gamma} \qquad (3.4)$$

2. Plot the values of H_T versus the corresponding values α. These values of H_T and α will define a "strength curve", as shown in Fig. 3.2.

3. Estimate the volume of tailings which would be involved in the flow, v_f. It is considered that the most appropriate assumption will often be that 100% of the tailings will flow.

4. For a number of assumed values of α, calculate H_T using this formula

$$H_T = \sqrt{A_1^2 H_c^2 + A_2 v_p} - A_3 H_c \qquad (3.5)$$

where

$$A_1 = \left(\frac{\tan \alpha}{\tan \alpha - \tan B}\right)^2 \qquad (3.6)$$

$$A_2 = \frac{2 \tan^2 \alpha}{\tan \alpha - \tan B} \qquad (3.7)$$

$$A_3 = \frac{\tan B}{\tan \alpha - \tan B} \qquad (3.8)$$

$$H_c = \frac{4 S_u}{\gamma} = \text{the critical vertical height} \qquad (3.9)$$

v_f = volume of material which flows.

These values of H_T and the corresponding values of α will define a "volume curve" as shown in Fig. 3.2.

5. Where the strength curve and the volume curve intersect, all conditions with regard to strength and geometry are satisfied simultaneously, with a factor of safety equal to one. The values of H_T and α at the point of intersection are those corresponding to the "limiting stability condition". The values of the flow distance, L, can be calculated according to Fig. 3.1, as follows:

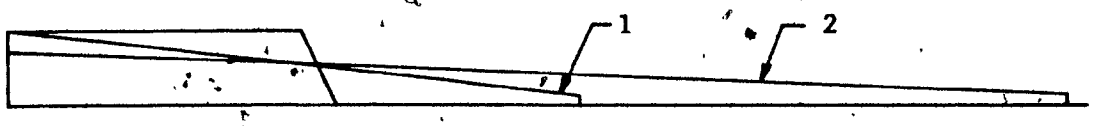

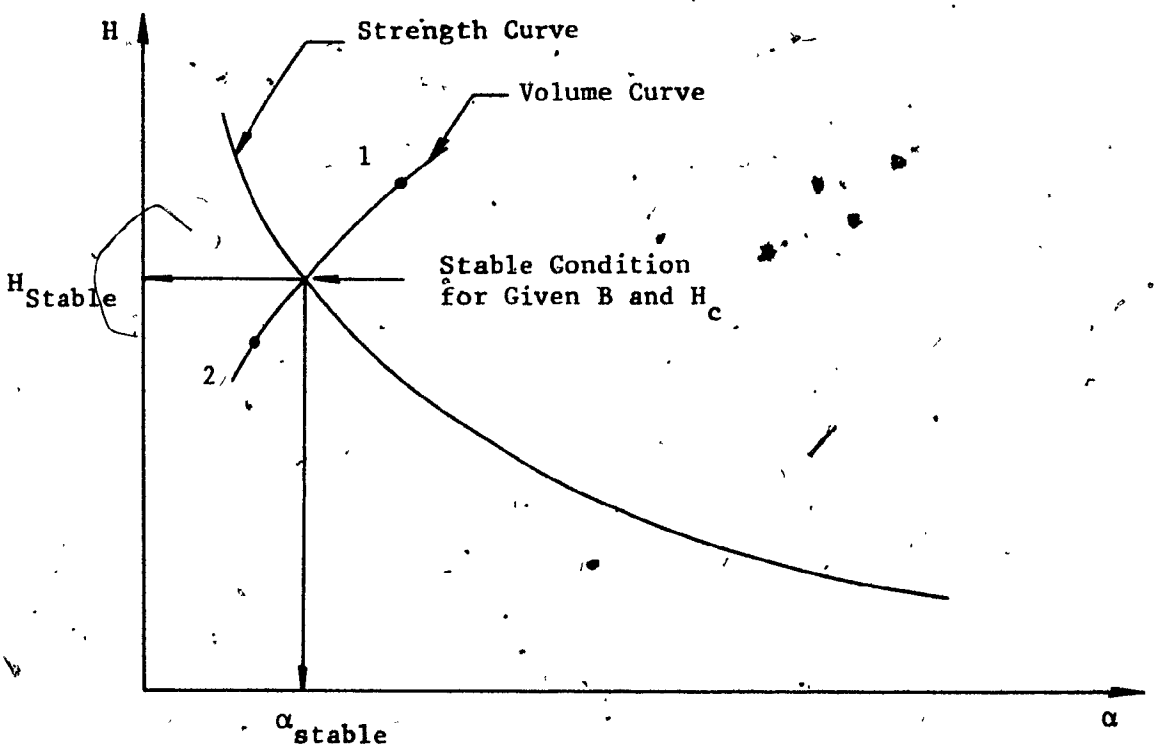

Fig. 3.2 Prediction of Distance of Flow
(Lucia, Duncan, and Seed 1980)

$$L = \frac{H_T - H_c}{\tan \alpha} \qquad (3.10)$$

3.3 Suggested Approach for Predicting the Distance and the Time of Flow (for infinite slope)

In this approach the inertia forces are considered as acting forces during and after the earthquake. The system analyzed is also different from that of Seed et al (1980) in the sense that an infinite slope is analyzed.

Assume the profile of the tailings deposits is as follows: a layer of sand is overlying a continuous layer of saturated slimes of an inclination, θ. The flow of the overlying layer will be studied here during three phases as shown in Fig. 3.3. These phases are: Phase I during the earthquake, Phase II and Phase III after the earthquake ceases. During Phase II the shear strength of the slime increases until it reaches its maximum value τ_{cr}. During Phase III, the shear strength of the slime is constant and equal to τ_{cr}.

3.3.1 During the earthquake (Phase I)

The shear stress induced by the earthquake alternating motions liquefies the underlying slime layer (as observed in tests of Chapter 2 of this thesis). Hence, the slime loses its shear strength and cannot resist the shear stress applied by the overlying sand layer. The sand layer will flow over the liquefied slime layer without any resistance to to its movement. So, according to Fig. 3.4a:

The Shear Stress = Inertia Force

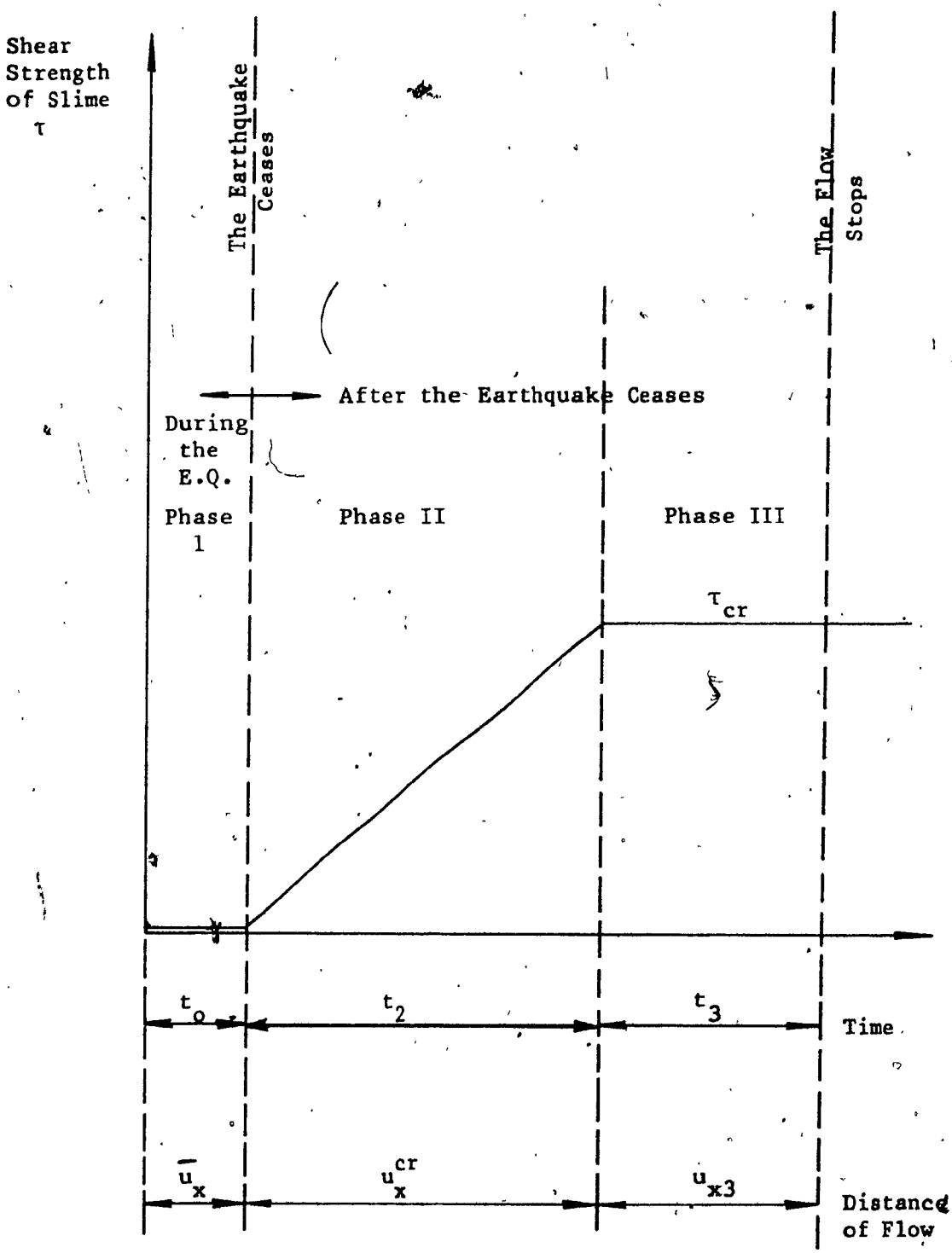

Fig. 3.3 The Three Phases of Flow Due to Earthquake Forces

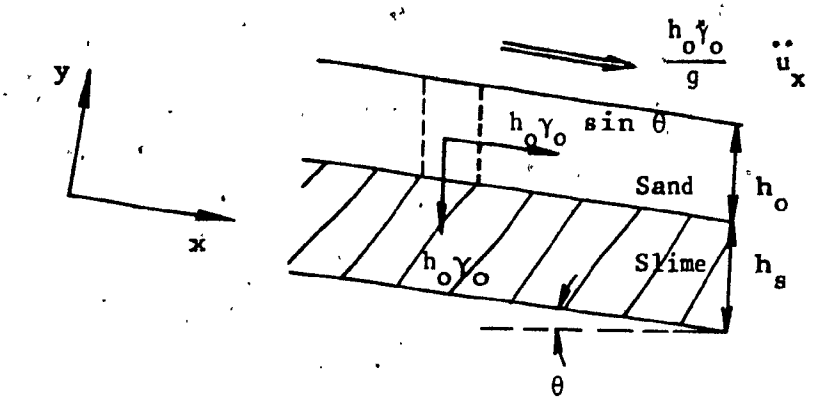

(a) Phase I

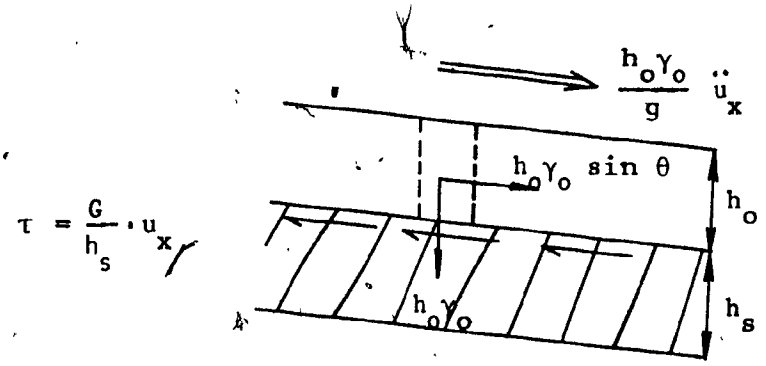

(b) Phase II

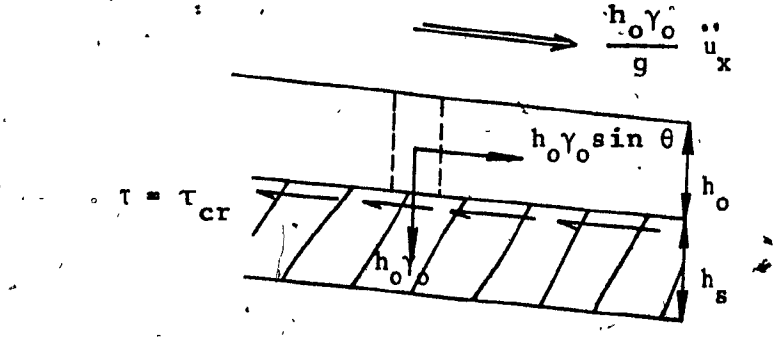

(c) Phase III

Fig. 3.4 Predicting the Distance and the Time of Flow

$$h_o \gamma_o \sin\theta = \frac{h_o \gamma_o}{g} \ddot{u}_x \qquad (3.11)$$

where γ_o: the total unit weight of the overlying layer

g: the gravity acceleration

$\ddot{u}_x$: the acceleration of the overlying sand layer flow in the x-direction

So, for $t = 0 \rightarrow t_o$ from equation (3.11)

where t_o: is the duration of the earthquake,

$$\ddot{u}_x = g \sin\theta$$

$$\dot{u}_x = \int \ddot{u} \cdot dt = g \sin\theta \cdot t$$

$$u_x = \int \dot{u}_x \cdot dt = g \sin\theta \cdot \frac{t^2}{2}$$

where $\dot{u}_x$: the velocity of the overlying sand layer flow.

u_x: the distance of flow of the overlying sand layer.

At the end of the earthquake period, $t = t_o$

$$\bar{\dot{u}}_x = g \sin\theta \cdot t_o$$

$$\bar{u}_x = g \sin\theta \cdot \frac{t_o^2}{2} \qquad (3.12)$$

Equation (3.12) represents the distance of flow of the overlying layer at the instant the earthquake ceases.

3.3.2 After the earthquake ceases (Phase II)

After the earthquake stops, the slime will gradually regain the shear strength it lost during the cyclic loading of the earthquake, (as indicated in Chapter 2 of this thesis, the slime has an angle of internal friction of 52.5^o, as the applying static loading following liquefaction

at axial strain equal to 13%.) Hence, the underlying slime layer will resist the shear stress applied by the overlying sand layer. The sand layer will continue flowing but its flow will be resisted by the shear strength of the slime, as shown in Fig. 3.4b.

The shear stress - slime shear strength = Inertia force -

$$h_o \gamma_o \sin\theta - \tau = \frac{h_o \gamma_o}{g} \ddot{u}_x \qquad (3.13)$$

τ = shear modulus, G · Engineering shear strain, γ_{xy} (3.14)

$$G = \frac{E}{2(1+\mu)}$$

where E is the elasticity modulus = $\frac{\text{Normal stress}}{\text{axial strain}}$

μ is the Poisson ratio $\simeq$ 0.5 for the saturated soil

$$G \simeq \frac{E}{3}$$

Strain tensor, $\varepsilon_{ij} = \frac{1}{2}[u_{i,j} + u_{j,i}] = \frac{1}{2}\left[\frac{du_i}{dj} + \frac{du_j}{di}\right]$

so, with reference to x,y axis the shearing strain, ε_{xy} is defined as:

$$\varepsilon_{xy} = \frac{1}{2}[u_{x,y} + u_{y,x}] = \frac{1}{2}\left[\frac{du_x}{dy} + \frac{du_y}{dx}\right]$$

Because there is almost no movement in y-direction, i.e. $\frac{du_y}{dx} \simeq 0$, hence

$$\varepsilon_{xy} = \frac{1}{2}\frac{du_x}{dy}$$

$$\gamma_{xy} = 2\,\varepsilon_{xy} = \frac{du_x}{dy} \qquad (3.15)$$

Substituting Eq. (3.15) in Eq. (3.14), we get:

$$\tau = G \cdot \frac{du_x}{dy}$$

$$\int du_x = \int \frac{\tau}{G} \cdot dy$$

$$u_x = \frac{\tau}{G} [y]_0^{h_s}$$

$u_x = \frac{\tau}{G} \cdot h_s$ at the surface of the slime layer

$$\tau = \frac{G}{h_s} \cdot u_x \qquad (3.16)$$

Substituting Eq. (3.16) in Eq. (3.13) we get:

$$h_o \gamma_o \sin\theta - \frac{G}{h_s} \cdot u_x = \frac{h_o \gamma_o}{g} \ddot{u}_x$$

$$\ddot{u}_x = g \sin\theta - \frac{G g}{h_o \gamma_o h_s} \cdot u_x$$

Let $\frac{G g}{h_o \gamma_o h_s} = \beta^2$

$$\ddot{u}_x = g \sin\theta - \beta^2 u_x$$

$$\ddot{u}_x + \beta^2 u_x = g \sin\theta \qquad (3.17)$$

The typical solution of the second degree differential equation (3.17) is

$$u_x = \frac{h_o \gamma_o h_s}{G} \sin\theta + a \cos\beta t + b \sin\beta t \qquad (3.18)$$

where a, b are constants and can be determined as follows: at $t = 0$ $u_x = 0$, substituting in Eq. (3.18),

$$a = -\frac{h_o \gamma_o h_s}{G} \sin\theta \qquad (3.19)$$

Substituting Eq. (3.19) in Eq. (3.18), we get:

$$u_x = -a + a \cos\beta t + b \sin\beta t \qquad (3.20)$$

$$\dot{u}_x = -a\beta \sin \beta t + b\beta \cos \beta t \tag{3.21}$$

at $t = 0$, substituting in Eq. (3.21):

$$\dot{u}_x = b\beta$$

$$b = \frac{\dot{u}_x}{\beta}$$

But, $t = 0$ for Phase II means that $t = t_o$ of Phase I, i.e.

$$\dot{u}_x = \bar{\dot{u}}_x = g \sin\theta \cdot t_o = b\beta$$

$$b = \frac{g \sin \theta \cdot t_o}{\beta} \tag{3.22}$$

Substituting from Eq. (3.19), (3.22) in Eq. (3.20), we get:

$$u_x = \frac{h_o \gamma_o h_s}{G} \sin \theta (1 - \cos \beta t) + \frac{g \sin \theta \cdot t_o}{\beta} \sin \beta t \tag{3.23}$$

where $\beta = \sqrt{\frac{G g}{h_o \gamma_o h_s}}$

Equation (3.23) represents the distance of flow of the overlying layer at any time after the earthquake ceases, before the underlying slime layer regains its maximum shear strength τ_{cr}. Eq. (3.23) can be differentiated to obtain the velocity of flow, $\dot{u}_x$. $\dot{u}_x$ equal to zero at the instant the flow stops. The time elapsed until the flow stops can be determined by solving the $\dot{u}_x$ equation when $\dot{u}_x = 0$ with the aid of the computer. By substituting this time in Eq. (3.23), we can determine the distance of flow, u_x.

Phase III

During phase III, the slime has constant shear strength, τ_{cr}.

where $\tau_{cr} = (\sigma - u) \tan \phi'$ (3.24)

where u: is the pore water pressure with minimum value of -14.7 psi, assuming that it is = -7 psi, considering that the soil is not fully saturated in the field.

σ: is the total stress on the slime layer. Assume $\sigma = 0$ to get the least value of τ_{cr}.

ϕ': is the angle of internal friction = 52.5^{o} (from test results of Chapter 2 of this thesis).

Substituting the values of u, σ, and ϕ' in Eq. (3.24), we get

$$\tau_{cr} = 7 \tan 52.5^{o} = 9.12 \text{ psi} \approx 641 \text{ gm/cm}^2 \quad (3.25)$$

$$u_x = \frac{\tau}{G} \cdot h_s \text{ at the surface of the slime layer} \quad (3.16)$$

$$u_x^{\text{critical}} = \frac{\tau_{cr}}{G} \cdot h_s \quad (3.26)$$

where u_x^{cr}: is the distance of flow after the earthquake ceases at the instant the slime reaches its maximum shear strength. The corresponding time of flow, t_2, can be determined by substituting the value of u_x^{cr} from Eq. (3.26) in Eq. (3.23) (i.e. $u_x^{cr} = u_x$)

If u_x from Eq. (3.23) is less than or equal to u_x^{cr}:

Phase I and Phase II only, will be considered. Hence, the total distance of flow during and after the earthquake can be predicted by adding the value of Eq. (3.12) to the value of Eq. (3.23).

If u_x from Eq. (3.23) is greater than u_x^{cr}:

The distance of flow after the earthquake ceases will be

$$u_x = u_x^{cr} + u_{x3} \text{ as shown in Fig. 3.3} \qquad (3.27)$$

where u_x^{cr} can be determined from Eq. (3.26)

u_{x3} will be obtained as follows:

According to Fig. 3.4c during Phase III:

The shear stress - the slime shear strength = inertia force

$$\gamma_o h_o \sin\theta - \tau_{cr} = \frac{\gamma_o h_o}{g} \ddot{u}_{x3}$$

$$\int(\gamma_o h_o \sin\theta - \tau_{cr})\, dt = \frac{\gamma_o h_o}{g} \int \ddot{u}_{x3} \cdot dt$$

$$(\gamma_o h_o \sin\theta - \tau_{cr})\, t_3 = \frac{\gamma_o h_o}{g} \dot{u}_{x3} + C_1 \qquad (3.28)$$

At $t_3 = 0$ $\qquad \dot{u}_{x3} = \dot{u}_x^{cr} \qquad (3.29)$

Substituting from Eq. (3.29) in Eq. (3.28)

$$C_1 = -\frac{\gamma_o h_o}{g} \dot{u}_x^{cr}$$

Substituting the value C_1 in Eq. (3.28), we get:

$$(\gamma_o h_o \sin\theta - \tau_{cr})\, t_3 = \frac{\gamma_o h_o}{g} \dot{u}_{x3} - \frac{\gamma_o h_o}{g} \dot{u}_x^{cr}$$

$$\frac{\gamma_o h_o}{g} \dot{u}_{x3} = (\gamma_o h_o \sin\theta - \tau_{cr})\, t_3 + \frac{\gamma_o h_o}{g} \dot{u}_x^{cr}$$

$$\int \frac{\gamma_o h_o}{g} \dot{u}_{x3} \cdot dt = \int(\gamma_o h_o \sin\theta - \tau_{cr})\, t_3 \cdot dt + \int \frac{\gamma_o h_o}{g} \dot{u}_x^{cr} \cdot dt$$

$$\frac{\gamma_o h_o}{g} u_{x3} = (\gamma_o h_o \sin\theta - \tau_{cr}) \frac{t_3^2}{2} + \frac{\gamma_o h_o}{g} \cdot \dot{u}_x^{cr} \cdot t_3 + C_2 \qquad (3.30)$$

At $t_3 = 0$ $\quad u_{x3} = 0$ (3.31)

Substituting from Eq. (3.31) in Eq. (3.30), we get:

$$C_2 = 0$$

Substituting the value of C_2 in Eq. (3.30), we get:

$$u_{x3} = \left[\frac{\sin\theta}{g} - \tau_{cr} \cdot \frac{g}{\gamma_o h_o}\right] \frac{t_3^2}{2} + \dot{u}_x^{cr} \cdot t_3 \tag{3.32}$$

$$\dot{u}_{x3} = \left[\frac{\sin\theta}{g} - \tau_{cr} \cdot \frac{g}{\gamma_o h_o}\right] t_3 + \dot{u}_x^{cr}$$

At the instant the flow stops, $\dot{u}_{x3} = 0$

$$\left[\frac{\sin\theta}{g} - \tau_{cr} \cdot \frac{g}{\gamma_o h_o}\right] t_3 + \dot{u}_x^{cr} = 0$$

$$t_3 = \frac{-\dot{u}_x^{cr}}{\left[\frac{\sin\theta}{g} - \tau_{cr} \cdot \frac{g}{\gamma_o h_o}\right]} \tag{3.33}$$

Equation (3.33) determine the time of flow during Phase III.

Substituting Eq. (3.33) into Eq. (3.32), we get:

$$u_{x3} = \frac{(\dot{u}_x^{cr})^2}{2\left[\frac{\sin\theta}{g} - \tau_{cr} \cdot \frac{g}{\gamma_o h_o}\right]} - \frac{(\dot{u}_x^{cr})^2}{\left[\frac{\sin\theta}{g} - \tau_{cr} \cdot \frac{g}{\gamma_o h_o}\right]}$$

$$u_{x3} = \frac{-(\dot{u}_x^{cr})}{2\left[\frac{\sin\theta}{g} - \tau_{cr} \cdot \frac{g}{\gamma_o h_o}\right]}$$

$$u_{x3} = \frac{(\dot{u}_x^{cr})^2}{2\left[\tau_{cr} \cdot \frac{g}{\gamma_o h_o} - \frac{\sin\theta}{g}\right]} \tag{3.34}$$

where $\dot{u}_x^{cr}$ is obtained from Phase II by substituting for the value of t_2 in Eq. (3.21)

τ_{cr} can be determined from Eq. (3.25).

Equation (3.34) determines the distance of flow during Phase III. Substituting Eq. (3.34) in Eq. (3.27) we get the distance of flow after the earthquake ceases:

$$u_x = \frac{\tau_{cr}}{G} \cdot h_s + \frac{(\dot{u}_x^{cr})^2}{2\left[\tau_{cr} \cdot \frac{g}{\gamma_o h_o} - \frac{\sin\theta}{g}\right]} \qquad (3.35)$$

The total distance of flow during and after the earthquake can be predicted by adding the value of Eq. (3.12) to the value of Eq. (3.35).

3.4 Quantitative Analysis of Settling and Liquefaction for Different Tailings Deposits Profiles

3.4.1 In Case the Slime Layer Overlies Sand

Consider the soil profile of tailings deposits as shown in Fig. 3.5a. It consists of two uniform materials. First, an underlying loose, fine to medium sand layer with initial porosity n_i where the settling velocity of its grains is A. Above it lies a relatively dense, fine slime layer of initial porosity n_d. The settling velocity of its grains is C, which is much smaller than A.

An earthquake causes the underlying sand layer to liquefy, but not the overlying slime layer directly. As shown in Fig. 3.5b after the earthquake ceases, the suspended grains of the sand layer settle at velocity A to form a solidified soil at a new porosity, n_f. Removal of

the support of the soil grains of the sand layer from the bottom grains of the slime layer causes the former to unravel from the bottom at such a rate that the falling grains form a suspension at porosity n_s. Subsequently, in Fig. 3.5c, the lower sand layer has solidified entirely and the upper slime layer partially, to leave an intermediate zone of liquefied slime. No disturbance is as yet apparent on the surface. Finally, Fig. 3.5d, shows both materials solidified at their new porosities n_f,n_e, the case where liquefaction has reached ground surface (the liquefaction process is completed).

Condition of Liquefaction process to be completed (liquefaction reaches the ground surface)

In Fig. 3.5, the sand layer contracts forming a denser layer of porosity $n_f < n_i$, and the slime layer expands forming a looser layer of porosity $n_e > n_d$. If the slime layer is able to accomodate the porosity change induced by liquefaction entirely within its thickness, liquefaction does not reach the ground surface, and no surface subsidence takes place, although subsidence does occur at depths below the surface.

The contraction in thickness of the sand layer can be obtained by considering that the volume of the soil solids remains constant and it is found to be equal to $(n_i - n_f)h_o/(1-n_f)$. Similarly, if the entire slime layer liquefies, its expansion thickness is equal to $(n_e-n_d)h_s/(1-n_e)$. If the stable porosities and layer thicknesses are such that the latter value for maximum expansion of the slime layer exceeds the amount of contraction of the sand layer, the slime layer will not liquefy all the way to the ground surface. If the expansion is smaller, the slime layer

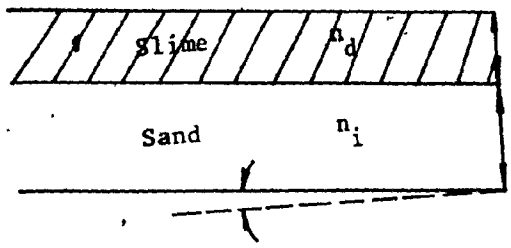

(a)

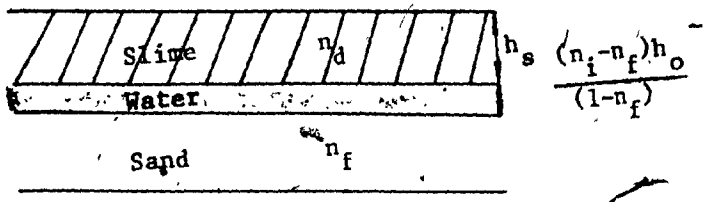

(b)

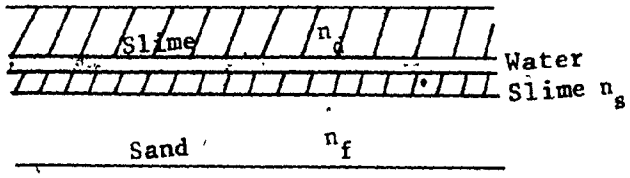

(c)

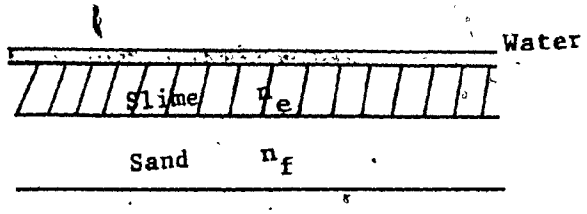

(d)

Process is complete

$n_f < n_i$ & $n_e > n_d$

Fig. 3.5 The Liquefaction Process Phases for the First Tailings Deposits Profile

will be entirely liquefied (Scott and Zuckerman 1967). Thus, the condition for complete liquefaction of the slime layer is

$$\frac{(n_e - n_d)}{(1 - n_e)} \; h_s \leq \frac{(n_i - n_f)}{(1-n_f)} \; h_o \qquad (3.36)$$

The estimated time of liquefaction process:

The particles of the upper surface of the sand layer begin settling as soon as the sand becomes liquefied at t = 0 after the earthquake ceases. They will continue to fall until they strike the solidification interface. The distance they fall is the contraction in the thickness of the sand layer, $(n_i - n_f)h_o/(1-n_f)$, and if they have a settling velocity A, the time t_f that they are in motion is:

$$t_f = \frac{(n_i - n_f)\, h_o}{(1-n_f)A} \qquad (3.37)$$

Similarly, the bottom grains of the slime layer begin falling as the sand grains settle at t = 0. The time it takes the bottom grains of the slime layer to fall the contraction distance of the sand layer, t_s, is:

$$t_s = \frac{(n_i - n_f)h_o}{(1-n_f)\, C} \qquad (3.38)$$

where C is the settling velocity of the slime grains.

t_s is a big value (minutes) and greater than t_f because C is much smaller than A.

Equation (3.38) determines the time elapsed until the liquefaction process is completed and reaches the ground surface. At the same time, t_s is the time along which the slime layer is susceptible to flow after the earthquake ceases, because during that time a layer of water (Fig.

3.5b,c) lays under the slime layer. This water has no shear strength to support the slime layer and to resist its flow. After time equal to t_s, the liquefaction will be completed all the way to the ground surface, and the slime layer will be supported again by a layer of sand (Fig. 3.5d) which has shear strength to resist its flow. In this case the total time of flow of the overlying slime layer is the time involved in liquefaction, t_s. Hence, the distance of flow after the earthquake ceases is:

$$u_x = g \sin\theta \cdot \frac{t_s^2}{2} \qquad (3.39)$$

This distance of flow during the earthquake is as before (Eq. 3.12). The total time of flow during and after the earthquake is the sum of the values of Eq. (3.12) and (3.39).

3.4.2 In Case the Slime Layer Underlies Sand

Consider the soil profile of tailings deposits as shown in Fig. 3.6a. An earthquake causes the underlying slime layer to liquefy, and the overlying sand layer to contract forming a dense layer of porosity n_f, Fig. 3.6b. The time for the liquefaction process to reach the ground surface is:

$$t_f = \frac{(n_i - n_f)\, h_o}{(1 - n_f)\, A}$$

In this case, during the liquefaction process phases, the overlying sand layer is supported by the underlying slime layer. No layer of water will appear between the two layers. (The velocity of sand particles are many times those of slime particles, so separation does not take place, and the analysis shown in Section 3.3 is applied).

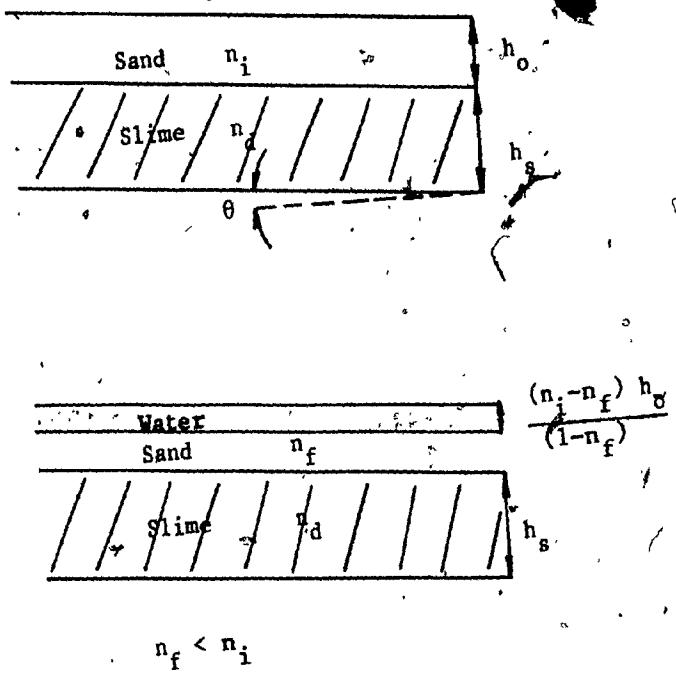

Fig. 3.6 The Liquefaction Process Phases for the Second Tailings Deposits Profile

3.5 A Suggested Tailings Deposits Profile

It is evident from the previous analysis that the most dangerous situation is when the slime layer is deposited on top of the sand layer. In this case a layer of water is encountered between the layers, the dissipation of which requires a long period of time. The dissipation may be achieved by installing drainage systems, like vertical sand or gravel drains. Quite apart from the fact that the installation of such drains are commercially unfeasible, they also suffer from the disadvantage of clogging. Hence, they become non-functional after a period of time.

An alternative method which is quite inexpensive to install and does not suffer from the clogging phenomenon is the method suggested here. The profile consists of two layers, an underlying loose sand layer in the shape of dunes, of height h_o, and an overlying layer of slime of height h_s at the sand dunes. During the earthquake the sand will contract and a layer of water will exist between the slime and the sand layers, as shown in Fig. 3.7a. After the earthquake ceases, the liquefaction process will proceed upward to the ground surface. The liquefaction will reach the ground surface at the sand dunes (where h_s is very much less than h_o) faster than it reaches the ground surface at other areas (according to equation (3.36) mentioned before), thus forming the so-called sand blows or sand boils, as shown in Fig. 3.7b,c. The excess pore water pressure developed in the underlying soil layer due to the earthquake induced forces, will be relieved by the venting of water and sand through these sand blows. The liquefaction process will be completed in a very short time, as shown in Fig. 3.7d. In other words, the time that the slime layer is susceptible to flow and hence the

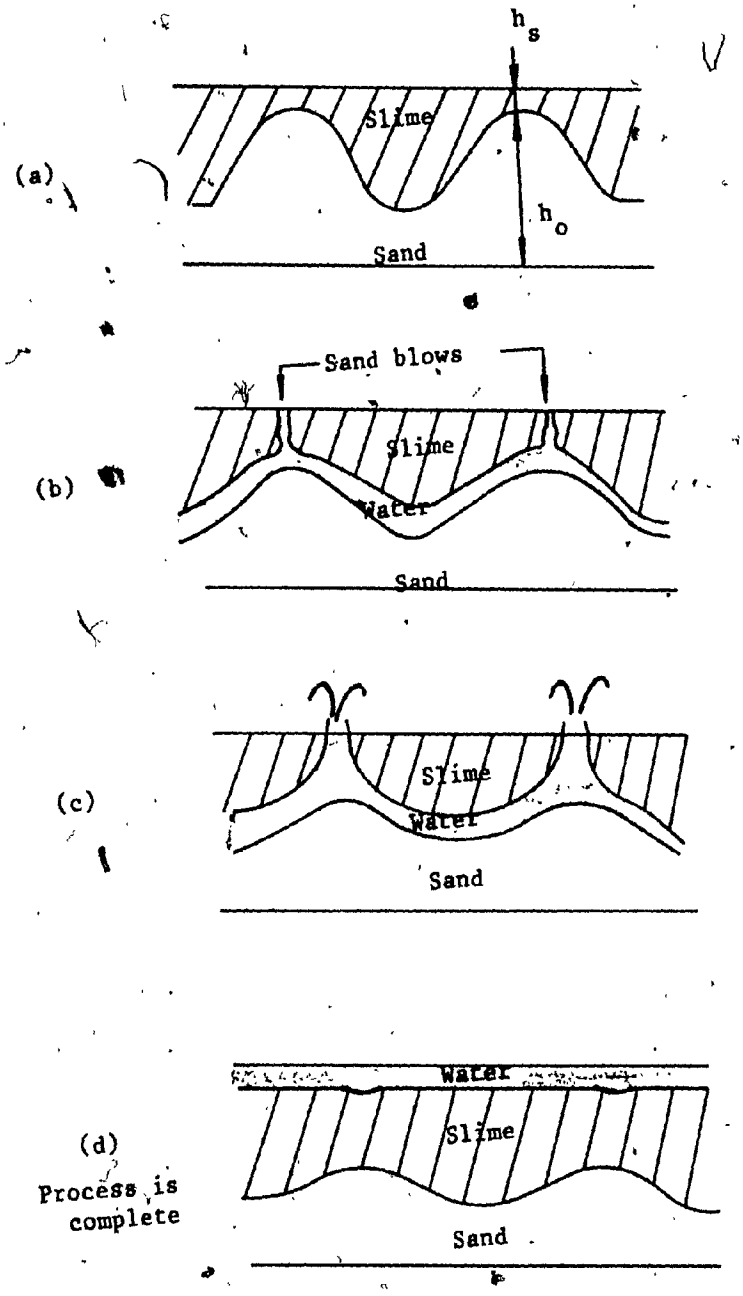

Fig. 3.7 The Liquefaction Process Phases for the Suggested Tailings Deposits Profile

distance of flow is short compared with that in the case of the original profile of the tailings deposits. Thus, the high pore pressure which causes the underlying soil to liquefy will dissipate, the soil will not liquefy and hence, will resist the flow of the overlying layer.

3.6. Experimental Study

Two tests were performed on two small models of the existing tailings deposits profile in the field, and the suggested one, to study the liquefaction process in each. The tests verified the preference of the suggested profile to speed up the liquefaction process and the development of the sand blows. Each model was positioned on the shaking table and subjected to vibrations of speeds of 3600 vpm and of a low amplitude 0.005 inch.

The first model is shown in Fig. 3.8a. Fig. 3.8b shows the beginning of the liquefaction process, as the sand contracts, developing a layer of water between the slime and the sand layer after vibrating the model for 15 sec. In Fig. 3.8c, the liquefaction process proceeds upwards towards the surface, as the slime particles start to settle after 30 sec. In Fig. 3.8d, the liquefaction process is completed and reaches the surface after 20 min, and the slime layer becomes supported by the sand layer again.

The second model is shown in Fig. 3.9a. After only 5 sec. of vibrating time, the sand blows began to develop at the sand dune forming small vents at the surface as shown in Fig. 3.9b. The liquefaction was complete and reached the surface after only 4 min, as shown in Fig. 3.9c. Fig. 3.9d shows the sand blows forming a uniform crack along the sand dune at the end of the liquefaction process.

The tests indicate that the suggested scheme is a fairly inexpensive and effective method of prevention of earthquake induced instability.

Fig. 3.8a Initial Condition, Time = 0

Fig. 3.8b Time = 15 seconds

Fig. 3.8 Stages in the Process of Liquefaction for the Existing Tailings Deposits Profile

Fig. 3.8c Liquefaction is Proceeding Upwards

Time = 30 seconds

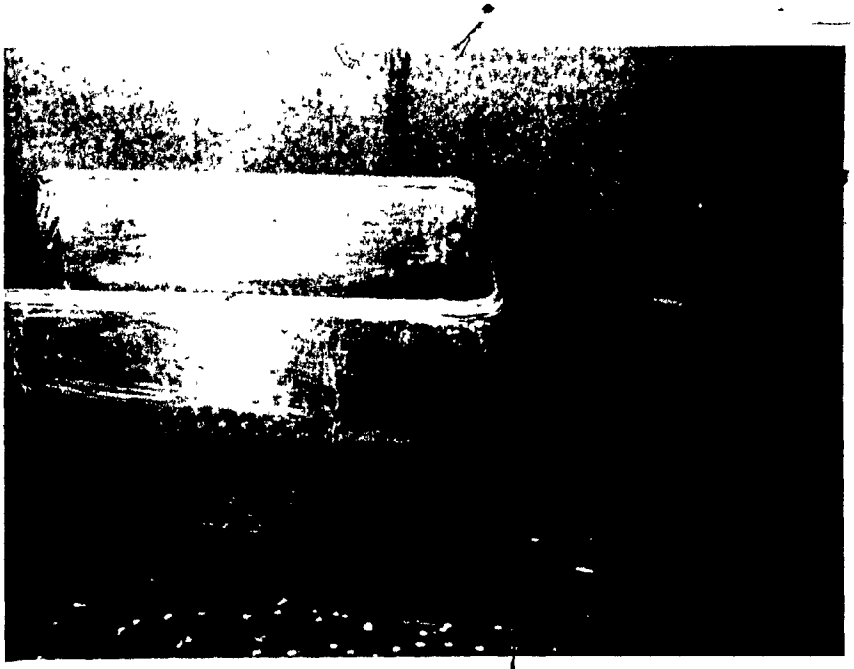

Fig. 3.8d Liquefaction Porcess is Complete

Time = 20 minutes

Fig. 3.8 Stages in the Process of Liquefaction for the Existing Tailings Deposits Profile

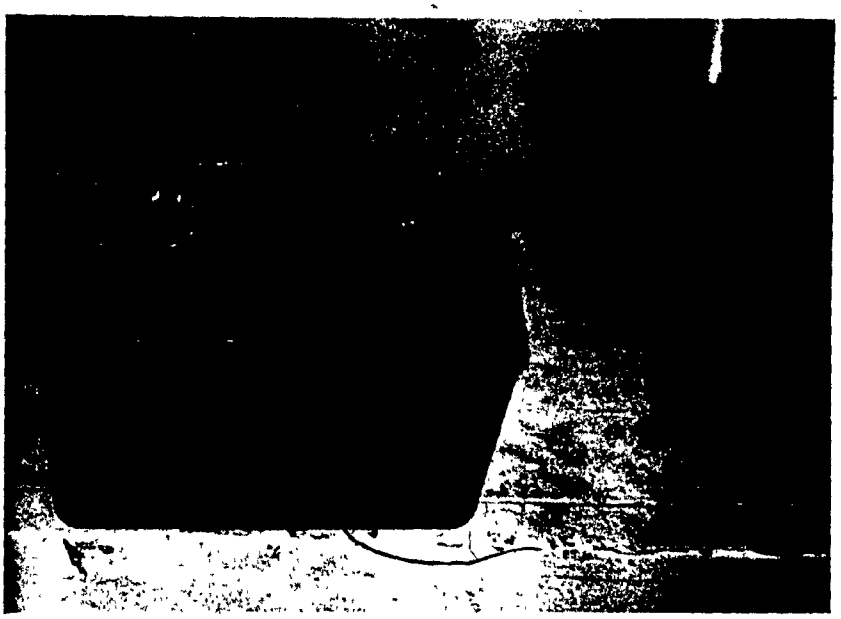

Fig. 3.9a Initial Condition, Time = 0

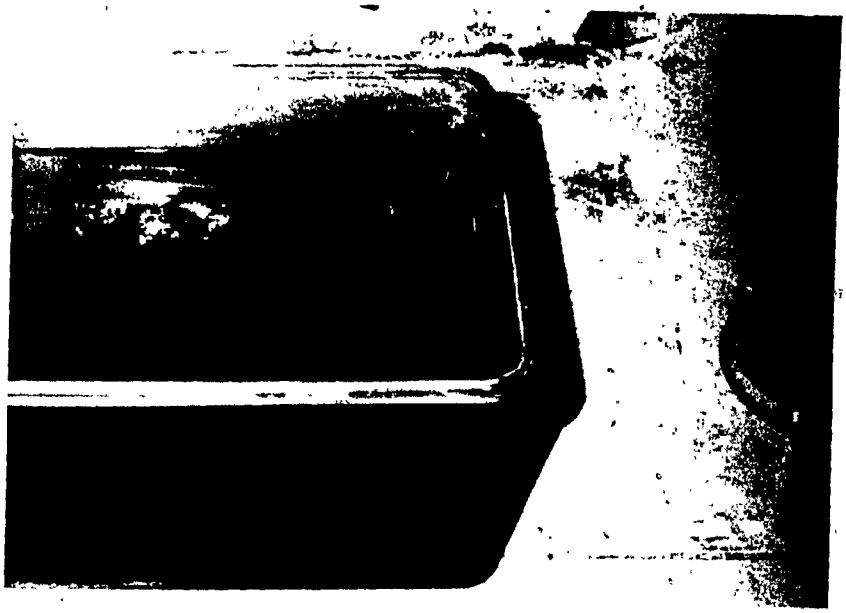

Fig. 3.9b Sand Blows Start to Develop, Time = 5 sec.

Fig. 3.9 Stages in the Process of Liquefaction for the Suggsested Tailings Deposits Profile

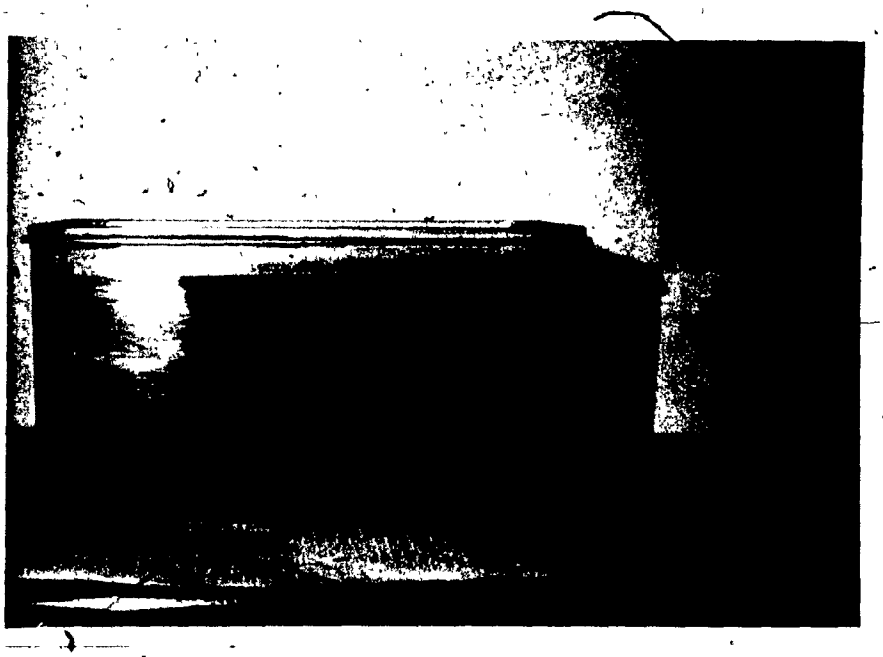

Fig. 3.9c Liquefaction Process is Complete
Time = 4 min.

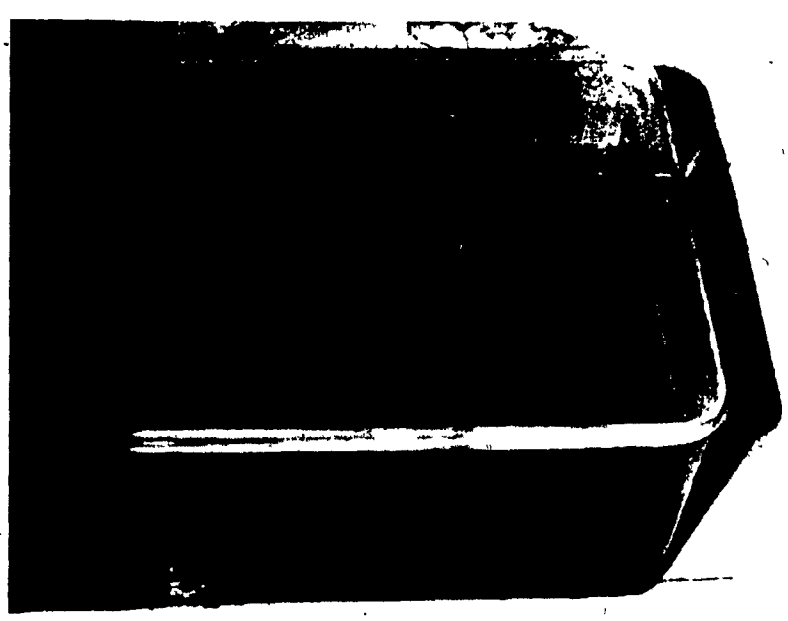

Fig. 3.9d Sand Blows Forming Continuous Crack

Fig. 3.9 Stages in the Process of Liquefaction for the Suggested Tailings Deposits Profile

CHAPTER 4

CONCLUSIONS

This research can be concluded as follows:

4.1 Liquefaction of Tailings Deposits Due to Earthquake Forces

The study of the slime behaviour under cyclic loading conditions of the triaxial cyclic loading tests (compression-extension tests) indicates that:

1. The slime experiences loss of shear strength, and hence, loss in its resistance to deformation during cyclic loading application. The pore water pressure increases gradually, which results in the effective stress applied to the soil decreasing, until the pore pressure reaches the value of the confining pressure (zero effective stress condition), i.e. the soil gets liquefied and looses all its shear strength and behaves like a liquid.
2. The slime of high water content is more susceptible to liquefaction under cyclic loading conditions than that of low water content.
3. The slime of certain water content subjected to low cyclic stress is more likely to liquefy than that of the same water content which is subjected to high cyclic stress, because the pore water pressure starts, in the later case, to dissipate during the cyclic loading application due to the tendency for the sample to dilate causing a decrease in the pore water pressure.

4. After the slime liquefies, if the cyclic loading is stopped (the earthquake ceases), and a static shear stress is applied to the liquefied slime (like weight component of the inclined slime layer in the field), the slime regains a high value of shear strength ($\phi' = 52.5^{\circ}$) and resists failure until it reaches high values of strain.

5. When a saturated slime is subjected to cyclic loading followed with no drainage by undrained compressive load to failure, the static undrained shear strength is higher than that for saturated slimes that fail without initial cyclic loading.

6. The comparative study between the static loading following liquefaction and the conventional static loading indicates that the cyclic stress required to induce liquefaction or failure is lower than the stresses required to cause failure under static loading conditions at the same confining pressure. This result confirms the important fact that soil behaviour under cyclic loading is quite different from that developed under static loading conditions. It is impossible at this stage, to predict soil behaviour under cyclic loading conditions from the results of tests performed under conventional static loading conditions.

7. The cyclic loading tests agreed with the concept of "Characteristic State" or "Critical State", which was proved, as discussed earlier, that these are essentially similar concepts. "Characteristic State" defines the stress level along which the soil experiences no volume change in drained conditions or no

pore water pressure generation in undrained conditions. When the stress applied to the slime is lower than the stress level associated with characteristic state line, it contracts if drainage is permitted; alternatively the pore pressure increases if drainage is not allowed. When the stress level is higher than the level corresponding to the CH.S.L., the slime dilates under drained conditions; alternatively the pore pressure decreases for the undrained conditions.

4.2 Instability of Tailings Deposits Due to Earthquake Forces

The study of an infinite slope of tailings deposits subjected to earthquake forces indicates that the overlying layer flows over the underlying liquefied layer.

4.2.1 In Case the Slime Layer Underlies Sand

The distance of flow during the earthquake, $\bar{u}_x$, is:

$$\bar{u}_x = g \sin\theta \cdot \frac{t_o^2}{2} \tag{3.12}$$

The distance of flow after the earthquake ceases u_x, can be obtained from the relationship:

$$u_x = \frac{h_o \gamma_o h_s}{G} \sin \quad (1-\cos \beta t) + \frac{g \sin\theta \cdot t_o}{\beta} \sin \beta t \tag{3.23}$$

In case $u_x < u_x^{cr}$

and

$$u_x = \frac{\tau^{cr}}{G} \cdot h_s + \frac{(\dot{u}_x^{cr})^2}{2\left[\tau_{cr} \cdot \frac{g}{\gamma_o h_o} - \frac{\sin\theta}{g}\right]} \tag{3.35}$$

In case $u_x > u_x^{cr}$

4.2.2 In Case the Slime Layer Overlies Sand

The distance of flow during the earthquake, $\bar{u}_x$, is given by Eq. (3.12). The distance of flow after the earthquake ceases, u_x, is:

$$u_x = g \sin\theta \cdot \frac{t_s^2}{2} \tag{3.39}$$

where t_s is a great value.

It is evident that the most dangerous case is when the slime layer is deposited on top of the flow sand layer, because the time of flow (and hence, the distance of flow) is greater than that obtained under the other condition. That is, because of the time differential between the slime particles and the sand particles settlement.

A new profile of tailings deposits of underlying sand layer of the shape of dunes overlayed by the slime layer, is suggested to solve the problems of liquefaction and flow of the desposits. When the new profile of the tailings deposits is subjected to earthquake forces, the liquefaction process will proceed from the sand dunes very rapidly to the ground surface, causing sand blows or sand boils. The excess pore water pressure developed due to the earthquake forces will dissipate through these sand blows. Hence, the underlying layer may not liquefy and will resist the flow of the overlying layer. The experiments proved this behaviour.

SUGGESTIONS FOR FURTHER RESEARCH

The following topics are considered suitable as an extension to the study described in this thesis:

1. A more detailed study of the phenomenon of liquefaction in the light of "Critical State" theory and recent criteria of yielding and instability.

2. Extension of the analysis of infinite slopes to cover the case of finite slopes.

3. A more detailed study of and preparation of design charts for the "dune" deposits, suggested here.

REFERENCES

1. Casagrand, A., "Characteristics of Cohesionless Soils Affecting the Stability of Slopes and Earth Fills", Journal, Boston Soc. of Civ. Engrs., January 1936.

2. Casagrand, A., "The Shearing Resistance of Soils and Its Relation to the Stability of Earth Dams", Proceedings, Soils and Foundation Conf. of the U.S. Engr. Dept., June, 1938.

3. Castro, G., and Christian, J.T., "Shear Strength of Soils and Cyclic Loading", Journal of the Geotechnical Engineering Division, ASCE, September 1976.

4. Dorby, R., and Alvarez, L., "Seismic Failures of Chilean Tailings Dams", Journal of the Soil Mechanics and Foundations Division, ASCE, November 1967.

5. Finn, W.D.L., Pickering, D.J., and Bransby, P.L., "Sand Liquefaction in Triaxial and Simple Shear Tests", Journal of the Soil Mechanics and Foundations Division, ASCE, April 1971.

6. Lee, K.L., and Chan, K., "Number of Equivalent Significant Cycles in Strong Motion Earthquakes", Proceedings of the International Conference on Microzonation for Safer Construction Research and Application, Seattle, Wash., October 1972.

7. Lee, L., and Seed, H.B., "Cyclic Stress Conditions Causing Liquefaction of Sand", Journal of the Soil Mechanics and Foundations Division, ASCE, January 1967.

8. Lucia, P.C., Duncan, J.M. and Seed, H.B., "Summary of Research on Case Histories of Flow Failures of Mine Tailings Impoundments", University of California at Berkeley. A paper prepared for presentation at the U.S. Bureau of Mines Technology Transfer Conference during Spring 1981 in Denver, Colorado, December 1980.

9. Luong, M.P., "Mechanical Performance of Granular Material Subjected to Cyclic and Transient Loading", Proceedings of the International Symposium on the Mechanical Behaviour of Structural Media, Ottawa, May 18-21, 1981.

10. Peacock, W.H., and Seed, H.B., "Sand Liquefaction Under Cyclic Loading Simple Shear Conditions", Journal of the Soil Mechanics and Foundations Division, ASCE, May 1968.

11. Poorooshasb, H.B. and Roscoe, K.H., "The Correlation of the Results of Shear Tests with Varying Degrees of Dilation", Proceedings of the 5th International Conference on Soil Mechanics and Foundation Engineering, 1961.

12. Poorooshasb, H.B., Holubec, I., and Sherbourne, A.N., "Yielding and Flow of Sand in Triaxial Compression", Part 1, Canadian Geotechnical Journal, November 1966.

13. Prakash, S., and Mathur, J.N., "Liquefaction of Fine Sand Under Dynamic Loads", Proceedings, 5th Symposium of the Civ. and Hydraulic Engrg. Dept., Indian Inst. of Science, Bangalore, India, 1965.

14. Scott, R.F., and Zuckerman, K.A., "Sand Blows and Liquefaction", California Institute of Technology. The Great Alaskan Earthquake of 1964, 1967.

15. Seed, H.B., "Soil Liquefaction and Cyclic Mobility Evaluation for Level Ground During Earthquakes", Journal of the Geotechnical Engineering Division, ASCE, February 1979

16. Seed, H.B., et al, "Representation of Irregular Stress Time Histories by Equivalent Uniform Stress Series in Liquefaction Analysis", Report No. EERC75-29, Earthquake Engineering Research Centre, University of California, Berkeley, Calif., October 1975

17. Seed, H.B. and Idriss, I.M., "Simplified Procedures for Evaluating Soil Liquefaction Potential", Journal of the Soil Mechanics and Foundation Division, ASCE, September 1971.

18. Seed, H.B. and Lee, K.L., "Liquefaction of Saturated Sands During Cyclic Loading", Journal of the Soil Mechanics and Foundation Division, ASCE, November 1966.

19. Seed, H.B., Mori, K., and Chan, C.K., "Influence of Seismic History on Liquefaction of Sands", Journal of the Geotechnical Engineering Division, ASCE, April 1977.

20. Seed, H.B., and Peacock, W.H., "Test Procedures for Measuring Soil Liquefaction Characteristics", Journal of the Soil Mechanics and Foundation Division, ASCE, August 1971.